DAMAGE ANALYSIS IN ASPHALT CONCRETE MIXTURES

BASED ON PARAMETER RELATIONSHIPS

A Dissertation

by

INJUN SONG

Submitted to the Office of Graduate Studies of
Texas A&M University
in partial fulfillment of the requirements for the degree of

DOCTOR OF PHILOSOPHY

August 2004

Major Subject: Civil Engineering

DAMAGE ANALYSIS IN ASPHALT CONCRETE MIXTURES

BASED ON PARAMETER RELATIONSHIPS

A Dissertation

by

INJUN SONG

Submitted to Texas A&M University
in partial fulfillment of the requirements
for the degree of

DOCTOR OF PHILOSOPHY

Approved as to style and content by:

Dallas N. Little (Chair of Committee)	Robert L. Lytton (Member)
Dan Zollinger (Member)	Eyad Masad (Member)
Christopher C. Mathewson (Member)	Paul N. Roschke (Head of Department)

August 2004

Major Subject: Civil Engineering

ABSTRACT

Damage Analysis in Asphalt Concrete Mixtures Based on Parameter Relationships. (August 2004)

Injun Song, B.S., Hanyang University;

M.S., Hanyang University

Chair of Advisory Committee: Dr. Dallas N. Little

Asphalt pavements experience damage due to traffic loading under various environmental conditions. Damage can be caused by viscoplastic flow and microcracks, fracture due to fatigue cracking, or fracture due to thermal cracking. Asphalt pavements have the capability to remediate some of this damage depending on binder surface and rheological properties, filler surface properties, and length of rest periods.

Asphalt mastic (asphalt and fine aggregates) properties play an important role in controlling damage and healing. This dissertation addresses the development of a comprehensive methodology to characterize damage and healing in asphalt mastics and mixtures. The methodology relies on nondestructive imaging techniques (X-ray CT), principles of continuum damage mechanics, and principles of micromechanics. The X-ray CT yields a damage parameter that quantifies the percentage of cracks and air voids in a specimen. The continuum damage model parameters are derived from the relationship between applied stress and pseudo strain. The micromechanics model

relates the damaged mastic modulus to a reference undamaged modulus. This relationship is a function of internal structure properties (void size, film thickness, and percentage of voids), binder modulus, aggregate modulus, and bond energy between binder and aggregates. The internal structure parameters are all obtained using X-ray CT and correlated.

The developed methodology was used to characterize damage in asphalt mastic and mixture specimens tested using the Dynamic Mechanical Analyzer (DMA) and dynamic creep test. The damage parameter measured using X-ray CT correlated very well with the predictions of the continuum and micromechanics models. All damage parameters were able to reflect the accumulation of damage under cyclic loading and were also able to capture the influence of moisture conditioning on damage. Although this dissertation focused on fatigue cracking at room temperatures, the methodology developed can be used to assess damage due to different mechanisms such as permanent deformation and low temperature cracking.

DEDICATION

To my parents, my wife, and my daughter

ACKNOWLEDGMENTS

I would like to express my deep gratitude and sincere appreciation to my advisor, professor Dr. Dallas N. Little for his valuable guidance, encouragement, and suggestions to complete this dissertation. I am greatly indebted to Dr. Dallas N. Little for giving me the opportunity to conduct research at the Texas Transportation Institute. It has been an honor for me to have the privilege of Dr. Dallas N. Little as an advisor. I also wish to express my special thanks to Dr. Eyad Masad for his valuable comments and helpful suggestions.

My sincere gratitude is also extended to Dr. Robert L. Lytton, Dr. Dan Zollinger, and Dr. Christopher C. Mathewson for their excellent service as my academic committee advisors.

I would also like to thank the Korean students at A&M and the staff members at the Texas Transportation Institute for all their assistance and help.

Finally, I would like to express my deep gratitude to my parents, Jin-Hoi Song and Kyung-Sook Moon, for their prayers, encouragement and support through these years of study. My beloved wife Sun Young and daughter Yoonah will always be remembered for their love and encouragement.

TABLE OF CONTENTS

TABLE OF CONTENTS (Cont'd)

TABLE OF CONTENTS (Cont'd)

LIST OF FIGURES

LIST OF FIGURES (Cont'd)

LIST OF FIGURES (Cont'd)

LIST OF FIGURES (Cont'd)

LIST OF FIGURES (Cont'd)

LIST OF FIGURES (Cont'd)

LIST OF TABLES

LIST OF TABLES (Cont'd)

CHAPTER I

INTRODUCTION

Fatigue cracking has been considered one of the three main distresses in asphalt concrete pavements along with permanent deformation, and thermal cracking. Fatigue cracking can be defined as the damage results from the accumulation of damage under repeated loading in asphalt pavements (Ghuzlan 2001). Therefore, characterizing damage has been considered one of the valuable methods in the models for improving design of pavements. Studies regarding damage in engineering materials have been performed by researchers such as Miner (1945), Kachanov (1958), and Perzyna (1984). They tried to define the effects of applied stresses, and temperature on damage accumulation. However, the accurate prediction of pavement performance still difficult because of complex and time consuming tasks as well as complexity of material behaviors.

RESEARCH OBJECTIVES AND METHODOLOGY

Texas Transportation Institute (TTI) successfully used the dynamic mechanical analysis (DMA) which is simple and easy method to evaluate the damage mechanics of the mastic as well as the microcrack healing potential of the mastic.

This dissertation follows the style and format of the *Journal of Materials in Civil Engineering*, ASCE.

X-ray computed tomography (CT) is a completely nondestructive technique for visualizing features in the interior of opaque solid objects to obtain digital information on their three-dimensional (3-D) geometry and properties (Denison et al. 1997). The suggested two methods can be used to characterize damage in asphalt mixtures and monitor the progression of the damage. Therefore, the key tools used to evaluate damage in the mixtures are DMA and X-ray CT experiment in this research.

Specific objectives of this research are as follows:

- Development of two critical points on both permanent deformation and fatigue cracking.
- Validating DMA as a simple and accurate method does indeed monitor the progression of microcrack damage through tomography and micromechanics model.
- Identification of X-ray CT as a valuable method to characterize damage in asphalt mixtures.
- Investigation of damage levels at different loading status.
- Investigation of the parameter relationships among three different damage indicators.
- Identification of characteristics of damage in asphalt mixtures in the presence of water.
- Development of methods to relate damage parameters.
- Validating cohesive and adhesive model in asphalt mixtures.
- Identification of correlation between DMA and X-ray CT method.

The methodology for using the DMA was fully developed in the previous study. Damage in the DMA experiment is monitored by decay in the normalized shear modulus and also by the accumulation of dissipated pseudo strain energy (DPSE). TTI used a micromechanics approach to monitor damage. This approach related the decay in modulus to microcrack growth in the sample tested. As the microcrack density and/or average crack length increased, the normalized modulus would decrease. This micromechanics relationship also included bond energy properties of the mixture. TTI also developed a protocol to measure surface energies of the aggregate and bitumen. Surface energies of the filler and bitumen can be used to calculate cohesive and adhesive bond strength of the asphalt mixture.

X-ray CT was used to measure the damage in the DMA dry and wet specimens at four different loading cycles or loading steps. It is critically important to validate the damage that occurs during the DMA testing. They are truly related to microcrack development and propagation. Fortunately, a tool exists by which this can be assessed, computer assisted tomography. Although former studies successfully characterized asphalt mixtures using image analysis, they didn't monitor the real progression of damage in the specimens since they used only the images just at initial (undamaged) and final (failure) stage. HMA and sand asphalt specimens before and after dynamic creep and DMA fatigue test were scanned by X-ray to capture the microstructures at different four steps with dry and wet condition. Damage parameter ξ from X-ray CT was adopted to quantify the damage levels at each step in both HMA and sand asphalt specimens.

RESEARCH ORGANIZATION

Three damage parameters were selected to represent the status of damaged and undamaged asphalt mixtures after reviewing literatures. There are two main approaches which were used to calculate the damage parameters in asphalt mixtures, those are, the void area approach and the damage approach. Perzyna (1984) introduced the void area approach which is based on the area of voids and cracks in the mixture. Kim et al. (1997) also showed the constitutive damage approach.

Most commonly used materials in the asphalt research were selected and used for this research. Performance grade (PG) binder, granite, and Ottawa standard sand were used for this study. Two sizes of specimens were fabricated for the two types of mechanical tests. Three laboratory experiments of DMA, dynamic creep, and X-ray CT were conducted to get mechanical properties. The mechanical properties from DMA and dynamic creep test were used to calculate and analyze damage indicators while image analysis was performed based on the results from X-ray CT.

The methods for comparing and validating results from the experiments were suggested and presented.

Figure 1.1 shows the research procedures in brief.

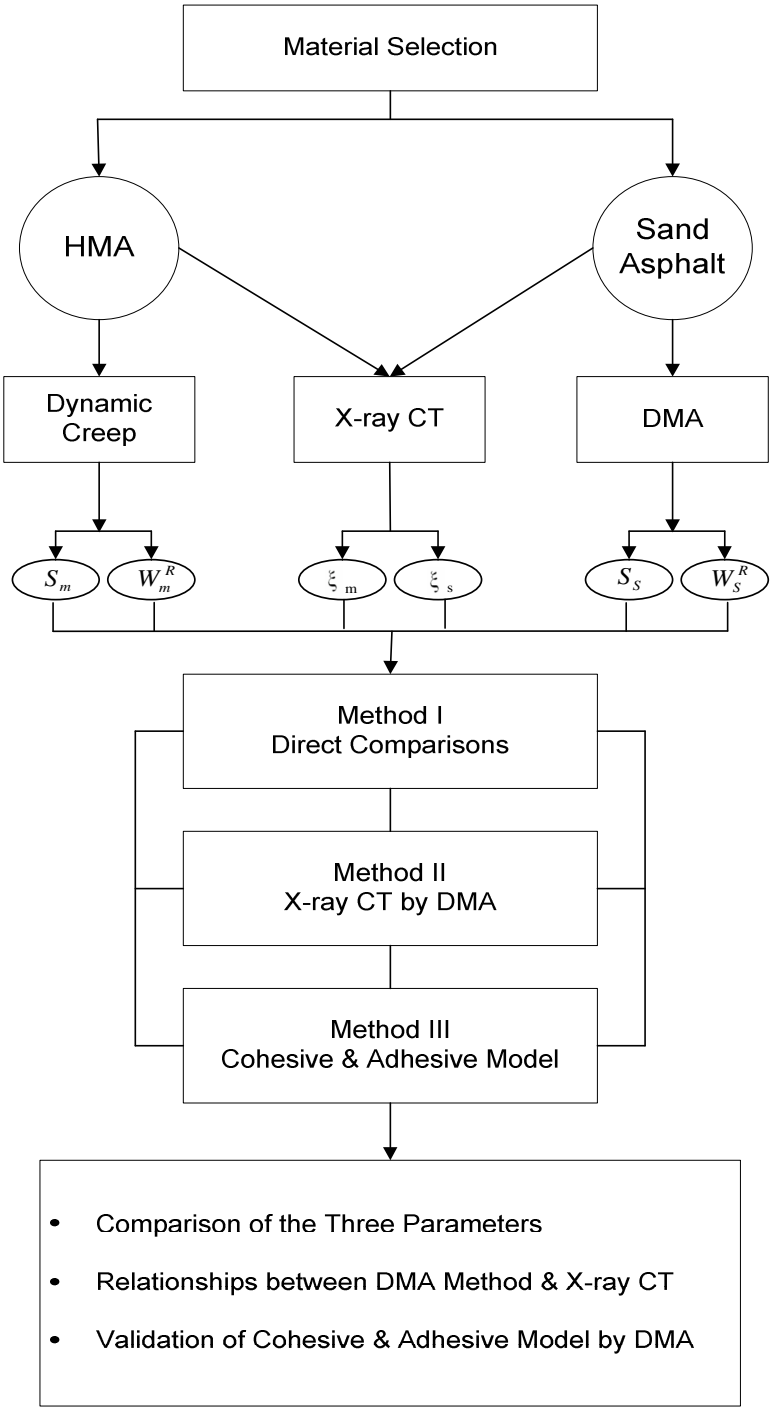

Figure 1.1. Chart for Research Procedures.

CHAPTER II

DAMAGE CHARACTERIZATION

DEFINITION AND THEORIES

Ghuzlan (2001) defined the mechanics of damage in his dissertation. Damage mechanics is the study of the mechanisms of deterioration of the material under loading by means of mechanical variables. Damage can be studied in three levels the microscale, mesoscale and the macroscale. At the microscale level, damage is the accumulation of micro stresses in the neighborhood of the defects or interfaces and the breaking of bonds, which damage the material. In the mesoscale level the microcracks and microvoids grwow and coalescence together to initiate one crack in a representative volume element. At the macroscale level, this is the growth of that crack. The microscale and mesoscale levels may be studied through the damage variables of the mechanics of the continuous media. The macroscale level is studied through the fracture mechanics with variables defined at the macroscale level.

Lytton (2000) defined undamaged materials behaving linear viscoelastically under loading and unloading if its hysteresis does not change with repeated loading. Accumulated damage will be occurred when a material is subjected to repeated loading. After the material becomes damaged enough to the point it can not carry any more loads it will fail. Damage, therefore, can be defined as the deterioration occurring prior to failure by the reduction in the structural integrity of the material under repeated loading. As defined above, damage has been considered important components in the distresses

and used for characterizing them. Thus, finding out the way to characterize asphalt mixture distresses in terms of relationships of damage parameters with more easy and simple methods is the main focus in this research.

Miner (1945) is one of the first researchers who related failure of the material to damage. Continuum damage mechanics model was first developed for ductile materials by Kachanov (1958) in 1958. He introduced the variable ψ, which called "continuity" in his paper. Years later the variable $D = 1 - \psi$ was introduced as the international state variable. The D variable varies between 0 and 1 where the undamaged material will be with D = 0 and the damaged material will have D = 1. The main developments of damage theory occurred in 1970' and 1980', later the principles of thermodynamic and micromechanics were introduced. In 1984, Perzyna modified his simple model of an elastic-viscoplastic solid with internal imperfections due to the nucleation, growth and diffusion of voids in such a way that he introduced the additional information about the final stage of the necking process.

Perzyna's analysis of damage, that the rate of damage is a function of the rate of viscoplastic energy, confinement pressure, and effective viscoplastic strain as follows:

$$\dot{\xi} = f(\dot{W}_{vp}, \dot{I}_1, \dot{\bar{\varepsilon}}_{vp}) \qquad (2.1)$$

Where $\dot{W}_{vp}$ = the rate of viscoplastic energy,

$\dot{I}_1$ = the rate of change in the first stress invariant, and

$\dot{\bar{\varepsilon}}_{vp}$ = the effective viscoplastic strain rate.

Kim et al. (1997) tried constitutive damage approach for studying damage in asphalt concrete mixtures. They used continuum damage theory to model the damage during cyclic loadings and healing during rest periods. The continuum damage model consists of: 1) pseudo strain energy density function, 2) stress-strain relationship, and 3) damage evolution law as follows:

$$W^R = W^R(\varepsilon^R, S_m) \tag{2.2}$$

$$\sigma = \frac{\partial W^R}{\partial \varepsilon^R} \tag{2.3}$$

$$\dot{S}_m = \left(-\frac{\partial W^R}{\partial S_m} \right)^{\alpha_m} \tag{2.4}$$

Where W^R = pseudo strain energy,

ε^R = pseudo strain,

S_m = internal state variables (or damage parameters),

$\dot{S}_m$ = damage evolution rate, and

α_m = material constant.

This constitutive model predicts the damage growth and healing in asphalt concrete under monotonic loading with varying strains for both controlled-stress and

controlled-strain modes of loading. Perzyna (1984) showed that damage in metals grows at a small rate at the beginning of the deformation process until it reaches a critical value, which corresponds to a sudden loss in the material yield strength. Thereafter, damage grows rapidly at a very high rate leading to complete failure. However, asphalt concrete at relatively high temperatures typically behaves as a ductile material. It is, therefore, expected that damage does not evolve in such an exponential pattern, as is the case in brittle metals.

Additionally, recent studies indicate that the average percent air void has been related to rutting (Brown and Cross 1992), fatigue cracking (Tayebali et al. 1994), low temperature cracking (Hiltunen and Roque 1994), stripping and permeability characteristics of asphalt mixtures (Roberts et al. 1996).

Paris and Erdogan (1963) found the crack growth rate and Paris' law is expressed as the damage evolution law in Equation 2.5.

$$\frac{dc}{dN} = AK^n \tag{2.5}$$

Where c = crack length,

N = number of loading repetitions,

A, n = parameters dependent on the material and on the experimental conditions, and

K = stress intensity factor.

ξ AND *S* AT ASPHALT MIXES

Since the Equations 2.4 and 2.5 show that the physical meaning of the damage parameter can be considered amount of damage, the crack length and/or dissipated energy due to crack development with increasing number of loading cycles can be used for calculating damage parameters. Therefore, Chapter VI introduced the correlation methods which adopted DPSE and two damage parameters which are based on crack length and dissipated energy are shown in this chapter.

In this research, it was determined to adopt the damage definitions based on the amount of voids and stiffness changes. The two damage parameters were calculated by two main approaches which were conducted to study damage in asphalt concrete mixtures, that is, the void area approach and the constitutive damage approach. The void area approach is based on the area of void and crack in the mixture and the constitutive damage approach is a microscale level study of damage. Two damage parameters which were introduced by Perzyna (1984) and Kim et al. (1997) were included and compared each other in this research to find the relationships so that quantify the damage level simple and easily.

Following the procedure as Tashman et al. (2004) and Lee et al. (2000a) proposed in their paper, two damage parameters ξ and *S* can be determined for asphalt concrete mixtures. The damage parameter ξ is expressed in terms of the ratio of area of cracks and voids to the total cross sectional area. Using the three laboratory experiments, the parameters in Equations 2.6 and 2.7 below can be acquired.

$$\xi = \frac{Av}{S} \tag{2.6}$$

$$S = Av + As \tag{2.7}$$

Where ξ = damage parameter,

A_v = the area of cracks and voids,

S = total cross sectional area of the specimen, and

A_s = solid phase area, which includes the aggregate and asphalt binder,

In the previous paper of Perzyna (1984) a simple model of an elastic-viscoelastic solid with internal imperfections due to the nucleation, growth and diffusion of voids was proposed. He showed that damage in metals grows at a small rate at the beginning of the deformation process until it reaches a critical value, which corresponds to a sudden loss in the material yield strength. Thereafter, damage grows rapidly at a very high rate leading to complete failure. Perzyna (1984) assumed that internal imperfections are generated from the nucleation, growth and transport of voids as follows:

$$\dot{\xi} = (\dot{\xi})_{nucleation} + (\dot{\xi})_{growth} + (\dot{\xi})_{transport} \tag{2.8}$$

$$(\dot{\xi})_{nucleation} = \frac{h}{1-\xi} tr(\sigma D^P) + l\dot{J}_1 \tag{2.9}$$

$$(\dot{\xi})_{growth} = (1-\xi) tr(\Xi D^P) \tag{2.10}$$

$$(\dot{\xi})_{transport} = (\dot{\xi})_{diffusion} = D_0 \nabla^2 \xi(x,t) \tag{2.11}$$

Where h,l = nucleation material function,

$\dot{J}_1$ = the first invariant of the Cauchy stress tensor,

D^P = rate of permanent deformation tensor,

Ξ = the matrix of the material function,

D_0 = diffusion constant for constant temperature, and

∇^2 = Laplasian operator.

In a room temperature, the Equation 2.9 is neglected and Ξ is replaced by one scalar material growth function Θ.

$$\dot{\xi} = \frac{h}{1-\xi} tr(\sigma D^P) + l\dot{J}_1 + (1-\xi) tr(\Theta D^P) \tag{2.12}$$

Tashman et al. (2004), however, found that asphalt concrete behave is different from that of brittle metals. They, therefore, proposed an empirical power law for damage evolution law.

$$\xi = \xi(W_{vp}, I_1, \bar{\varepsilon}_{vp}) = \xi_o + Hc\left(W_{vp}\right)^{Hp} + Lc\left(I_1\right)^{Lp} + Ec\left(\bar{\varepsilon}_{vp}\right)^{Ep} \tag{2.13}$$

Where ξ_0 = initial damage value,

W_{vp} = viscoplastic energy,

I_1 = the first invariant of the stress tensor,

$\bar{\varepsilon}_{vp}$ = effective viscoplastic strain, and

H_c, H_p, L_c, L_p, E_c, and E_p = fitting coefficients.

Damage parameter S can be defined from the evolution law shown in Equation 2.4 and the pseudo strain energy density function are introduced in Equation 2.26. Combining the two equations by using chain rule Equation 2.14 yields Equation 2.15 as follows:

$$\frac{dC}{dS} = \frac{dC}{dt}\frac{dt}{dS} \tag{2.14}$$

$$\frac{dS}{dt} = \left[-\frac{I}{2}\frac{dC}{dS}(\varepsilon_m^R)^2 \right]^{\alpha} \tag{2.15}$$

Substituting Equation 2.14 into Equation 2.15 is expressed as:

$$\frac{dS}{dt} = \left[-\frac{I}{2}\frac{dC}{dt}(\varepsilon_m^R)^2 \right]^{\alpha/(1+\alpha)} \tag{2.16}$$

Finally, the equation is rearranged by means of integrating.

$$S \cong \sum_{i=1}^{N} \left[\frac{I}{2}(\varepsilon_{m,i}^R)^2 (C_{i-1} - C_i) \right]^{\alpha/(1+\alpha)} (t_i - t_{i-1})^{1/(1+\alpha)} \tag{2.17}$$

Lee et al. (2000a) also used the time-dependent damage evolution process of asphalt concrete and defined that damage in continuum damage mechanics is any structural changes in a system. Kim et al. (2002) adopted the damage evolution law for their study on fatigue and healing potential of asphalt binders in sand asphalt mixtures. They used above equation by substituting γ_m^R for ε_m^R for their torsional controlled-strain mode fatigue test as shown in Equation 2.18.

$$S \cong \sum_{i=1}^{N} \left[\frac{I}{2} (\gamma_{m,i}^R)^2 (C_{i-1} - C_i) \right]^{\alpha/(1+\alpha)} (t_i - t_{i-1})^{1/(1+\alpha)} \tag{2.18}$$

Where S = the damage parameter at each discrete cycle,

$\gamma_{m,i}^R$ = the peak pseudo strain,

C_i = the pseudo stiffness, and

t_i = the corresponding time.

The material constant α is initially assumed and then varied until cross-plotting the measured C against *S* at several different load-levels results in closure.

Figure 2.1 shows a typical relationship between pseudo stiffness C and damage parameter *S*.

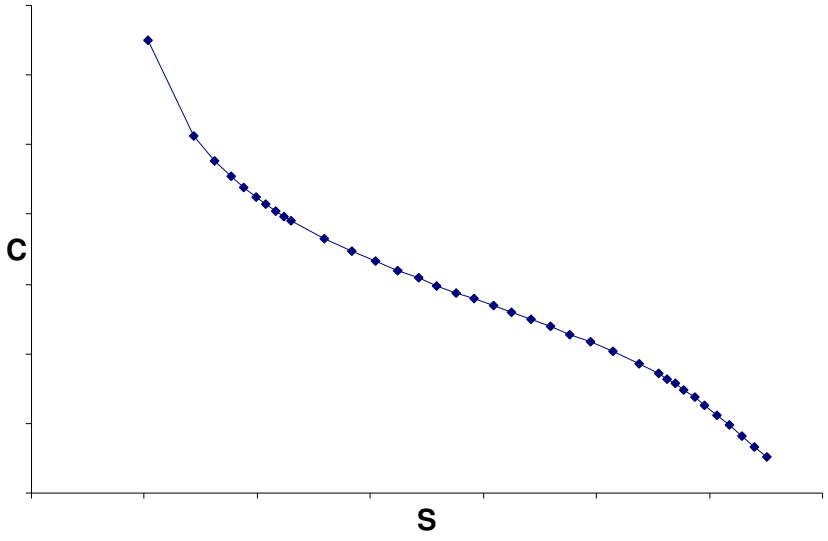

Figure 2.1. Typical Relationships between Pseudo Stiffness C and Damage Parameter *S*.

PSEUDO STIFFNESS AND DISSIPATED PSEUDO STRAIN ENERGY

Pseudo stiffness eliminates a material behavior from viscoelasticity.

Using DPSE instead of dissipated strain energy let time dependent viscoelastic behavior be eliminated as long as the initial stress or strain is negligible (Kim 1988). Also, the DPSE is a real damage indicator. Therefore, pseudo stiffness and DPSE provide more accurate way to characterize damage in the material.

Figures 2.2 and 2.3 show typical undamaged linear and nonlinear viscoelastic material behavior under repeated loading conditions. The hysteresis loop area under loading and unloading in Figure 2.3 represents a DPSE.

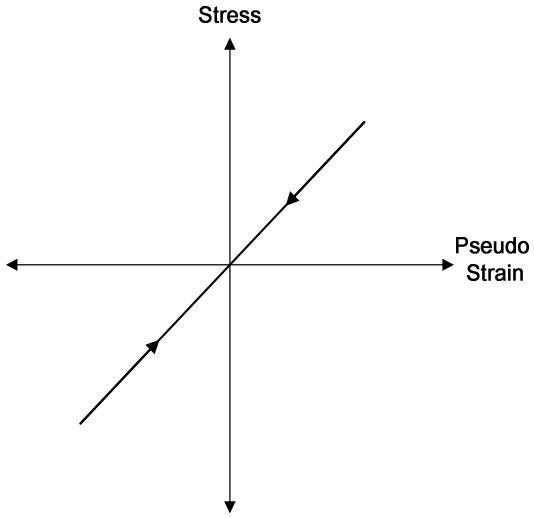

Figure 2.2. Typical Stress vs. Pseudo Strain Plot from Undamaged Linear Viscoelastic Material.

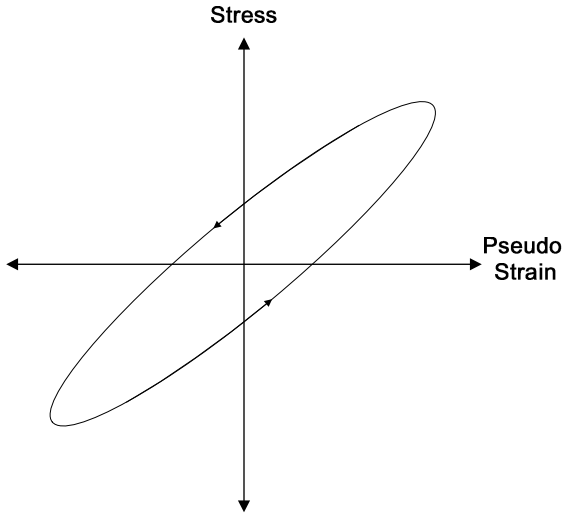

Figure 2.3. Typical Stress vs. Pseudo Strain Plot from Undamaged Nonlinear Viscoelastic Material.

Lee et al. (1998) defined secant pseudo stiffness and proposed a uniaxial pseudo strain energy density function W^R as follows:

$$S^R = \frac{\sigma_m}{\varepsilon_m^R} \tag{2.19}$$

Where S^R = pseudo stiffness,

ε_m^R = peak pseudo strain in each stress-pseudo strain cycle, and

σ_m = stress corresponding to ε_m^R.

$$W^R = \frac{I}{2} MC(S)(\varepsilon_e^R)^2 + \frac{I}{2} G(\frac{\varepsilon^R}{\varepsilon_L^R}, \varepsilon_0^R)(\varepsilon_e^R)^2 \tag{2.20}$$

Figure 2.4 shows a general graph plot of pseudo stiffness change with increasing number of cycles at controlled- stain mode in terms of measured stress against calculated pseudo strain.

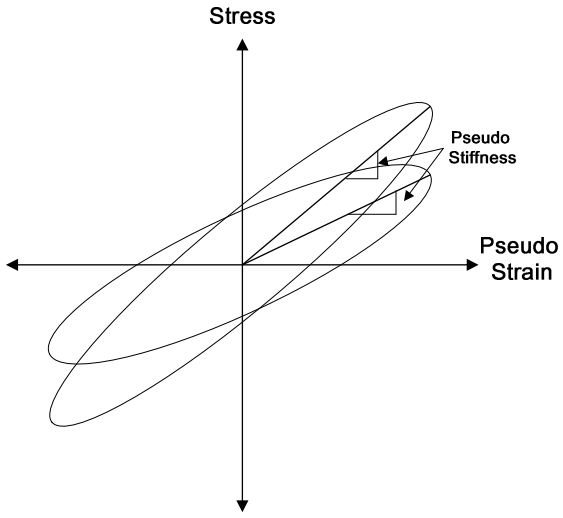

Figure 2.4. Pseudo Stiffness Change with Increasing Number of Cycles at Controlled- Stain Mode.

Based on the Equation 2.3, stress-strain relationship becomes

$$\sigma = \frac{\partial W^R}{\partial \varepsilon_e^R} = I\left[MC(S) + G(\frac{\varepsilon^R}{\varepsilon_L^R}, \varepsilon_0^R) \right] \varepsilon_e^R \tag{2.21}$$

The Equations 6.20 and 6.21 are simplified as follows when pseudo strain ε^R becomes ε_m^R and M $(\varepsilon_m^R - \varepsilon_S^R) = \varepsilon_m^R$. With the previous assumption, G becomes 0 since the ratio of ε^R to ε_m^R is 1.

$$W_m^R = \frac{I}{2} C(S) \varepsilon_m^R \varepsilon_{me}^R \tag{2.22}$$

Viscoelastic body with damage can be identified by Equation 2.23.

$$\sigma = C(S_m)\varepsilon^R \tag{2.23}$$

We can get the general form of the constitutive equation for a viscoelastic body during damage is presented as:

$$\sigma_m = IC(S)\varepsilon_m^R \tag{2.24}$$

The time-dependent damage evolution law for viscoelastic materials is typically rate-dependent and is expressed as:

$$\dot{S} = \left(-\frac{\partial W_m^R}{\partial S} \right)^{\alpha} \tag{2.25}$$

Only for controlled-strain condition is considered in this research and hence $\varepsilon_m^R = \varepsilon_{me}^R$.

Finally, the Equation 2.22 can be expressed as follows:

$$W_m^R = \frac{I}{2} C(S)\left(\varepsilon_m^R\right)^2 \tag{2.26}$$

Kim et al. (2002) applied the Equation 2.26 for torsional controlled-strain mode fatigue test as shown in Equation 2.27.

$$W_m^R = \frac{I}{2} C(S)(\gamma_m^R)^2 \tag{2.27}$$

A typical graph of stress versus pseudo strain curve under cyclic loading is shown in Figure 2.5 in which pseudo stiffness and pseudo strain energy density function are depicted.

Figure 2.5 depicted a hysteresis loop which is obtained after getting a plot of stress against pseudo stiffness and then DPSE is calculated based on the area of the hysteresis loop.

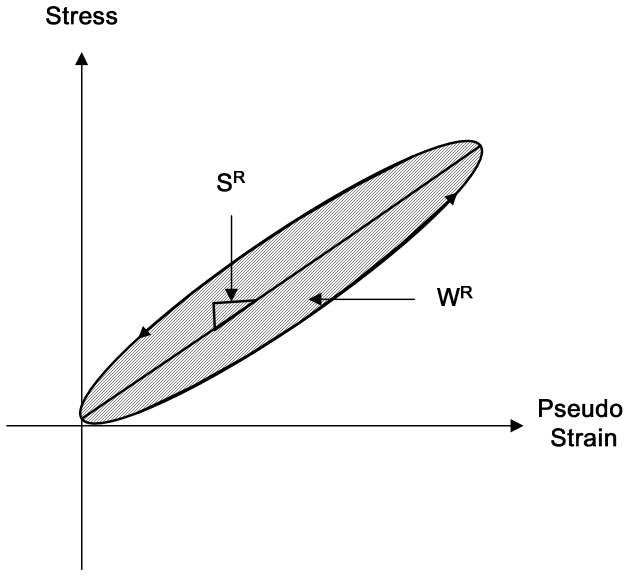

Figure 2.5. Pseudo Stiffness and Pseudo Strain Energy Density Function.

To represent the change in the slope of stress-strain loops under controlled-stress loading, the defined pseudo stiffness (S^R) in Equation 2.19 was defined and shown in Figure 2.6.

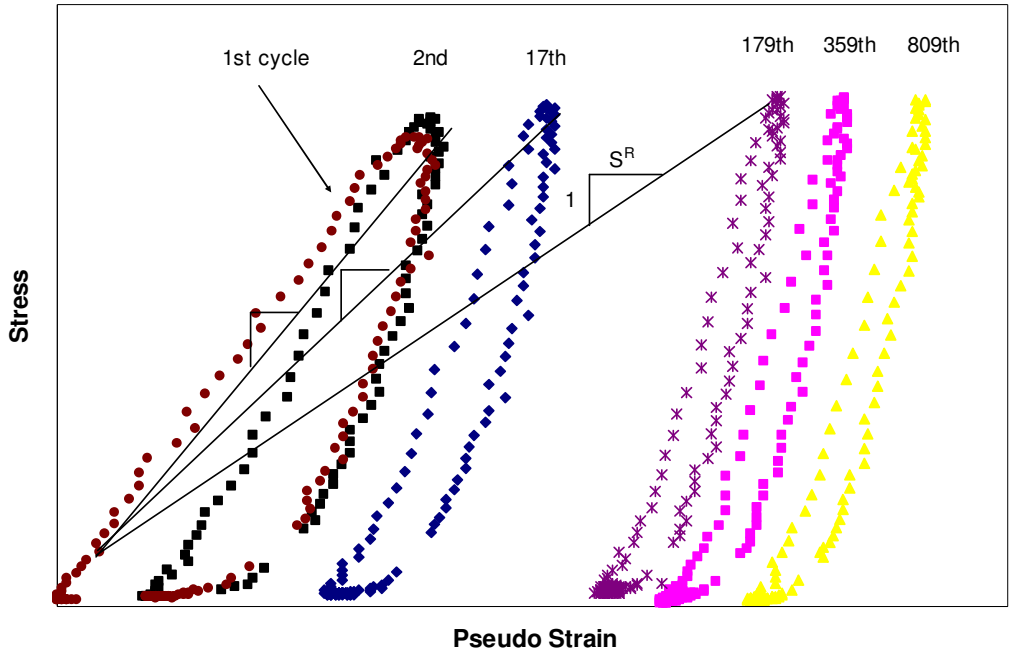

Figure 2.6. Stress-Pseudo Strain Plot and Pseudo Stiffness Changes with Increasing Loading Cycles in Controlled-Stress.

Figure 2.6 shows pseudo stiffness changes by number of cycles as well as stress-pseudo strain hysteresis loops at different loading cycles under controlled-stress mode.

Dissipate Pseudo Strain Energy for Asphalt Concrete Mixture

Schapery (1984) proposed the extended elastic-viscoelastic correspondence principle, which can be applied to both linear and nonlinear viscoelastic materials. The correspondence principle stated that constitutive equations for certain viscoelastic media are identical to those for the elastic cases, but stresses necessarily physical quantities in the viscoelastic body. Instead, they are pseudo variables.

The peak pseudo strain above at a current time t under a constraint strain amplitude ε_0 of cyclic loading can be represented as follows (Lee, 1996):

$$\varepsilon_m^R(t) = \frac{\varepsilon_0}{2}\left[E(t) + \left|E^*\right|\right] \tag{2.28}$$

Where ε_0 = strain amplitude,

$E(t)$ = relaxation modulus, and

$\left|E^*\right|$ = dynamic modulus.

Equation 2.29 having generalized power law and its parameters were determined by performing a 10000 sec creep test on a single specimen. The dynamic modulus also can be calculated with Equations 2.30, 2.31 and 2.32 proposed by Kim et al. (1995).

$$D(t) = D_0 + D_1 t^n \tag{2.29}$$

$$\left|E^*\right| = \frac{1}{\sqrt{(D')^2 + (D'')^2}} \tag{2.30}$$

$$D' = D_0 + D_1\Gamma(n+1)(2\pi f)^{-n}\cos(\frac{n\pi}{2}) \quad (2.31)$$

$$D'' = D_1\Gamma(n+1)(2\pi f)^{-n}\sin(\frac{n\pi}{2}) \quad (2.32)$$

Pseudo strain calculation requires the relaxation modulus test as we can see in Equation 2.28, but the test has large load response as a result of the immediate increase in strain input. A simpler test, therefore, such as creep test is desirable to predict the relaxation modulus for practical purposes. Linear viscoelastic theory allows one to predict the modulus as long as the load level in the creep testing is within the linear range. Kim et al. (1995) suggested a method to predict the relaxation modulus from the calculated creep compliance $D'(t) = D_1 \times t^{n'}$ in creep test as shown in Equation 2.33.

$$E(t) = \frac{1}{D'(t)} \cdot \frac{\sin(n'\pi)}{n'\pi} \quad (2.33)$$

It is possible to calculate pseudo strain energy for the asphalt concrete mixture using Equation 2.22 after getting the pseudo stiffness from the asphalt concrete mixture by Equation 2.19, and Equation 2.29 to Equation 2.33.

Dissipated Pseudo Strain Energy for Sand Asphalt

Schapery (1984) defined elastic-viscoelastic correspondence principle and it is applied to torsional shear pseudo strain:

$$\gamma^R \equiv \frac{1}{G_R}\int_0^t G(t-\xi)\frac{\partial \gamma}{\partial \xi}d\xi \tag{2.34}$$

Where γ^R = pseudo strain in the shear mode,

G_R = reference shear modulus that is an arbitrary constant,

$G(t)$ = shear relaxation modulus, and

γ = time-dependent shear strain.

Kim et al. (1994 and 1995) introduced pseudo stiffness (S^R) as shown in Equation 2.19, and which was modified for torsional stress mode:

$$S^R = \frac{\tau_m}{\gamma_m{}^R} \tag{2.35}$$

Where S^R = pseudo stiffness,

$\gamma_m{}^R$ = peak pseudo strain in each physical stress-pseudo strain cycle, and

τ_m = physical stress corresponding to $\gamma_m{}^R$.

The analytical harmonic representation of the shear strain component at time t under the zero mean cyclic strain condition can be expressed as:

$$\gamma(t) = \gamma_0 \sin(\omega t + \theta) H(t) \tag{2.36}$$

Where γ_0 = shear strain amplitude,

ω = angular velocity,

θ = regression constant, and

$H(t)$ = Heaviside step function.

Kim et al. (2002) replaced the pseudo strain in Equation 2.34 by Equation 2.36 and it yields the respective pseudo strain at time, t as:

$$\gamma^R(t) = \frac{1}{G_R}[\gamma_0 \left|G^*\right| \sin(\omega t + \theta + \phi)] \tag{2.39}$$

Where $\left|G^*\right|$ = linear viscoelastic dynamic modulus in shear mode, and

ϕ = linear viscoelastic phase angle.

Therefore, Equation 2.37 is used for Equation 2.27 which makes it possible to calculate the DPSE in the sand asphalt with torsional stress mode loading. Figures 2.7 and 2.8 which illustrate the parameters θ and ϕ. As shown in Figure 2.7, the parameter θ represents the time lag between the real strain and ideal strain. In Figure 2.8, the parameter ϕ also can be defined as the time lag between the applied stress and the resulting strain.

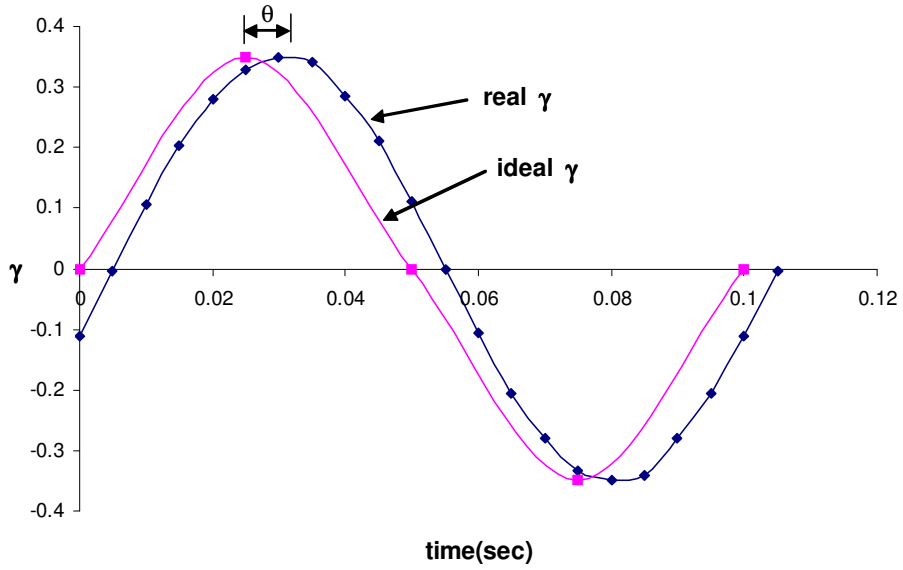

Figure 2.7. Graph for θ.

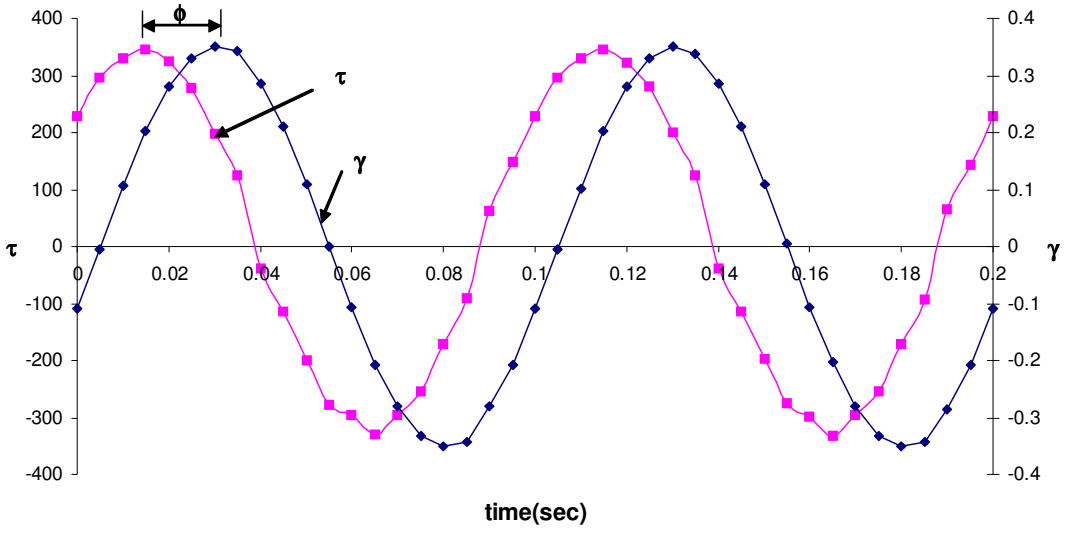

Figure 2.8. Graph for ϕ.

CHAPTER III

FATIGUE CRACKING

Fatigue cracking due to repeated traffic loading is one of the major distresses in asphalt concrete pavements. Perzyna (1984) proposed three mechanisms of the nucleation, the growth, and the transport of voids that drive the damage in the material. Similarly, Kim et al. (1997) introduced fatigue crack mechanism that starts from microcracks and later propagate, densify, and coalesce due to tensile or shear stress or combinations of both to form macrocracks.

Either controlled-stress method when a constant stress amplitude is applied, or controlled-strain when a constant strain amplitude is applied is selected for general fatigue tests. Also, applying a constant stress amplitude appears to be good for thick asphalt pavements under repetitive loading, while the controlled-strain method is suitable for thin pavements (Yoder 1975, Tangella 1990, and Tayebali 1994). Kim et al. (2002) used DMA in their study with cylindrical sand asphalt mixtures to characterize fatigue damage and healing effects during controlled-strain, torsional testing at the temperature of 25 °C.

The energy approach has been used for predicting fatigue behavior and life of the asphalt mixtures. In this research, DPSE concept was applied for damage analysis of the asphalt mixtures.

THE FIRST AND SECOND INFLECTION POINT

The first inflection point (FIP) defines a decreasing rate of change in stiffness associated with microcracking in the sample. The second inflection point (SIP) also infers a mechanical behavioral change possibly associated with the macrocracking. A transition point between the two inflection points represents the shift from microcracking to macrocracking. The rate of stiffness reduction abruptly increases at this transition point. As Rowe and Bouldin (2000) skillfully proposed, the meaning of the transition point can be explained mathematically using the Taylor's series expansion.

$$E^* = E_o^* + n\frac{dE^*}{dn} + \frac{n^2}{2!}\frac{d^2E^*}{dn^2} + \frac{n^3}{3!}\frac{d^3E^*}{dn^3} + ... \tag{3.1}$$

$$E^* n = E_o^* n + n^2\frac{dE^*}{dn} + \frac{n^3}{2!}\frac{d^2E^*}{dn^2} + \frac{n^4}{3!}\frac{d^3E^*}{dn^3} + ... \tag{3.2}$$

Where E^* = stiffness or modulus,

E_o^* = initial stiffness or modulus, and

n = number of load cycles.

THEORY OF VISCOELASTICITY

Schapery (1984) suggested the extended elastic-viscoelastic correspondence principle applicable for both linear and nonlinear viscoelastic materials and proposed pseudo strain equations as calculated linear viscoelastic stress divided by a reference modulus.

$$\varepsilon_{ij}^{R} = \frac{1}{E_R}\int_0^t E(t-\tau)\frac{\partial \varepsilon_{ij}}{\partial \tau}d\tau \tag{3.3}$$

$$\sigma_{ij}^{R} = E_R\int_0^t D(t-\tau)\frac{\partial \sigma_{ij}}{\partial \tau}d\tau \tag{3.4}$$

Where σ_{ij}, ε_{ij} = physical stresses and physical strains,

σ_{ij}^{R}, ε_{ij}^{R} = pseudo stresses and pseudo strains,

E_R = reference modulus that is an arbitary constant, and

$E(t)$, $D(t)$ = relaxation modulus and creep compliance, respectively.

Stress-strain relationship for linear viscoelastic materials is expressed as:

$$\sigma = \int_0^t E(t-\tau)\frac{\partial \varepsilon}{\partial \tau}d\tau \tag{3.5}$$

Equation 3.5 is presented by using Equation 3.3 as:

$$\sigma_{ij}^{R} = E_R\varepsilon^{R} \tag{3.6}$$

Where $\varepsilon^{R} = \frac{1}{E_R}\int_0^t E(t-\tau)\frac{\partial \varepsilon}{\partial \tau}d\tau$.

Kim et al. (2002) extended the above equations for torsional shear pseudo strain such that:

$$\tau_{LVE}(t) = \int_0^t G(t-\xi)\frac{\partial \gamma}{\partial \xi} d\xi \tag{3.7}$$

$$\tau_{LVE}(t) = G_R \gamma^R \tag{3.8}$$

Where $\gamma^R \equiv \frac{1}{G_R}\int_0^t G(t-\xi)\frac{\partial \gamma}{\partial \xi} d\xi$,

$\tau_{LVE}(t)$ = calculated linear viscoelastic stress,

ξ = time history at which strains were measured,

γ^R = pseudo strain in the shear mode,

G_R = reference shear modulus that is an arbitrary constant,

$G(t)$ = shear relaxation modulus, and

γ = time-dependent shear strain.

The analytical harmonic representation of the shear strain component at time t under the zero mean cyclic strain condition can be expressed as:

$$\gamma(t) = \gamma_0 sin(\omega i + \theta)H(t) \tag{3.9}$$

Where γ_0 = shear strain amplitude,

ω = angular velocity,

θ = regression constant, and

$H(t)$ = Heaviside step function.

Pseudo strain defined in Equation 3.8 is replaced by Equation 3.9 yields the Equation 3.10 for pseudo strain at time t as follows:

$$\gamma^{R}(t) = \frac{1}{G_R}\left[\gamma_0 \left|G^*\right| sin(\omega i + \theta + \phi)\right] \tag{3.10}$$

Where $\left|G^*\right|$ = linear viscoelastic dynamic modulus in shear mode, and

ϕ = linear viscoelastic phase angle.

Equation 3.10 can be rewritten by assuming the value of G_R to be unity and it becomes Equation 3.11.

$$\gamma_m^R = \gamma_0 \left|G^*\right| \tag{3.11}$$

Where γ_m^R = peak pseudo strain in each cycle.

Therefore, linear viscoelastic dynamic modulus $\left|G^*\right|$ and strain amplitude are the only ones to calculate the peak pseudo strain at any loading cycle.

Generally, the complex modulus of a viscoelastic material is composed of a storage (elastic) modulus and a loss (viscous) modulus. Therefore, the dynamic modulus is defined by Equation 3.12 in terms of measuring the values of peak stress and peak strain amplitude or storage and loss modulus when a repeated cyclic test is performed.

$$\left|G^*\right| = \frac{\tau_o}{\gamma_o} = \sqrt{\left(G'\right)^2 + \left(G''\right)^2} \tag{3.12}$$

Where τ_o, γ_o = peak stress and strain amplitude at each cycle, respectively,

G' = storage modulus, and

G'' = loss modulus.

The phase angle due to time lag between stress and strain can be easily expressed as:

$$\phi = tan^{-1}\left(\frac{G''}{G'}\right) \tag{3.13}$$

In this approach, only the peak pseudo strain within each cycle is typically used. The pseudo strain reaches the peak when the sine function in Equation 3.10 becomes 1. Linear viscoelastic material properties such as the linear viscoelastic dynamic modulus and the phase angle are usually determined by means of a dynamic frequency sweep test. In addition, the peak pseudo strain in Equation 3.11 is equal to the maximum stress in Equation 3.12 in the linear viscoelastic region for G_R = 1.

Equation 3.14 represents the static relaxation modulus by which is calculated the linear viscoelastic modulus.

$$G(t) = G_{\infty} + G_1 t^{-n} \tag{3.14}$$

Where $G(t)$ = shear relaxation modulus,

G_{∞} = long-time equilibrium modulus,

G_1 = regression constant, and

n = regression constant representing the slope between modulus and time.

The storage and loss modulus in frequency domain can be calculated as:

$$G'(\omega) = G_{\infty} + G_1 \Gamma(1-n)\omega^n cos(\frac{n\pi}{2}) \tag{3.15}$$

$$G''(\omega) = G_1 \Gamma(1-n)\omega^n sin(\frac{n\pi}{2}) \tag{3.16}$$

Where Γ = gamma function.

The linear viscoelastic dynamic shear modulus is easily determined by using Equations 3.12, 3.15, and 3.16.

CHAPTER IV

PERMANENT DEFORMATION

Rutting is defined as a surface depression in the wheel paths (Huang 1993). It stems from the small amount of permanent deformation in any of the pavement layers and/or the subgrade. Accumulation of the small deformation during each time a load is applied is developed as a pavement distress. Rutting is considered one of the most significant distresses that can cause severe damage in asphalt concrete pavements, along with fatigue cracking, low-temperature cracking, and moisture damage. The distress decreases the pavement service life and causes safety problems such as hydroplaning from entrapped water following deformed wheel paths. Water also can penetrate into the unbound base and then failure is accelerated due to excessive water. Therefore, it has long been a problem in hot mix asphalt (HMA) pavement. Through the years, researchers have used different kinds of fundamental, empirical and simulative test methods to estimate the rutting performance of HMA. Permanent deformation characterized by appropriate methodologies can help us to improve pavement performance.

In fundamental tests, unconfined and confined cylindrical specimens in creep, repeated, or dynamic loading; cylindrical specimens in diametral creep or repeated loading; and Superpave shear tester (SST) repeated shear at constant height (RSCH); shear modulus; quasi-direct shear; and shear strength tests have been used. In empirical tests, Marshall and Hveem tests were used. In simulative tests, Georgia loaded wheel

tester, asphalt pavement analyzer (APA), Hamburger wheel tracking device (HWTD), Laboratoire Central des Ponts et Chaussees (Paris) wheel tracker, Purdue University laboratory wheel tracking device, Nottingham pavement testing facility, and model mobile load simulator are being used (Sousa et al. 1991, TRC E-C016 2000).

A lot of wheel tracking test devices like APA and HWTD have been developed and used for simulating field conditions in laboratories. Recently a couple of studies gave some absolute values and acceptable rut depth criteria generated from wheel tracking devices (Wang et al. 2002; Kandhal and Mallick 1999, Shami et al. 1997), but there are no current methods to explain rutting development in the laboratory tests.

The APA has shown some promise results as a rut testing equipment (Shami et al. 1997). Testing with the APA will be conducted according to the procedure recommended by the Georgia Department of Transportation test method GDT-115. Hose pressure and wheel load will be 690 kPa and 445 N will be carried out to 8,000 cycles and rut depth measured continuously. A cylindrical sample 100 mm diameter by 150 mm from a Superpave gyratory compactor is subjected to a static axial load for creep and strength tests. The tests are performed with several different confining pressures.

LABORATORY PERMANENT DEFORMATION TESTS

Repeated Shear at Constant Height (RSCH)

The RSCH test with SST is used to evaluate rutting resistance of HMA mixtures for the Superpave volumetric analysis system. The RSCH is a good tool to compare empirically two or more samples. The test is generally used for Superpave performance

tester. It is used to estimate relative rutting performance (Sousa 1995). A haversine shear load is applied to a HMA specimen. A standardized method for the test is introduced in AASHTO TP7 procedure F.

Hamburg Wheel Tracking Device (HWTD)

The HWTD developed in Germany and has been used for evaluating rutting and stripping of pavements. It carried out 20,000 passes with a steel wheel rolls across the surface of HMA specimens and rut depth measured continuously.

Asphalt Pavement Analyzer (APA)

As described in Chapter VII, the APA is an automated, new generation Georgia load wheel tester. The standardized method is the Georgia Department of Transportation test method GDT-115. In general, hose pressure is 690 kPa. One set of back and forth movement is considered one cycle and 8,000 cycles are performed with measuring rut depth continuously. There have been a number of studies to match the APA test results to field data or other laboratory tests such as Kandhal and Mallick (1999). They presented fair correlations between permanent deformation from APA and from RSCH conducted with the Superpave shear tester.

RUTTING PREDICTION

Permanent strain deformation in HWTD and RSCH test results are expected by following two equations (Wang et al. 2002).

$$\varepsilon^p(N) = \varepsilon^p(L) + a\log N \tag{4.1}$$

$$\log\varepsilon^p(N) = \log\varepsilon^p(L) + b\log N \tag{4.2}$$

Where $\varepsilon^p(N)$ = permanent strain accumulated during N load applications, and

$\varepsilon^p(L)$, a, b = material constant.

Following Equations 4.3 and 4.4 are SHRP A-003A rut depth prediction model (Sousa 1995).

$$RD = 280 \times \varepsilon_m^p \tag{4.3}$$

Where RD = rut depth (mm), and

ε_m^p = maximum permanent shear strain.

$$\log(cycles) = -4.36 + 1.24\log(ESALs) \tag{4.4}$$

Asphalt Institute (1982) proposed the failure criteria for rutting by following equation.

$$N_d = 1.365 \times 10^{-9}(\varepsilon_c)^{-4.477} \tag{4.5}$$

Where N_d = allowable number of load repetitions to limit permanent deformation, and

ε_c = compressive strain at top of subgrade.

Generally, the creep test appears to be useful to estimate rutting potential in asphalt mixtures. The creep test data were also used by Finn et al. (1983) with the same form of the equation suggested by Shell researchers for expecting permanent deformation.

$$\Delta h_{1-i} = C_{m-1} \times h_{1-i} \times \frac{\sigma_{avs}}{S_{mix}} \tag{4.6}$$

Where Δh_{1-i} = change in layer thickness,

h_{1-i} = layer thickness,

h_{1-i} = average vertical compressive stress,

S_{mix} = creep modulus at particular time of loading and temperature, and

C_{m-i} = correction factor.

Kandhal and Mallick (1999) used granite, gravel and limestone mixes and measured rutting in APA to correlate with the film thickness. They found that granite and limestone mixes tend to have more rutting with film thickness increase, for gravel the rutting decreased with film thickness increase.

$$RD = 2.53 + 0.035 \times (D_f)^2 \tag{4.7}$$

Where D_f = film thickness (mm).

A relation for binder courses with granite and limestone is presented as:

$$RD = 37.05 - 6.137(D_f) + 0.2754 \times (D_f)^2 \quad (4.8)$$

For wearing gravel courses, the best relation was found to be:

$$RD = 19.39 - 14.017 \log_{10}(D_f) \quad (4.9)$$

Shami et al. (1997) introduced a temperature-effect model based on APA test results as presented in Equation 4.10 in terms of given test temperature and a given number of cycles.

$$\left(\frac{R}{R_0}\right) = \left(\frac{T}{T_0}\right)^{2.625} \left(\frac{N}{N_0}\right)^{0.276} \quad (4.10)$$

Where R = predicted rut depth,

R_0 = reference rut depth obtained at reference test conditions T_0 and N_0,

T, N = temperature and number of load cycles at the rut depth sought, and

T_0, N_0 = reference temperature and load cycles at R_0.

Brown and Bell (1977, 1979) compared rut depth results between theoretical prediction and measured values in the Nottingham Test Track. The comparisons between them indicated reasonable agreement.

Another rutting prediction model was presented by Kirwan et al. (1977). The model used layer-strain approach and a nonlinear finite element computer program. In-place rutting is somewhat less than expected value from the model.

The layer-strain method for predicting deformation was also used by Monismith et al. (1977). In the paper, he used material properties from repeated load triaxial test and the elastic computer program ELSYS was used to calculate pavement deformation.

CHAPTER V

IMAGE ANALYSIS

Digital image analysis can be defined that converting pictures into a digital form and extracting some information from the pictures by means of various mathematical procedures. This information may be characteristic of cracks or any damage on a pavement surface area. In this research, asphalt concrete mixture and sand asphalt specimens representing asphalt pavement surface area were used to get pictures for damage parameters.

The advent of computer imaging technology and nondestructive techniques has made it possible to characterize engineering materials based on the distribution of its internal structure (Denison et al. 1997, Masad et al. 1999a and b). Digital image analysis has been used to study asphalt concrete structure quantitatively. Eriksen and Wegen (1993) conducted microscopic analysis of air voids in asphalt concrete mixtures at the Danish Road Institute. Coarse aggregates in asphalt concrete mixture were analyzed using image analysis by Yue et al. (1995).

An image analysis technique is generally consist of three major steps such as image acquisition, image processing and image analysis as shown in Figure 5.1.

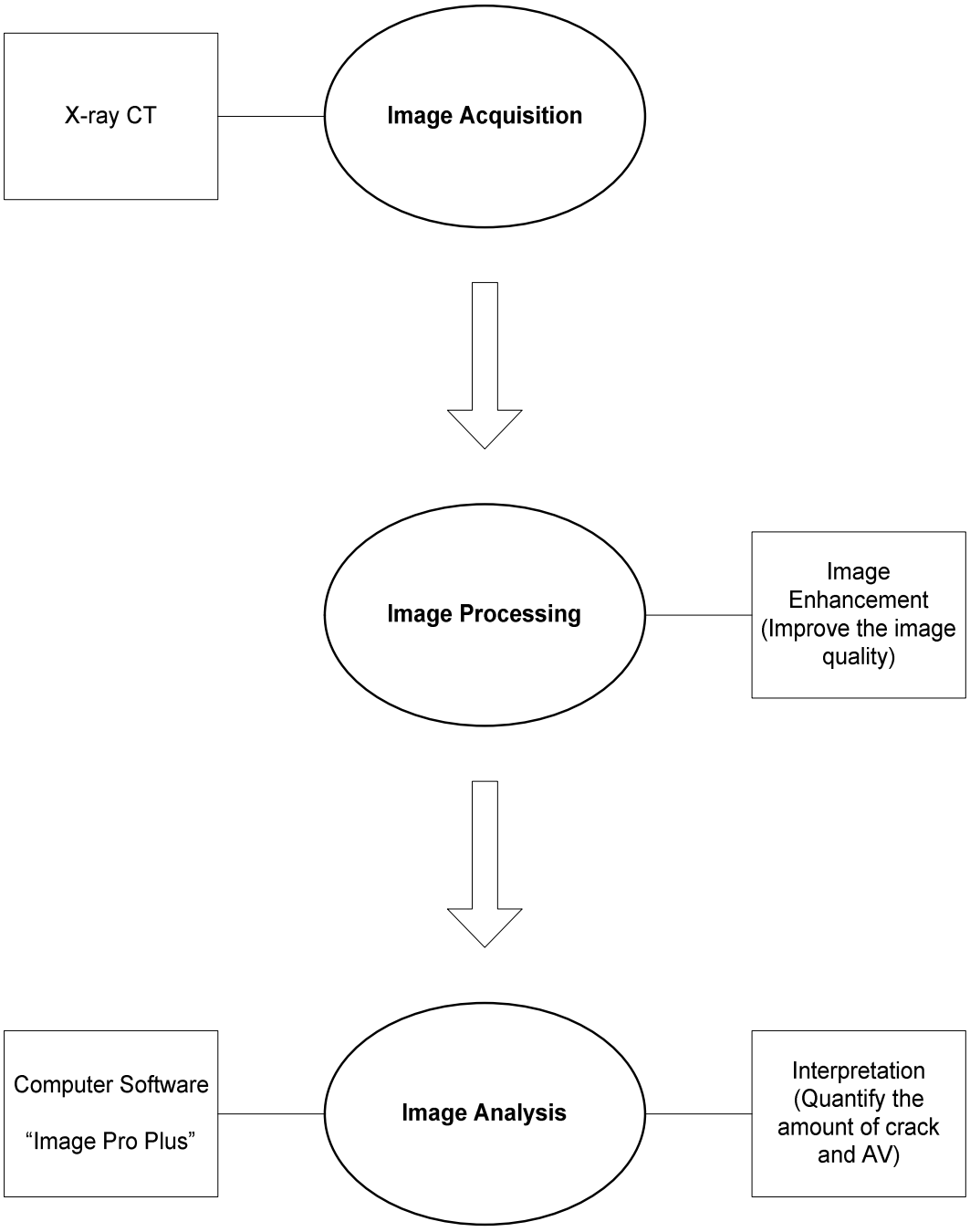

Figure 5.1. Three Major Steps Consisting Image Analysis Technique.

It is well established that air voids play an important role in determining resistance of asphalt mixtures to major pavement distress including rutting, fatigue cracking, and low-temperature cracking (Monismith 1992). Air voids and cracks determine damage parameter values in asphalt mix specimens. Using X-ray CT system along with digital image analysis techniques, air voids and cracks are detected for damage parameters in the asphalt mix specimens. X-ray CT imaging has been used increasingly in civil engineering material research in recent years and it is a completely nondestructive technique for visualizing features in the interior of opaque solid objects to obtain digital information on their three-dimensional (3-D) geometry and properties (Denison et al. 1997). In the meanwhile, X-ray CT method can be performed with the sample before or after destructive test since it is a nondestructive test. Therefore, X-ray CT is the most effective method for destructive micro and macro-property tests such as fatigue or rutting and it can be used to study the relationship between microstructure and macro-property.

X-ray CT system consists of a source and a detector with the test specimen placed in between as shown in Figure 5.2. The source transmits X-ray radiation with certain intensity. As X-rays penetrate through a specimen, part of the radiation gets absorbed, part of it gets scattered, while the remaining part penetrates through the specimen. The intensities of these transmitted X-rays are recorded with an array of detectors placed at the other side of the specimen. X-rays passing through the specimen along several different paths in several different directions produce the set of CT images.

Scanning of a slice is complete after collecting the intensity measurements for a full rotation of the specimen and then it is shifted vertically by a fixed amount.

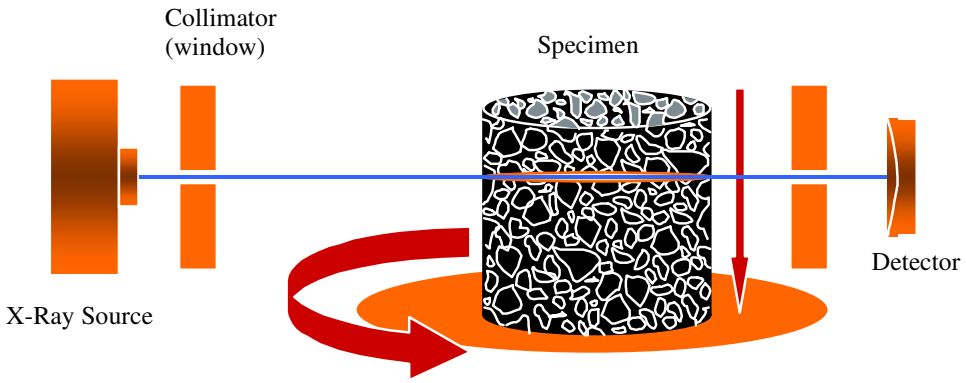

Figure 5.2. Components of X-ray CT System (Masad et al. 2002).

Digital images were captured to measure air void and crack size at different depths with asphalt mix specimens. Horizontal slices of sand asphalt specimens were captured every 0.03148 mm and those of HMA were 1 mm without offset. The captured images were saved in TIFF. As shown in Figure 5.3, two types of cylindrical samples with dimension of 100 mm × 150 mm for asphalt mixture and 12 mm × 50 mm for sand asphalt were used. The analysis did not include the top and bottom 22.5 mm of a mixture

and sand asphalt specimen to exclude the effect of surface voids on the distribution and the defections caused by experimental errors.

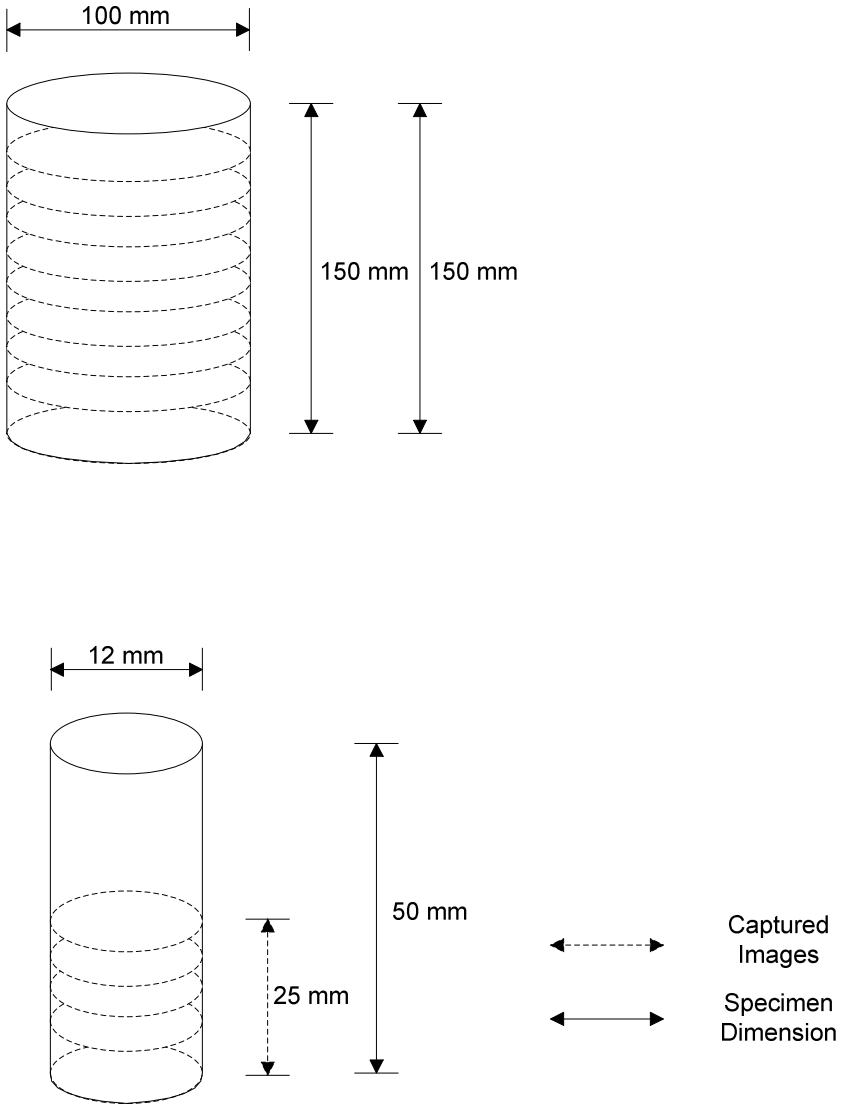

Figure 5.3. Configurations of Two Specimens for Image Analysis.

The image analysis technique was used in this research to identify and quantify air voids and cracks which are based on analyzing gray images. The captured images from X-ray CT system were used to identify air voids and cracks within the specimen. As presented in Figure 5.4, air voids and cracks are shown in black and aggregates are white. In order to identify air voids which have low density, a threshold gray intensity must be determined. The gray intensity measured on a given point may be higher or lower than this threshold. Accordingly, the point is assigned to be either part of the air void, cracking, asphalt binder or aggregate. Image analysis software, Image Pro Plus (1998), was used for the procedure. The software has a built in language, Image Pro Basic (IPBasic): IPBASIC is the interpreter built into Image Pro Plus.

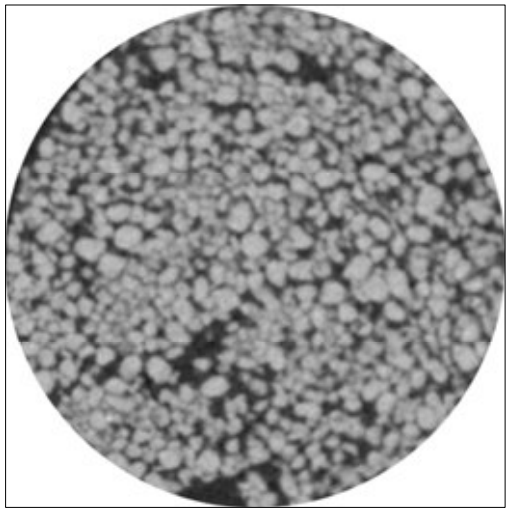

Figure 5.4. Gray-Scale Image of Sand Asphalt Sample from X-ray CT.

Following the settings as described in Chapter VII, dynamic creep test with asphalt mixture and DMA with sand asphalt were conducted to calculate the damage parameters from the image analysis. Four points were selected from the two tests based on each performance behavior. The last point means the starting point of tertiary flow in dynamic creep test and the SIP in DMA test. The second and the third point are determined after deciding the last point in each performance graph plot. The second is one third of initial point of tertiary flow or FIP of the DMA result. The first point represents a specimen having undamaged condition. Two replicates at each point with two conditions of dry and wet were scanned. Therefore, 16 samples each test for a total number of 32 were analyzed. Figure 5.5 briefly shows the selected four points at each dynamic test.

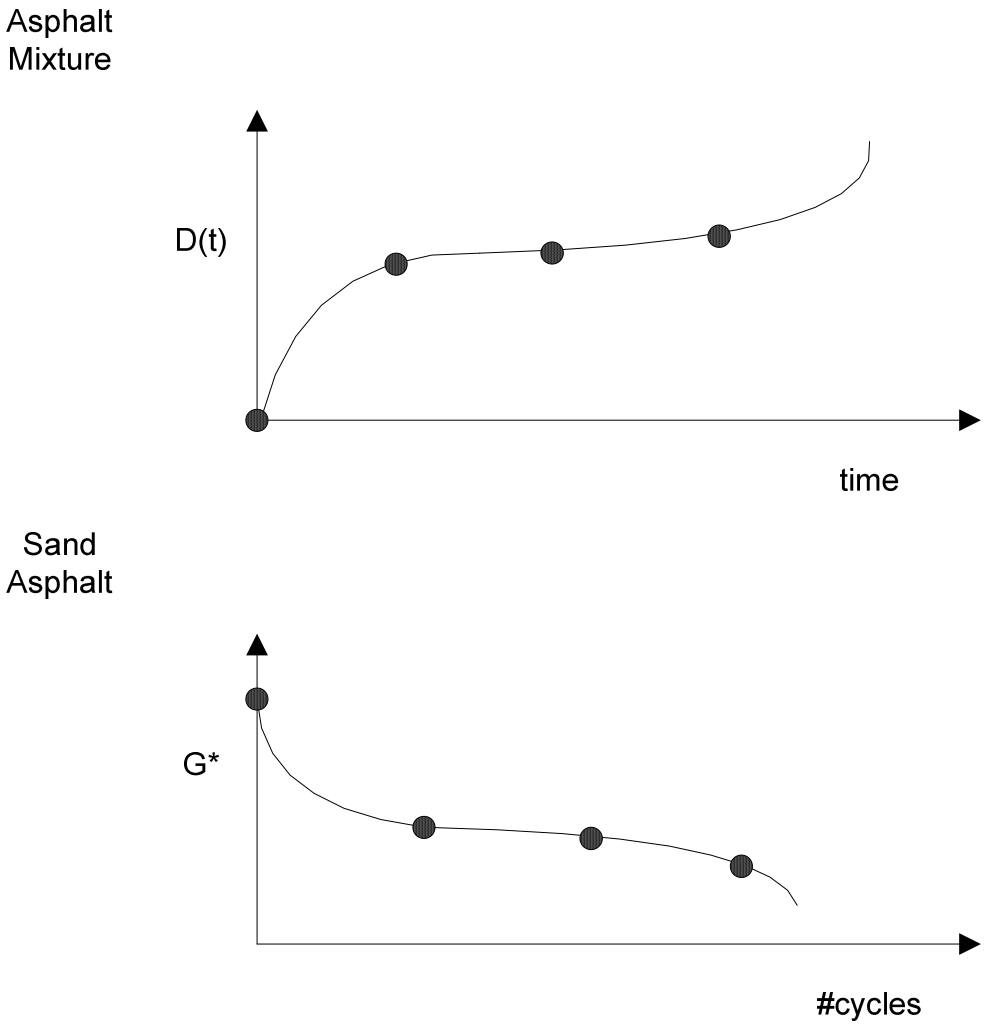

Figure 5.5. Typical Test Results from Creep and DMA test and Selected Four Points for Digital Image Analysis.

CHAPTER VI

THEORETICAL METHODOLOGY

TWO CRITICAL POINTS FROM LABORATORY TESTS

Permanent deformation is composed of two different mechanisms (Roberts et al. 1996, Lee et al. 2000b): densification and repetitive shear deformation. The densification occurs at the early stage of cyclic loading, while the shear deformation is a long-term process. Tseng et al. (1989), Lytton (2000) and Bhairampally (1998) showed that permanent deformation relates to microcracking and defined a transition point where microcracking starts. Mohammad et al. (2000) and Wang et al. (2002) introduced three stages of rutting performance in their laboratory wheel tracking tests. Si (2001) also described the mechanism of microcracks and permanent deformation in his dissertation. When an asphalt concrete is subjected to repeated loading, it hardens with accumulating plastic deformation. If there is no microcrack arrestor, nor the material heals rapidly, it will reach a point where it is stiff enough for microcracks to initiate and grow. The asphalt concrete starts accumulating more plastic deformation after beginning of microcracks, where is commonly called “tertiary flow”.

Fatigue in asphalt mixes is generally consisting of three states, those are crack initiation, crack propagation, and disintegration. The first step is crack initiation in which microcracks are developed and followed by crack propagation which shows the development of macrocracks out of microcracks resulting in stable crack growth. The last state is disintegration which represents the collapse and final failure of the materials

because of unstable crack growth (Jacobs 1995). Little and Kim (2002) also suggested that microcracking is associated with both fatigue cracking damage and the accumulation of permanent damage (rutting) under repeated loading. As Rowe and Bouldin (2000) also showed a typical fatigue behavior with classified performance regions as shown in Figure 6.1, Kim et al. (2002) suggested two regions with transition point. Little and Kim (2002) used DMA to evaluate microcraking damage potential in sand asphalt mixtures. Microcracking has been shown to be associated with the permanent damage as well as fatigue cracking.

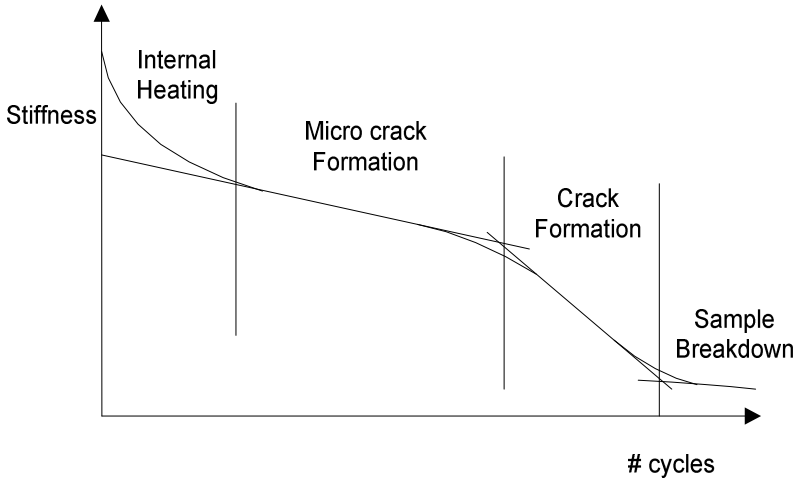

Figure 6.1 Regions of Fatigue Behavior (redrawn from Rowe and Bouldin 2000).

Generally, both permanent deformation and fatigue cracking can be evaluated by the ratio of predicted number of load repetition (n_{ij}) to allowable number of load

repetitions (N_{ij}) and damage ratio of end of year is defined by its summation as shown in Equation 6.1 (Huang 1993).

$$D_r = \sum_{i=1}^{p} \sum_{j=1}^{m} \frac{n_{ij}}{N_{ij}} \tag{6.1}$$

Where D_r = damage ratio at end of year,

n_{ij} = predicted number of load repetitions for load j in period i,

N_{ij} = allowable number of load repetitions,

p = number of periods in each year, and

m = number of load groups.

Since the prediction of load repetitions for the both two distresses is deeply related to the damage ratio that is the life of pavement, a lot of researches have been done to expect it by means of developing theoretical or empirical models from laboratory tests such as wheel tracking or creep test. After reviewing their models and how they were developed, we can propose methodologies to relate HMA pavement performance with damage parameters.

Permanent Deformation Prediction in Terms of the Two Critical Points

A method for predicting deformation in the asphalt concrete surface area of a road is described. The method is based on an analysis of the stiffness behavior of the HMA, the stiffness values of the bituminous samples being derived from a static creep, APA, and DMA test. Under compressive loading conditions of a simple wheel tracking test to the torsional shear stress in strain controlled DMA test, the correlation among the three lab tests was able to predict the permanent deformation of HMA mixtures. The FIP and SIP were introduced and used as two critical points to predict permanent deformation.

As described earlier, three sample sizes were used depending on their final use. Figure 6.2 shows geometric configurations of the asphalt mixtures and sand asphalt which were fabricated for the three tests.

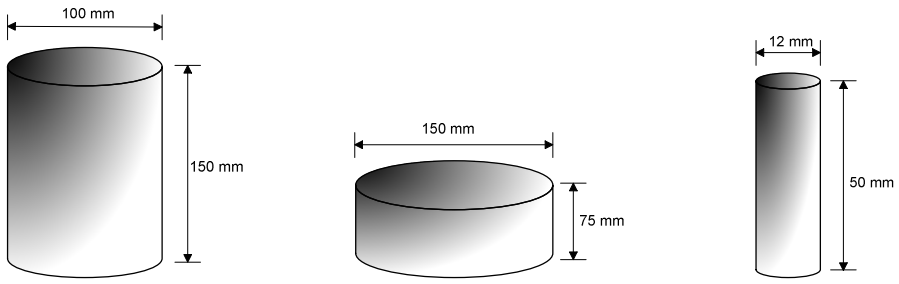

(a) Creep (b) APA (c) DMA

Figure 6.2. Sample Configuration for the Creep, APA, and DMA Test.

Detailed setups and materials for the laboratory tests which were used in this chapter are described in Chapter VII.

1. Stiffness Calculation

Stiffness or modulus of asphalt mixtures has been used for characterizing major distresses. Monismith and Tayebali (1988) considered stiffness for characterizing asphalt concrete pavement section and proposed stiffness with different traffic conditions as shown in Table 6.1.

Table 6.1. Proposed Stiffness Moduli for Austrian Traffic Conditions (Monismith and Tayebali 1988).

S_{mix} (MN/m^2)	Traffic Category
20-30	Minor traffic
30-45	Medium-heavy traffic
45	Extensive traffic

Calculating stiffness modulus allows the results of the three tests to be compared directly by plotting each data at two inflection points. In general, creep test result can

shows three major zones such as primary, secondary, and tertiary. DMA result also has two inflection points in the data plotting of dynamic shear modulus (G*) against number of cycles. On both tests, two inflection points of FIP and SIP are observed. The FIP and the SIP define a decreasing rate of changes in stiffness.

APA has been used for comparing permanent deformation susceptibility and shown good comparisons among the wheel tracking machines. The machine, however, doesn't have any mechanical properties in the result so it rarely used for mechanical analysis as creep test did. By means of direct comparison among the three tests, the correlations were found and used to predict permanent deformation in rutting test. DMA adopted to expect SIP in APA result and the prediction was validated in terms of creep test. Figure 6.3 shows measured stiffness from HMA and sand asphalt with APA result.

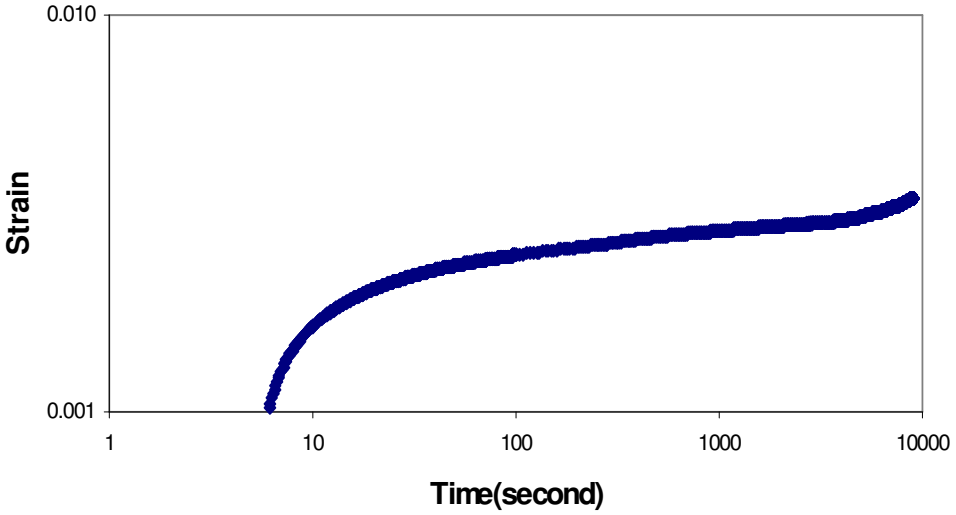

(a)

Figure 6.3. Measured HMA Stiffness from (a) Static Creep Test, (b) DMA and (c) APA result.

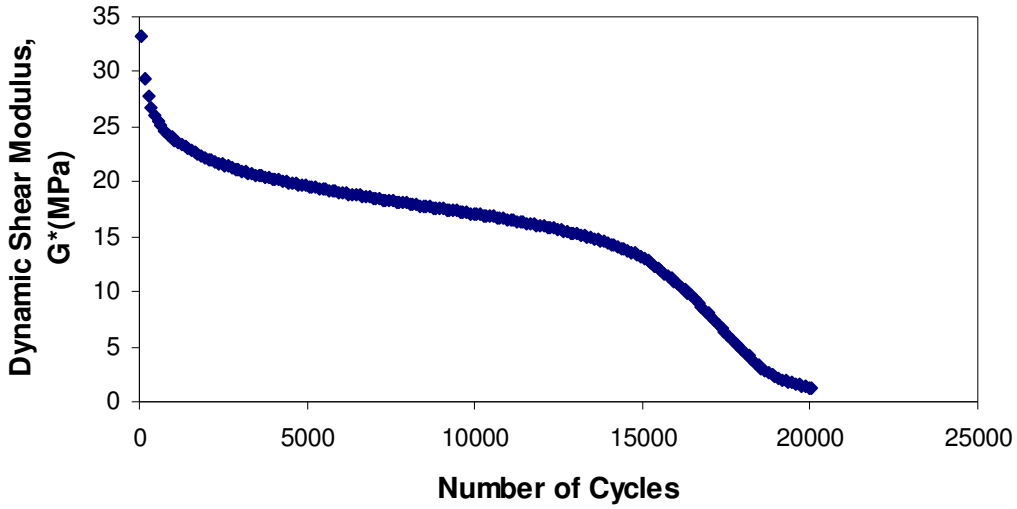

(b)

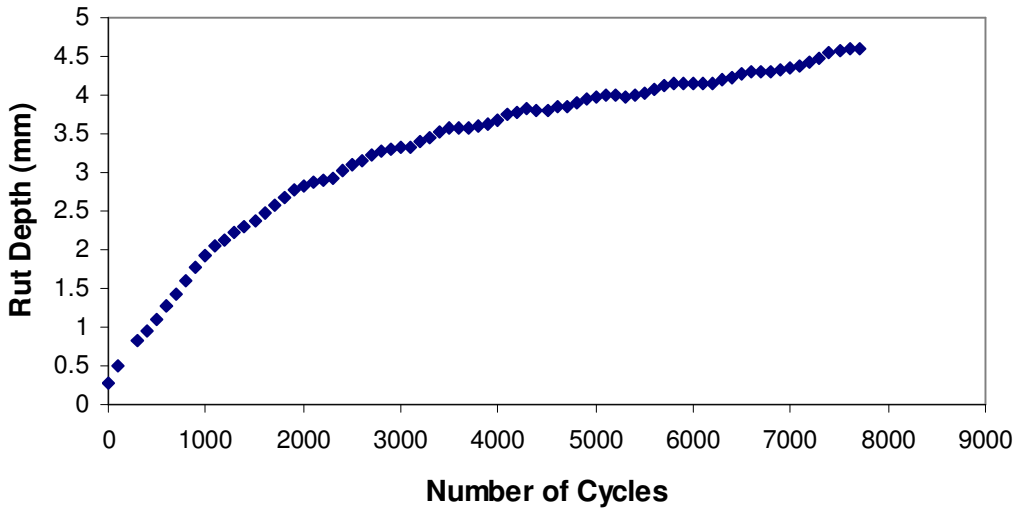

(c)

Figure 6.3. Continued.

(1) HMA stiffness (S_{mix})

Hills et al. (1974) suggested methods to calculate the stiffness of mixtures in creep and rutting test such as APA. In the creep test the strain (ε_{mix}) in the mix which is a function of the loading time was measured at a fixed temperature and then mixture stiffness was calculated with constant stress (σ_0) as shown in Equation 6.2.

$$S_{mix} = \frac{\sigma_0}{\varepsilon_{mix}} \tag{6.2}$$

Two graphs plotting the static creep test results as S_{mix} against deformation at two critical points were shown in Figure 6.4.

In general, the vertical surface displacement of an elastic layer on a rigid base, w, is expressed as follows (Ueshita et al. 1968):

$$w = \frac{p}{E} \cdot B \cdot I \tag{6.3}$$

Where p = uniformly distributed pressure on loaded area,

B = width of loaded area,

E = modulus of elasticity of upper layer, and

I = surface displacement influence value which is a function of Poisson's ratio of the upper layer, ratio of thickness T of upper layer to width of loaded area, shape of loaded area, and condition at the interface.

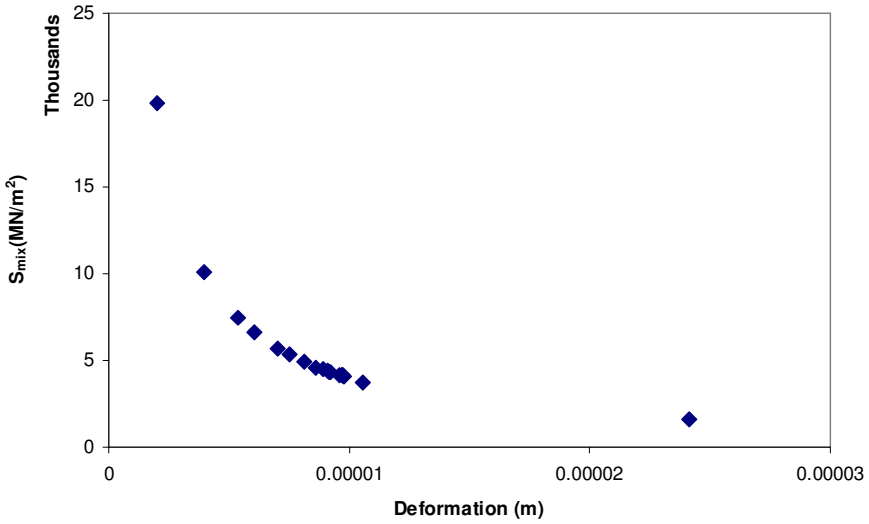

(a)

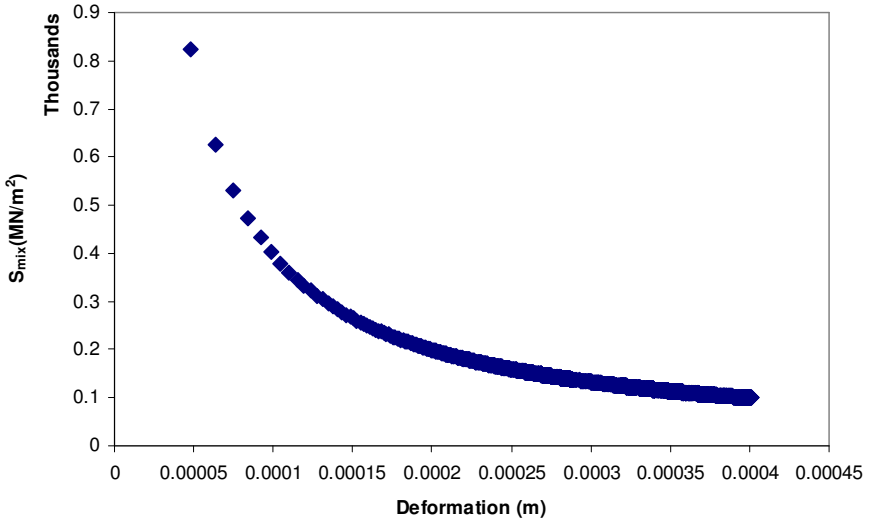

(b)

Figure 6.4. S_{mix} against Deformation in Static Creep Test for Calculating (a) FIP and (b) SIP.

For the laboratory rutting tests, elastic layer model for two layers was used by denoting I_{co} in Equation 6.4 based on the Equation 6.3.

$$I_{co} = \frac{w_{co} \cdot E}{p \cdot T} = f\left(\frac{a}{T}, \frac{E_{\infty}}{E}\right) \tag{6.4}$$

Where I_{co} = the displacement influence value,

w_{co} = the displacement at the center of the loaded area,

E_{∞} = modulus of elasticity of the lowest layer, and

a = the radius of the loaded circular area.

Other symbols are as explained before.

The fundamental assumptions of the APA test are that the two layers are infinite in horizontal direction and the lowest layer is infinite in the vertically downwards direction. Poisson's ratio of the layers υ and υ_{∞} take fixed values of 0.28. Needing numerical values for Equation 6.4, we plotted the equation as a graph of I_{co} against a/T and the results are shown in Figure 6.5. This was done by using ELSYM5 to calculate w_{co}. In the elastic analysis program E_{∞} is 10^4 times of assumed E (241150 MN/m^2) or greater because the cylindrical samples rested on steel base plate for APA tests.

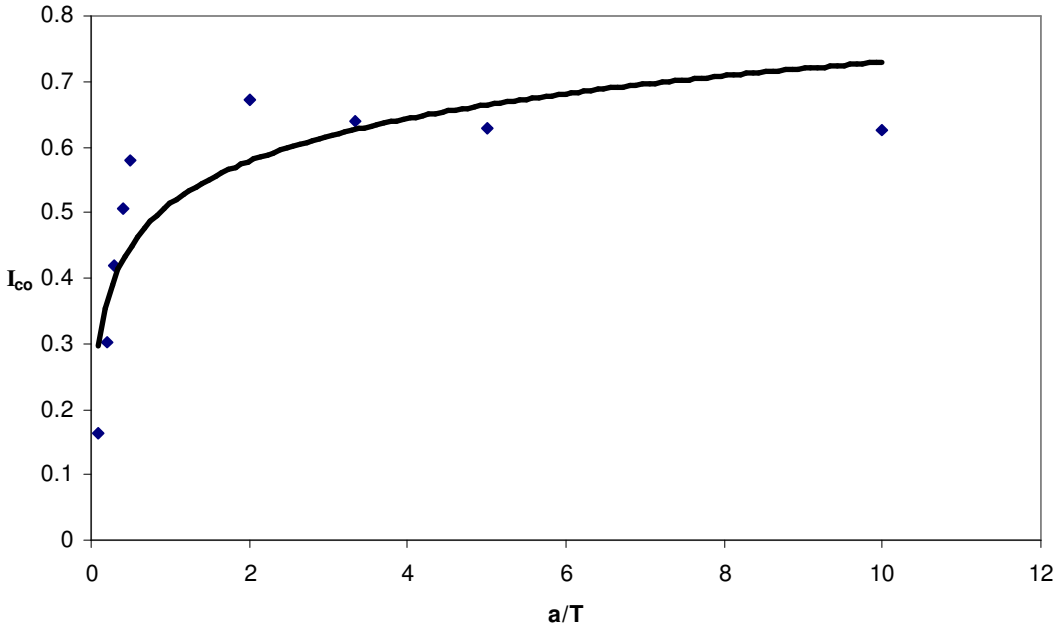

Figure 6.5. The Relationship between I_{co} and a/T Derived from ELSYM5 Analysis.

Substituting E = S_{mix} in Equation 6.4 gives Equation 6.5 as follows:

$$S_{mix} = \frac{I_{co} \cdot p \cdot T}{w_{co}} \tag{6.5}$$

Figure 6.6 plotted calculated stiffness from the Equation 6.5 against rut depth measured by APA.

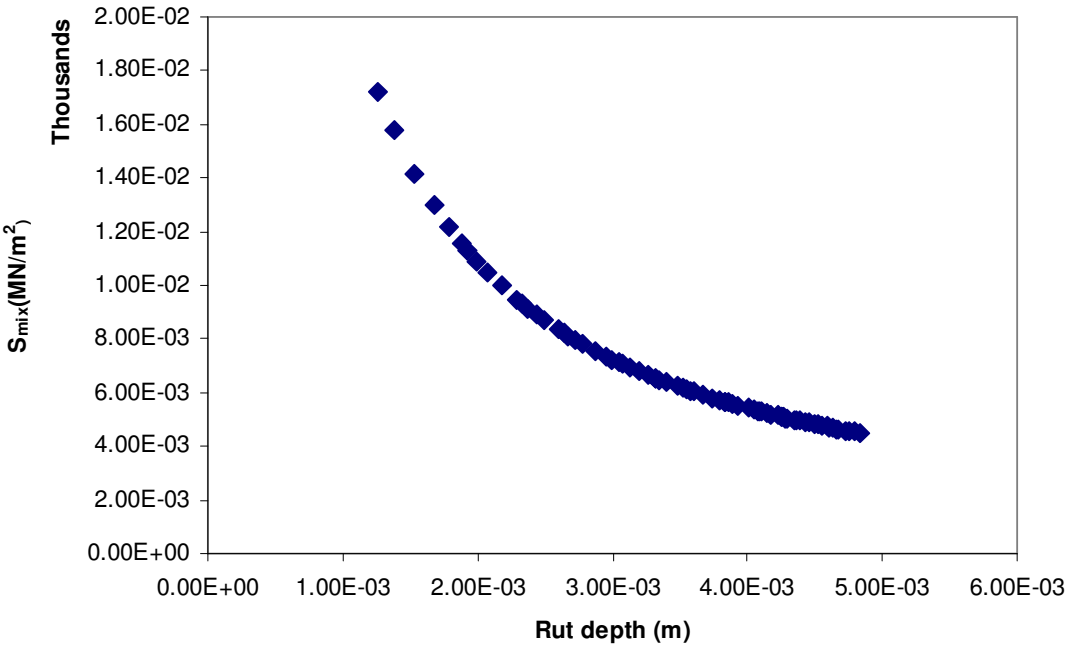

Figure 6.6. S_{mix} versus Rut Depth from APA.

(2) Dynamic Shear Modulus (G*)

As described above, the stiffness from mixture tests such as static creep and APA is calculated to compare with the result from DMA test with sand asphalt.

In repeated cyclic tests, the dynamic modulus is typically determined by monitoring the ratio of the peak stress to the peak strain amplitude or measuring storage and loss modulus:

$$\left|G^*\right| = \frac{\tau_o}{\gamma_o} = \sqrt{\left(G'\right)^2 + \left(G''\right)^2} \qquad (6.6)$$

Where τ_o = peak stress amplitude at each cycle,

γ_o = peak strain amplitude at each cycle,

G' = storage modulus, and

G'' = loss modulus.

The FIP and SIP can be monitored and calculated from DMA test. Figure 6.7 shows calculated G* against number of cycles in DMA test for calculating FIP and SIP.

2. Expecting the Second Inflection Point

After finding the two inflection points by using stiffness modulus from the DMA test, the SIP in APA and creep can be predicted with the following equation:

$$SIP_e = C_F \times (\frac{N_S}{N_F}) \quad (6.7)$$

Where SIP_e = expected SIP in creep or APA

C_F = number of loading cycles at FIP in creep or APA,

N_F = number of loading cycles at FIP in DMA, and

N_S = number of cycles at SIP in DMA.

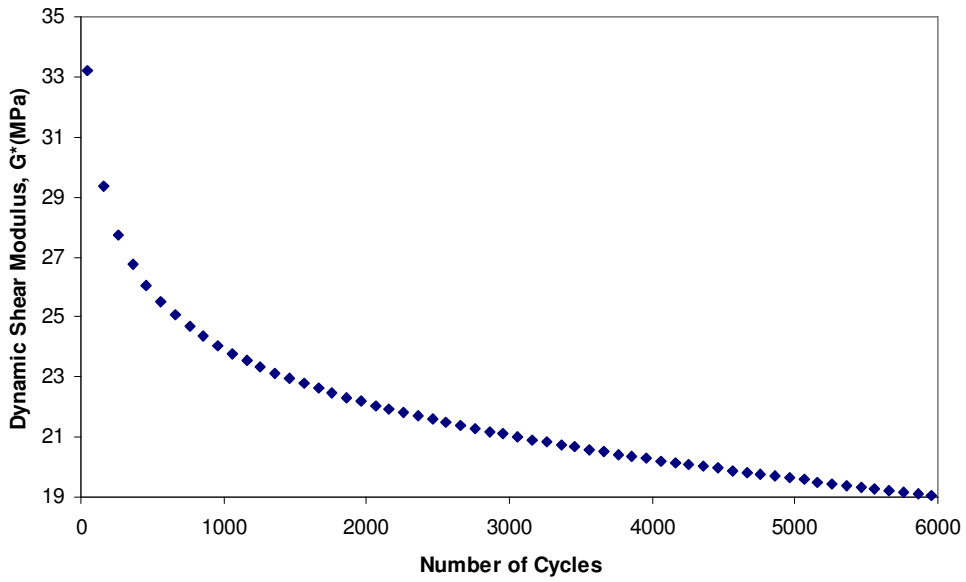

(a)

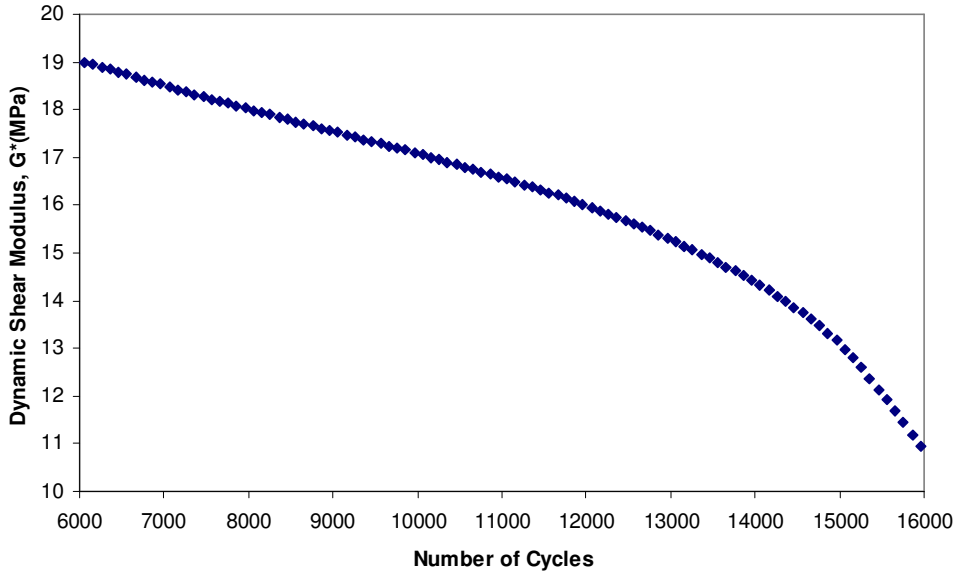

(b)

Figure 6.7. G* against Number of Cycles in DMA Test for Calculating (a) FIP and (b) SIP.

In Figure 6.8, the typical graph plots from DMA and APA were shown with two critical points. The SIP in creep or APA was also expected from the ratio of N_S to N_F. In addition to calculate SIP in creep from DMA test as shown in Equation 6.7, as defined earlier for FIP and SIP, second derivative method with creep test result was used as well.

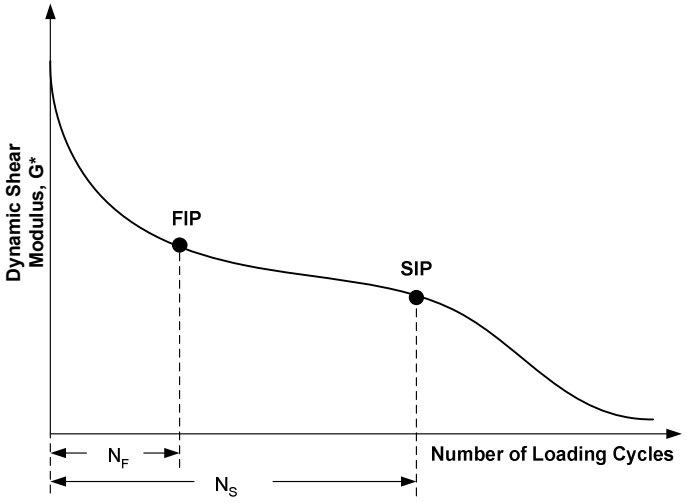

(a)

Figure 6.8. Typical Graph Plots from (a) DMA and (b) APA with Expected SIP Value Based on DMA Data.

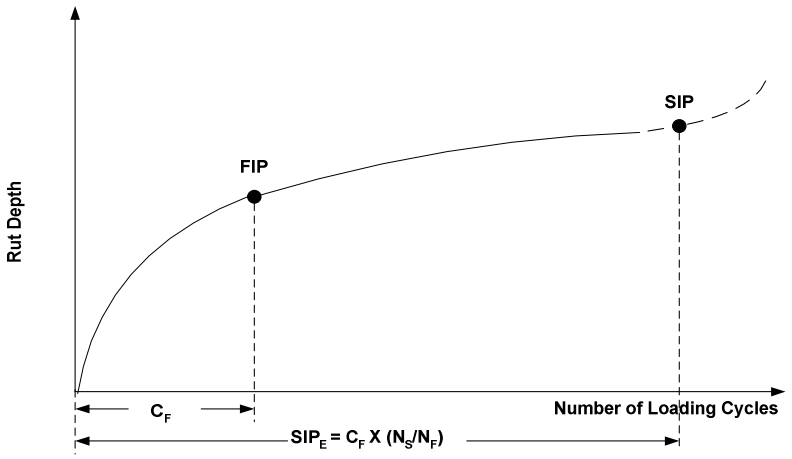

(b)

Figure 6.8. Continued.

DAMAGE PARAMETER COMPARISONS

The damage indicators parameters ξ, S and W^R were taking at four steps based on the previous studies which show that both permanent deformation and fatigue cracking have similar performance behaviors.

Three different comparing methodologies are proposed in this chapter to find out damage parameter the relationships among ξ, S, and W^R from sand asphalt mixtures by DMA, and from HMA by dynamic creep test. Thereafter, the relationships can be validated using creep, DMA, APA tests. The first method is to compare directly with same parameter by calculating each parameter values from dynamic creep test with asphalt concrete mixture and from DMA test with sand asphalt. The second is to compare the image analysis method with DMA method in terms of the parameters. In

other words, the damage parameter ξ for X-ray CT can be expected by *S*, and W^R that are calculated from DMA. The third is based on the micromechanic cohesive and adhesive model. Parameters in the models are calculated or measured from image analysis results.

Finally, the best fitting analysis method and parameters were selected based on the results from DMA and dynamic creep test after comparing the proposed three types of methods.

Method I: Characterizing Damage in Asphalt Mixtures by Damage Parameter Relationship

HMA and sand asphalt specimens were used to calculate parameters ξ, S, and DPSE W^R. Chapter II introduced and characterized the three parameters. The parameters represent damage states at previously defined points before and after failure of samples. As can be seen in Figure 6.9, the ξ values are obtained after performing X-ray CT for both HMA and sand asphalt specimens. In the meantime, others are directly obtained from mechanical tests. Once they are calculated, each one is compared so that the results from different mechanical tests show good agreements.

As Little et al (1998) showed in their report, one of the ways to quantify the damage is by using DPSE. Asphalt concrete shows viscoelastic characteristics which are time and history dependent under constant stress or strain. Therefore, analyzing the real behavior of asphalt concrete is more difficult under realistic testing conditions. The time-dependent viscoelastic behavior is eliminated by DPSE instead of dissipated strain

energy only if the initial strain or stress is negligible to induce any damage within the material (Kim and Little 1990).

DPSE concept was introduced previously and adopted for calculating and comparing the two damage parameters.

Method II: Correlate Parameters at Same Damage States

The second method to correlate the parameter ξ with S and W^R that are from dynamic creep test and DMA to compare the values at the same damage status of the specimens. Calculated ξ value in both HMA and sand asphalt are plotted with S and W^R that are calculated by the mechanical results from DMA. Figure 6.10 depicts the second method to show the concept to correlate X-ray CT result with DMA.

Method III: Cohesive and Adhesive Micromechanics Model

Cohesive and adhesive micromechanicsmodel were used to validate the relationships between parameters by using the results from X-ray CT and DMA.

Lytton (2004) developed an equation, based on micromechanicsanalysis of cohesive and adhesive damage in asphalt-aggregates mixture, for the ratio of the damaged modulus to the undamaged modulus of the binder. It is postulated here that this ratio is the same for the mastic as the reduction in the mastic modulus is due to the degradation in the binder modulus. Mechanical and chemical asphalt properties, i.e., stiffness, stress, and bond energy, were used to see the relation between damaged and undamaged modulus of asphalt.

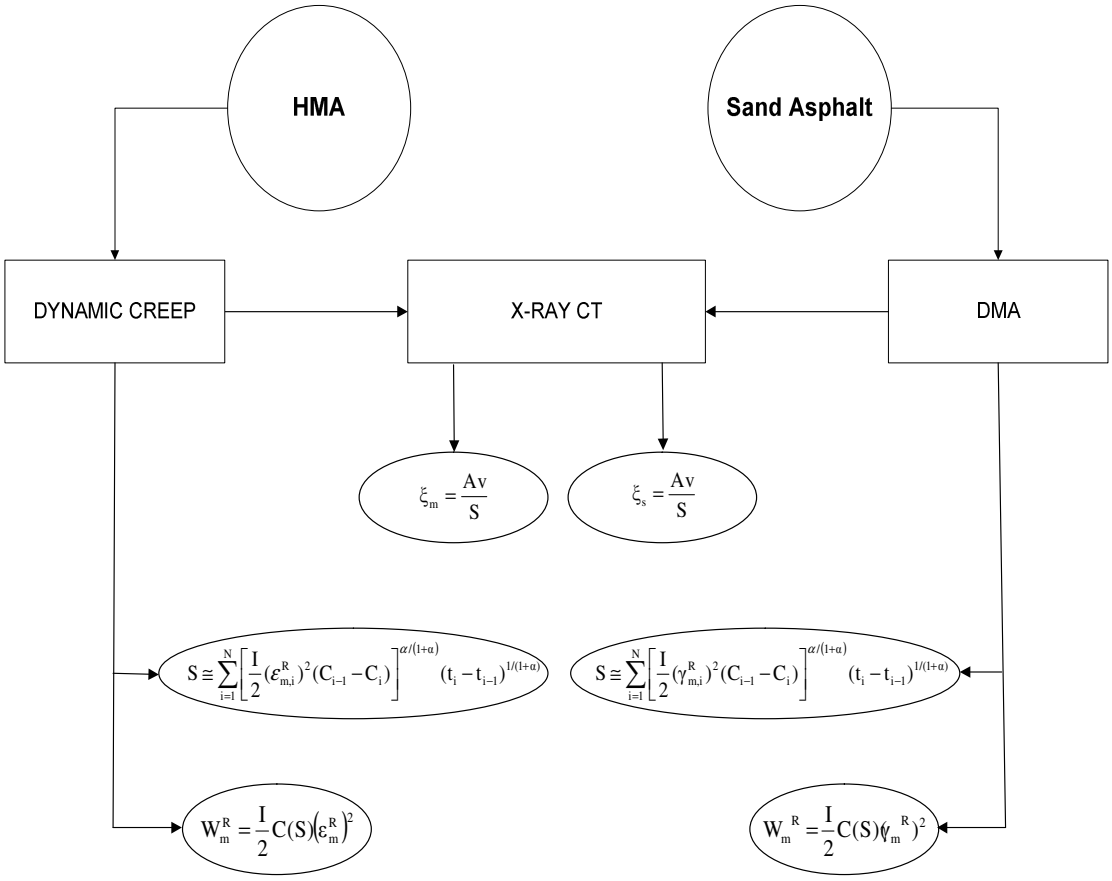

Figure 6.9. Flow Chart for Method I Using Pseudo Strain Energy.

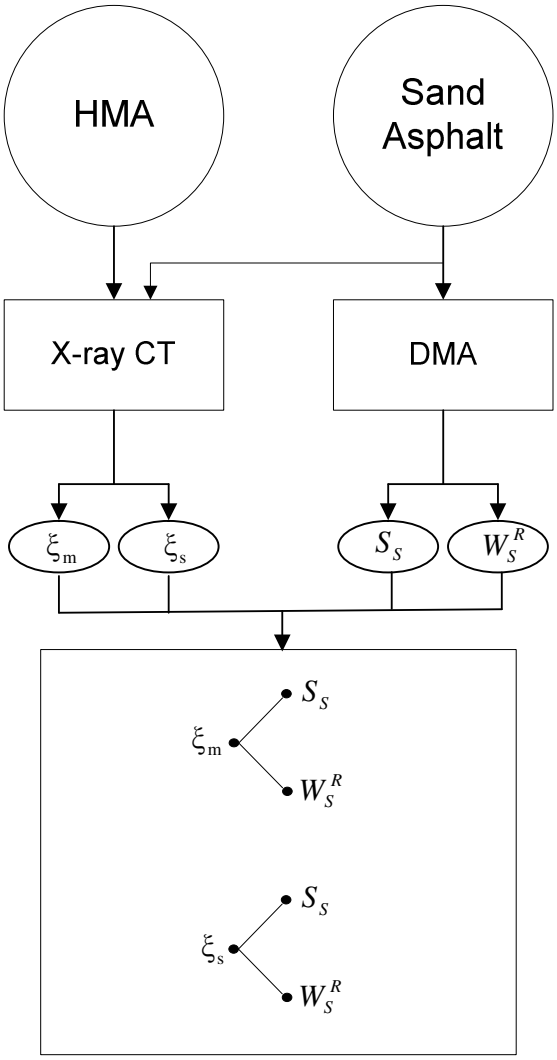

Figure 6.10. Damage Parameter Comparisons at Each Step (Method II).

CHAPTER VII

MATERIALS SELECTION AND EXPERIMENTAL SETUP

Materials used in this laboratory study consisted of asphalt binder, aggregate, and sand. It was determined to use the same asphalt binder PG 64-22 which is the most commonly used asphalt binder in the United States for the both HMA and sand asphalt to maintain consistency in the test. The aggregate used in the mixture composed of Georgia Granite provided by Vulcan Materials Co.

ASPHALT BINDER (PG 64-22)

PG binders were introduced in Superpave system. The binder grading system corresponds to the expected high (average 7-day max high pavement temperature at 20 mm depth) and low (minimum temperatures at pavement surface) temperatures of the location of the pavement. The asphalt binders are required to meet the minimum and/or maximum values when they were tested with specified tests for material properties. The Superpave performance based binder grades are selected based on the climate prevailing at the project site (Roberts et al. 1996). Table 7.1 gives the performance based binder grades in the specification.

The mixing and compaction temperature were determined by plotting viscosity against temperature as we can see in Figure 7.1.

A rotational coaxial cylinder viscometer (RV) was adopted in Superpave and described in ASTM D4402. The RV was used in this research to calculate binder

viscosity and determine mixing and compaction temperature for mixtures as shown in Table 7.2.

Table 7.1. Superpave Performance Based Asphalt Binder Grades (Roberts et al. 1996).

High Temperature Grades (°C)	Low Temperature Grades (°C)
PG 46	-34, -40, -46
PG 52	-10, -16, -22, -28, -34, -40, -46
PG 58	-16, -22, -28, -34, -40
PG 64	-10, -16, -22, -28, -34, -40
PG 70	-10, -16, -22, -28, -34, -40
PG 76	-10, -16, -22, -28, -34
PG 82	-10, -16, -22, -28, -34

Table 7.2. Mixing and Compaction Temperature As Defined by The Rotational Viscometer.

Temp (℃)	Pa·s	Mixing Temp(℃)	Compaction Temp(℃)
135	0.6110	158 ~ 166	148 ~ 153
175	0.0881		

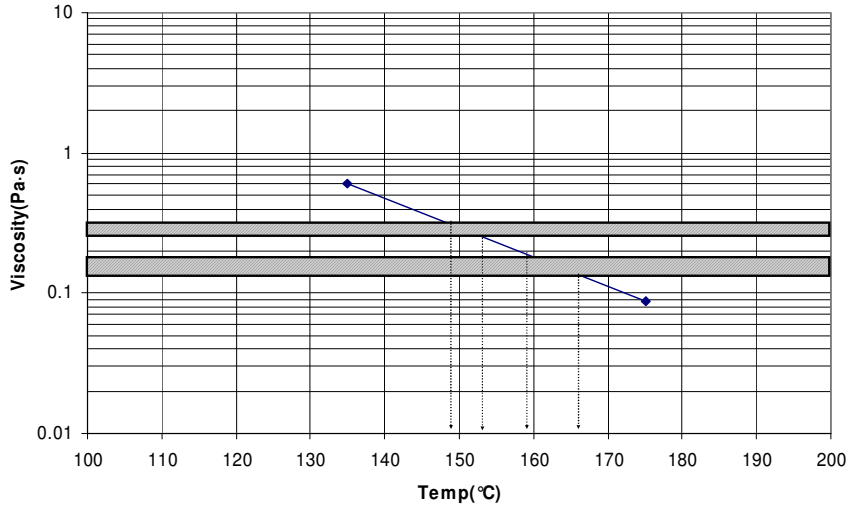

Figure 7.1. Determination of Mixing and Compaction Temperature.

SAMPLE FABRICATION

Creep and APA

Dense-graded HMA which were intended to dynamic and APA tests were designed according to Superpave specifications. A Superpave gyratory compactor was used for preparing specimens. Georgia granite was selected to produce the gradation shown in Figure 7.2. This gradation was selected in accordance with limits given in Superpave specifications. As stated earlier, PG 64-22 asphalt binder was selected and used to fabricate sand asphalt for asphalt concrete specimens.

After batching the aggregates, 4.5 % of asphalt binder by weight of mixture was mixed to meet the specified % of air voids (AV), voids in mineral aggregate (VMA), and voids filled with asphalt (VFA).

Two sample sizes were selected depending on their final use as shown in Figure 6.2. Compaction was performed in a split mold to fabricate cylindrical samples having 100 mm diameter and 150 mm height for creep test with 7% AV. The test specimens evaluated for APA were also fabricated with a diameter of 150 mm and a height of 75 mm. The same asphalt binder and gradation which were used for making samples for creep and APA test. Acceptable uniformity of all the fabricated samples was verified by means of bulk specific gravity and air void content.

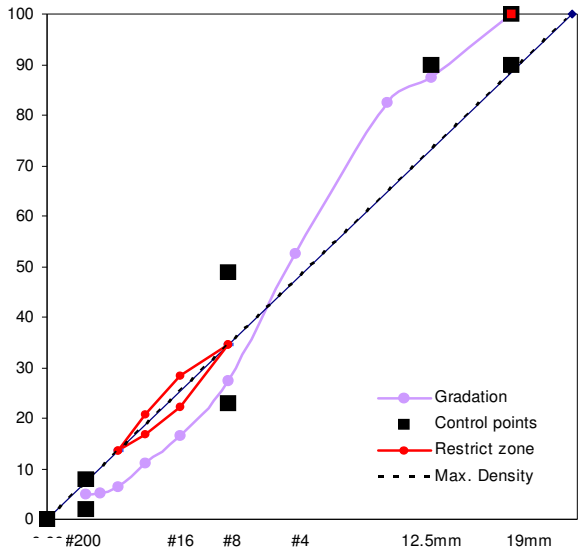

Figure 7.2. Dense Gradation for Georgia Granite.

Dynamic Mechanical Analysis (DMA)

Same asphalt binder of PG 64-22 was employed for sand asphalt to eliminate the variability caused by using different type of asphalt binder. Only the aggregates passing

sieve the #16 (1.18 mm sieve size) were used following the Ottawa standard sand gradation as can be seen in Figure 7.3 since the size of sand asphalt sample is much smaller than that of asphalt concrete mixtures for creep and APA test. The selected size of aggregates forms a sand asphalt mixture capable of maintaining its shape without plastic flow during testing and the selected gradation of the aggregates met the standard sand requirements provided by ASTM C 778.

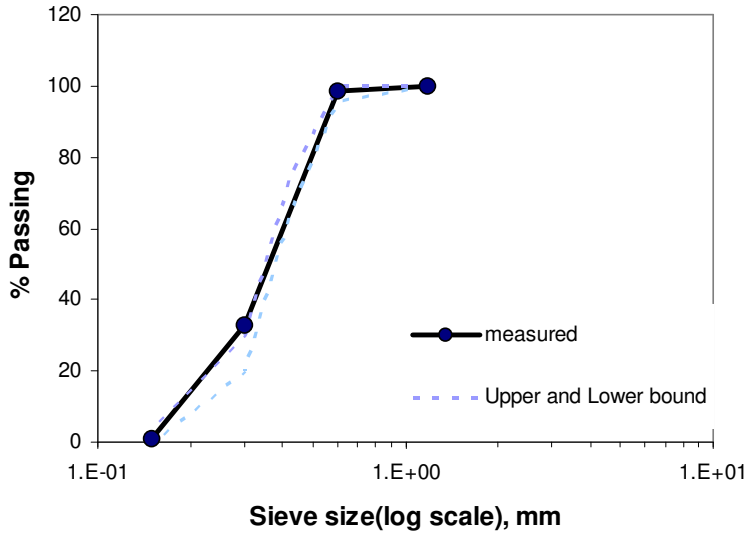

Figure 7.3. Ottawa Standard Sand Gradation with Upper and Lower Limit by ASTM C 778.

Eight percent of binder by weight of dried aggregate was added to make sand asphalt samples. Reasonable arbitrary value of the eight percent binder was selected to provide an average “film thickness” of approximately 10 microns. As described earlier,

AASHTO T 209 method which is to use rotational viscometer was adopted to determine mixing and compaction temperature for making samples.

Kim (2003) suggested a methodology in his dissertation to characterize fatigue damage by using DMA. Figure 7.4 shows a specially fabricated mold which was designed and used to fabricate the 11.0 grams of cylindrical sand asphalts for DMA test. The trial and error method was adopted to determine the required mass for one sample which has a 50 mm long with a 12 mm diameter. The schematic diagram of cylindrical sample of sand asphalt with holders in DMA is offered in Figure 7.5. The cylindrical sample for DMA test was adopted to avoid complex data analysis. To install the fabricated sample in DMA two sample holders and epoxy glue were used in this research.

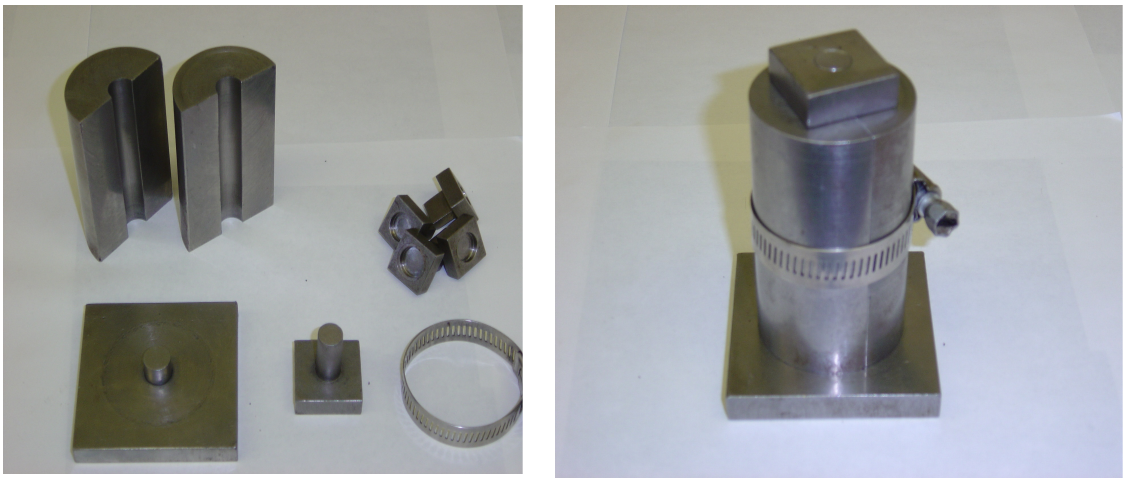

Figure 7.4. Compaction Mold Assembly for Sand Asphalt Sample Fabrication.

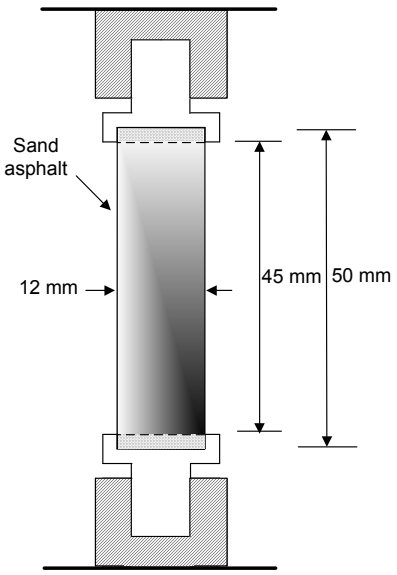

Figure 7.5. Geometric Dimension of Cylindrical Sand Asphalt Sample.

Sample Preparation for Wet Conditioned Test

This research follows AASHTO DESIGNATION: T283-89 (1993), title of "Resistance of Compacted Bituminous Mixture to Moisture-Induced Damage", for preparing wet conditioned samples. Figure 7.6 shows a vacuum apparatus for wet conditioned specimens. Table 7.3 summarizes the procedures step by step as follows:

.

Table 7.3. Procedures for Wet Conditioned Specimens.

Task	Content
1	Place the sample in the vacuum container
2	Fill the container with distilled water at room temperature so that the samples have at least 25mm of water above their surface
3	Apply a vacuum and leave the samples submerged in water for 5 minutes
4	Determine the bulk specific gravity by T 166 and calculate the percent saturation (should be between 55 percent and 80 percent). If volume of water is more than 80 percent, discard the sample
5	Soak the sample in a bath containing distilled water for 24±1 hours

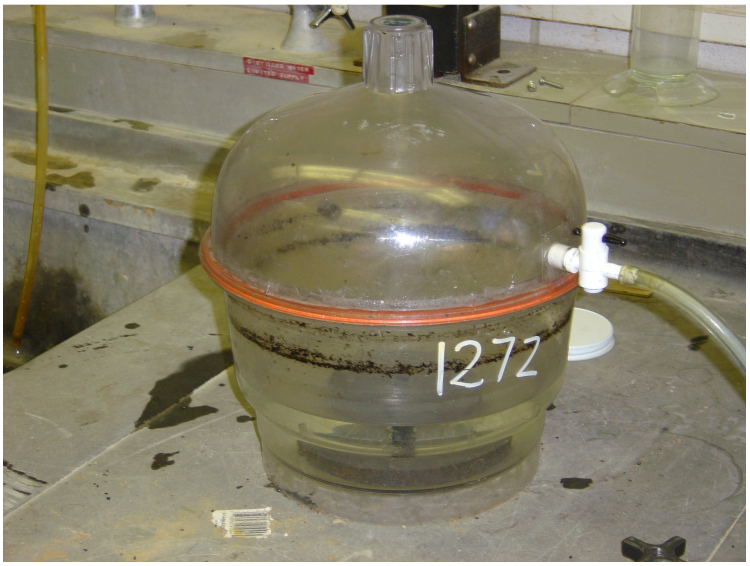

Figure 7.6. Vacuum Apparatus for Wet Conditioned Specimens.

EXPERIMENTAL SETUP

Dynamic Creep

The creep test has been used for many years to estimate the rutting potential of HMA. Creep test data can be used to evaluate the permanent deformation potential of asphalt concrete mixtures when the laboratory creep testing is performed in such a manner as to simulate realistic field stress conditions (Little et al. 1993). In a dynamic creep test, the strain in the mixture is measured as a function of time in the laboratory under unconfined conditions at a fixed temperature.

Figure 7.7 shows the dense grade asphalt mixture specimen installed in a materials testing system (MTS). The MTS machine was used for the dynamic creep test with dense graded asphalt concrete mixtures having 100 mm diameter 150 mm high as shown in Figures 6.2 and 7.8. A load system consisting of a testing machine, environmental chamber, measuring system, and specimen was used for the test.

Figure 7.7. Dense Grade Asphalt Mixture Installed in MTS.

Only one stress level of 0.45MPa was selected in this research in order to have a uniform basis for comparison. The selected stress level was determined based on trial tests to ensure that the test sample would exhibit tertiary flow within a reasonable testing time. To compare the DMA results, room temperature of 25˚C was applied.

The axial deformations were measured at two locations 180° apart (in a plain view) by using 100 mm length linear variable differential transformers (LVDTs). The experimental set up for dynamic creep test is shown in Figure 7.8 and Table 7.4 shows detail conditions for creep test.

Figure 7.8. Dynamic Creep Test Set Up with Axial LVDT.

Table 7.4. Conditions for Creep Test.

Condition	Value
Deviatory Stress (MPa)	0.45
Temperature (°C)	25
Gauge Length (mm)	100

Three basic zones which are primary, secondary and tertiary zones in a typical plot of the compliance against time a graph on a log-log scale were described by Kaloush and Witczak (2002) as can be seen in Figure 7.9. The primary zone is where the strain rate decreases sharply under static load and tends to stabilize reaching the secondary zone. In the secondary zone, the strain rate remains almost constant under the applied static load and starts increasing in the tertiary zone.

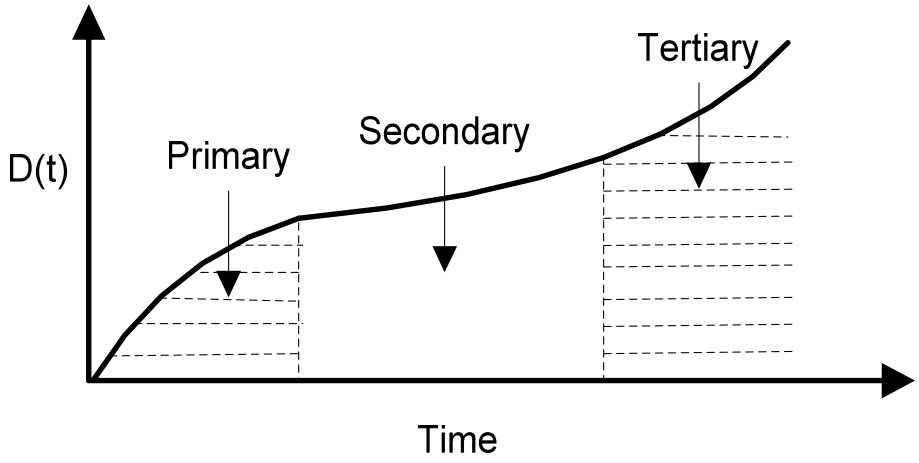

Figure 7.9. Typical Three Basic Zones in Creep Test by Plotting Creep Compliance against Time on Log Scale.

Since this test apply a specific stress level in a dynamic form, it needs an application and rest period. In general, 0.9 sec of rest periods followed by a stress application period of 0.1 sec is applied for the test. Figure 7.10 shows the input stress wave form for dynamic creep test.

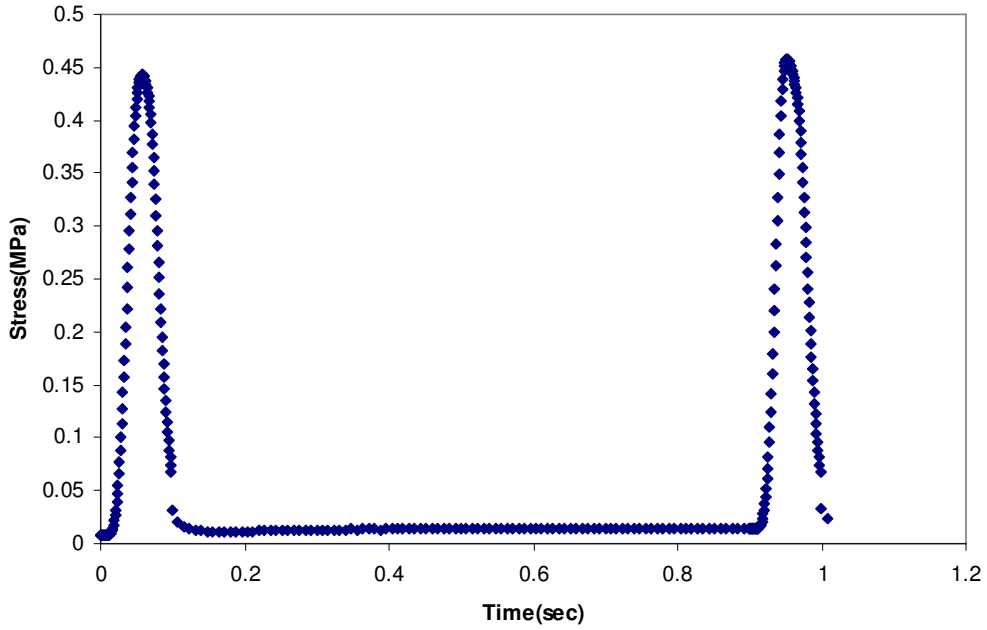

Figure 7.10. Input Stress Wave Form For Dynamic Creep Test.

Three basic zones of primary, secondary, and tertiary zone were detected from the dynamic creep test as well, when the permanent strain data were plotted versus the number of load cycles.

Asphalt Pavement Analyzer (APA)

Figure 7.11 shows an APA machine which is basically a modified and improved version of the Georgia load wheel tester. By far, the APA is the most popular and commonly used loaded wheel tester in the USA.

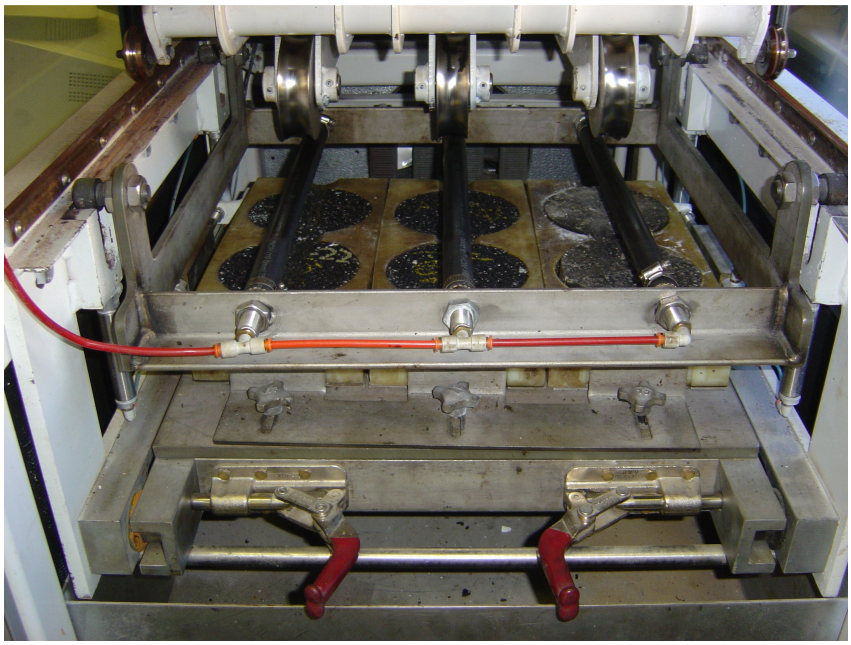

Figure 7.11. Test Specimens in Laboratory Wheel Tracking Tester APA.

Shami et al. (1997), Kandhal and Mallick (1999) used APA in his research for evaluating permanent deformation. Testing with the APA was conducted according to the procedure recommended by the Georgia Department of Transportation test method GDT-115. Hose pressure and wheel load were 690 kPa. The test carried out to 8000

cycles at 38°C and rut depth measured continuously. One set of forward and backward strokes comprise one cycle. All the tests conducted in this research were dry condition to emphasize the rutting behavior of the mixtures. Three pairs of samples were tested at a test. Data from each pair was recorded to one channel.

Dynamic Mechanical Analysis (DMA)

Each sample after following the procedures described above was mounted in the DMA instrument as shown in Figure 7.12. At least 20 minutes equilibrium time was applied with closing the chamber to allow equilibrate desired test temperature.

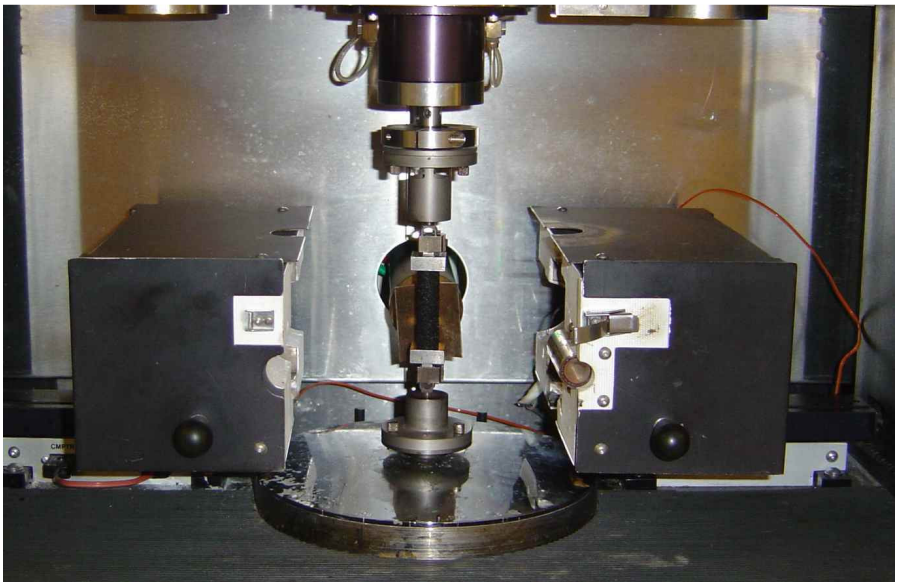

Figure 7.12. Cylindrical Sand Asphalt Sample Installed in DMA.

The torsional shear was used in a strain-controlled mode and the test data were collected by a data acquisition (DAQ) system with a 16-bit multi channel board. Considering traffic movements, damage simulation in the torsional loading would be better than that in the bending loads (Reese 1997).

Average values of stresses and strains from the following equations were used in this research:

$$\gamma = \frac{R\varphi}{H} \tag{7.1}$$

$$\tau = \frac{2T}{\pi R^3} \tag{7.2}$$

Where R = radius of cylinder,

H = length of cylinder,

φ = actuator angular displacement, and

T = transducer torque.

Figure 7.13 shows the dynamic loading mode which has sinusoidal wave form. Strain-controlled cyclic tests were performed at 0.28% strain level at 25°C with 10Hz of frequency. Stiffness reduction and phase angle change due to damage accumulation can be monitored as the number of loading cycles increase.

Kim et al. (2001) explained testing protocol above using this protocol in which a thermocouple wire was used to measure the history of heating and heat dissipation during torsional testing and rest periods.

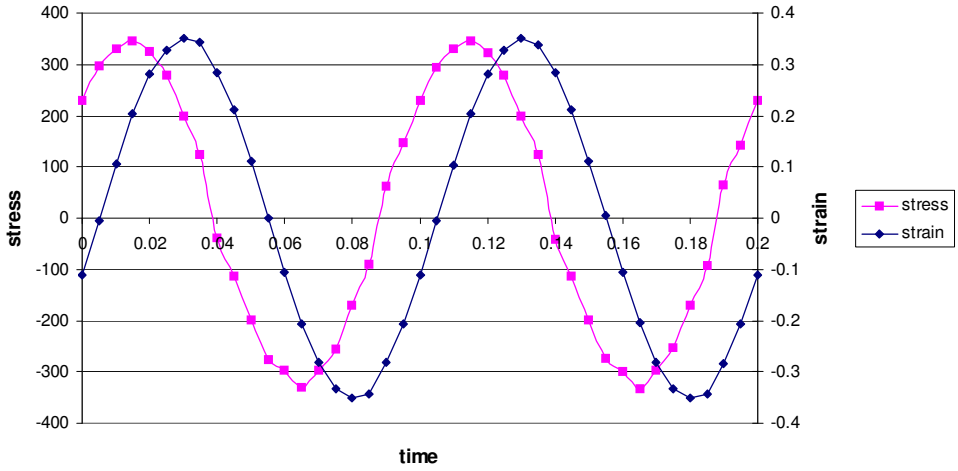

Figure 7.13. Typical Controlled-Strain Mode DMA Test Following Sinusoidal Dynamic Loading.

CHAPTER VIII

RESULTS AND CONCLUSIONS

DATA POINT DECISION BASED ON DYNAMIC TESTING

Basically, both damage parameter ξ and *S* are calculated from dynamic creep test with HMA and DMA with sand asphalt samples which were fabricated for dry and wet condition. Chapter VII introduced dynamic creep and DMA fatigue test settings for controlled-strain mode. Figure 8.1 plots the calculated creep compliance D(t) on the corresponding time from dynamic creep test. Figure 8.2 depicts how the stiffness from DMA decreases as number of cycles increase in both dry and wet condition. The plots in the two graphs show that wet conditioned samples are more sensitive to the stress.

The results from the mechanical tests are not only used for calculating parameters to show the damage by damage parameters and relate the parameters, but also they are used to determine two critical points. Third order polynomial equations were made on the each curve and then the two critical points in the graphs were obtained by second derivative of the equations. The asphalt mixture behavior, therefore, in dynamic loading have four distinct regions. The selected four points are illustrated below in Figures 8.1 and 8.2 and each point represents damage step until the test specimen reaches failure. Step1 is considered an initial condition without any damage. Generally, there are three distinct regions in creep test such as the primary, the secondary, the tertiary zone. Witczak et al. (2002) defined the secondary zone as the region in which strain rate decreases with loading time. Rowe and Bouldin (2000) also considered four

regions of fatigue behavior and the second region was the microcrack zone. Based on the results from this research and these previous studies, Step2 is defined as the FIP in the whole fatigue behavior. Step3 is the SIP matching with the start point of tertiary flow and macro cracking. Step4 represents the failed condition by the dynamic loading.

Table 8.1 summarized the values of the four points for HMA and sand asphalt specimens. The points are marked in Figures 8.1 and 8.2.

Table 8.1. Summary of the Four Points for Analysis.

(unit: sec (cycle))

Test	Condition	Step1	Step2	Step3	Step4
Dynamic Creep	Dry	0 (0)	219.8 (220)	549.6 (550)	1099.1 (1099)
	Wet	0 (0)	179.8 (180)	449.6 (450)	899.1 (899)
DMA	Dry	0 (0)	86.0 (860)	200.0 (2000)	336.0 (3360)
	Wet	0 (0)	100.0 (1000)	236.0 (2360)	436.0 (4360)

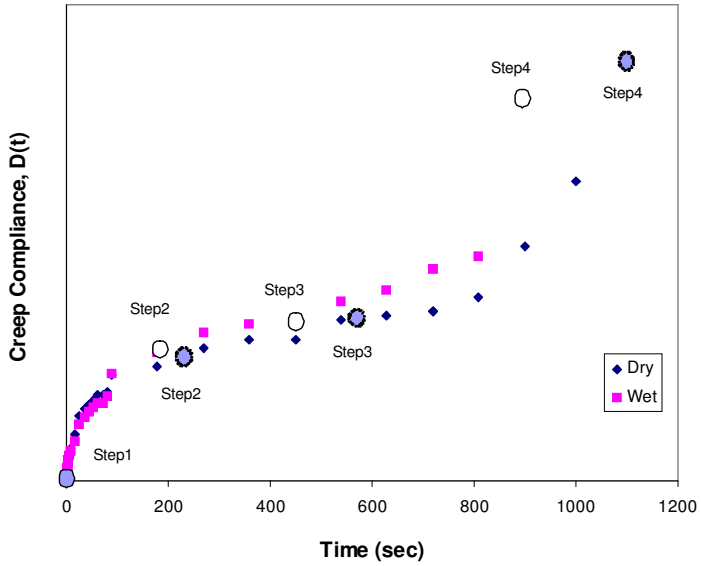

Figure 8.1. Creep Compliance versus Loading Time with Stress-Controlled Dynamic Creep Test.

DATA ANALYSIS FOR ξ

Former image analysis studies take the images just at initial and final (failure) stage of destructive tests or from material properties such as aggregate angularity and texture before fabricating samples, therefore, the procedures are hard to represent the real damage of tested specimens between initial and the failure status even though they can be used to estimate indirectly from their methods.

HMA and sand asphalt specimens before and after dynamic creep and DMA fatigue test were scanned by X-ray to capture the microstructures at different four steps with dry and wet condition. Damage parameter ξ was adopted to quantify the damage

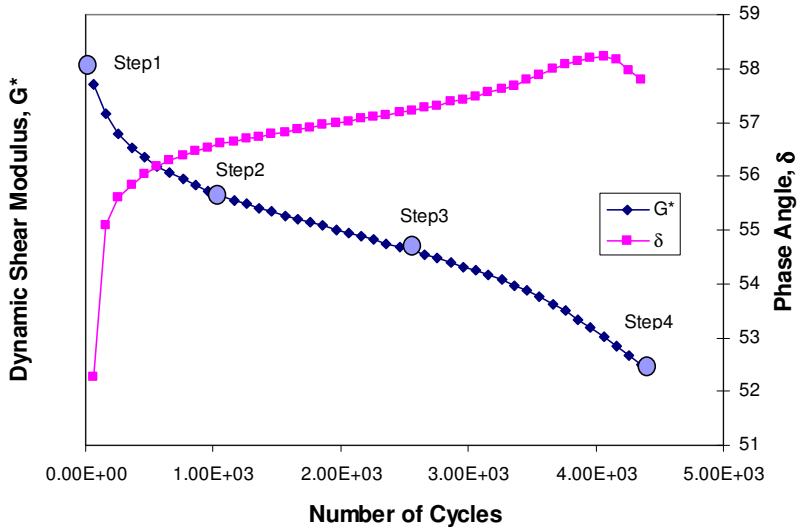

(a)

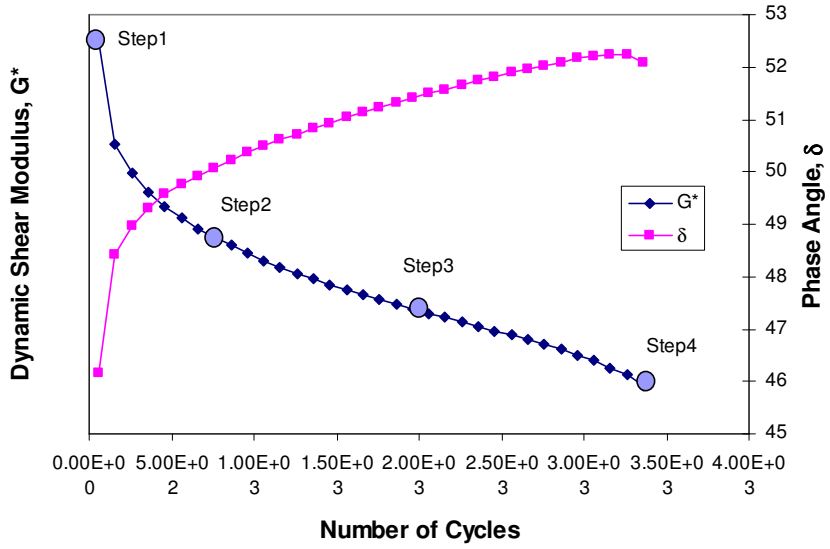

(b)

Figure 8.2. Stiffness versus Number of Cycles with Strain-Controlled DMA Test in (a) Dry Condition and (b) Wet Condition.

levels at each damage step in both HMA and sand asphalt specimens. Data analysis showed that the parameter was good to see the damage changes in both specimens. The degree of scattering in terms of standard deviation was used to show the differences of damage in HMA at each damage step.

Image analysis methods and steps are introduced in Chapter V. As described in the chapter, selecting proper threshold value is critical because the subsequent measurements are sensitive to its value.

Threshold levels were determined by focusing on the air voids in the initial step (undamaged specimens) with gray-scale images acquired through X-ray CT. In other words, threshold values were determined when they match up to the air voids measured by bulk specific gravity. Accordingly, measured gray intensity at a given point may be higher or lower than the threshold. Therefore, it is assigned to be either part of the air void, cracking, and aggregates. Following the threshold level decision, the gray-scale image was converted to black-and-white image based on the threshold level so that it is possible to calculate parameter values. Table 8.2 shows the determined threshold values for HMA and sand asphalt both in dry and wet condition.

Table 8.2. Determined Threshold Values for Image Analysis.

Specimen	Condition	Value
HMA	Dry	59
	Wet	90
Sand Asphalt	Dry	115
	Wet	130

Hot Mix Asphalt Concrete Mixture (HMA)

Figures 8.3 and 8.4 show the results of the damage parameter measurements at each damage step. Four curves are plotted for the same condition. Each curve is composed of 158 points representing results from horizontal sliced images and indicates the amount of damage measured at pre-determined steps. Each point in the figures is calculated values based on the 1 mm slice image from the HMA mixtures without offset. The height ratio is defined as the ratio of vertical distance from the top of the specimen to the total height of sample because there were slight different heights among the fabricated samples.

Figure 8.3 shows that the damage parameter ξ values decreased initially and then they increased up to 0.2 in the rest of steps. As can be seen in Figures 8.3 and 8.8,

the damage parameter values in both the two types of specimens exhibited slight changes in the first three damage steps in dry condtion.

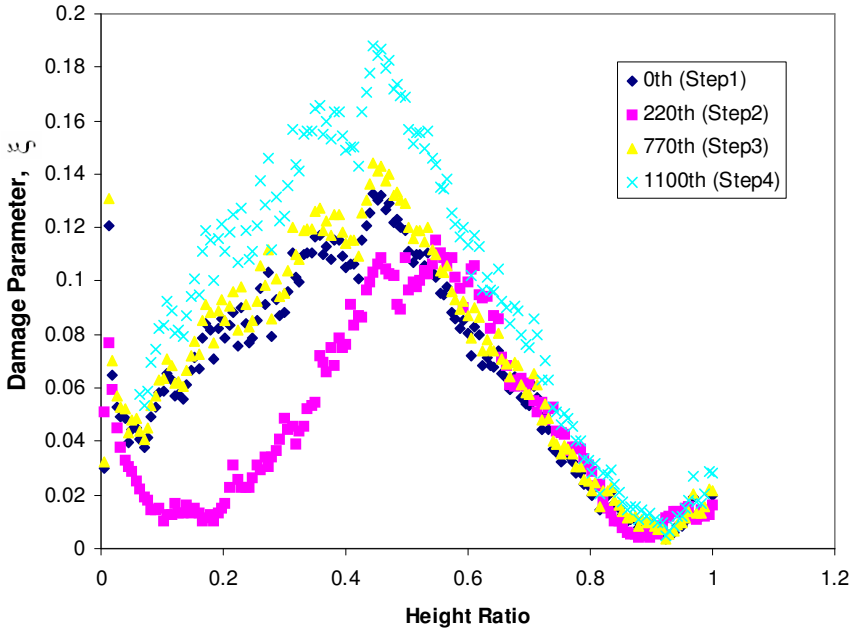

Figure 8.3. Damage Parameter ξ Distribution in HMA (Dry Condition).

There were significant changes of ξ occurred between Step1, undamaged condition, and Step2 and the results were shown in Figures 8.4 and 8.9.

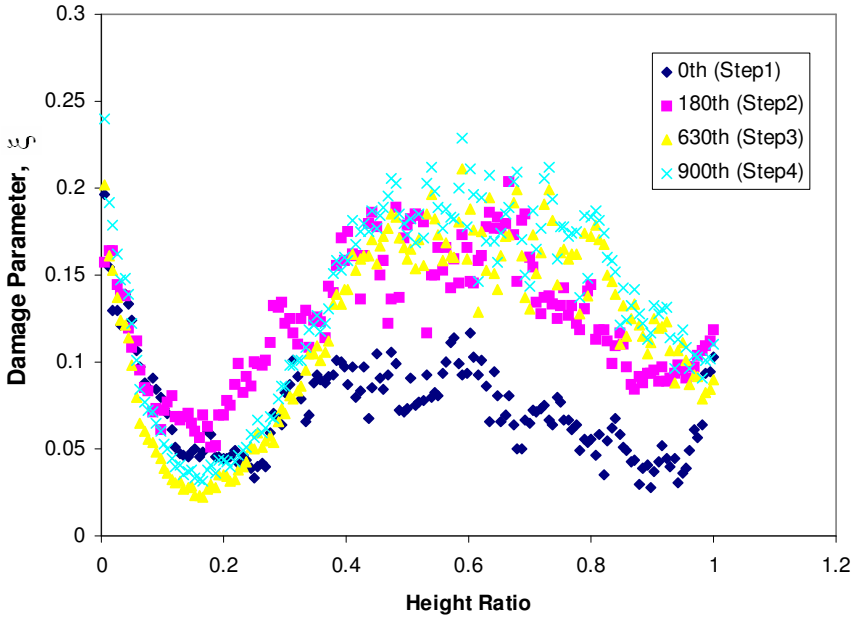

Figure 8.4. Damage Parameter ξ Distribution in HMA (Wet Condition).

HMA images showed that there were distinct regions with respect to damage parameter ξ as shown in Figures 8.3 and 8.4. Approximately, the first and last 10 percent of the height of HMA specimens have high void contents because of the direct contact with the gyratory plates causing restriction in the mobility of the aggregates and reducing the efficiency of the kneading action (Tashman et al. 2001). The three regions were separated by 15 percent for the top and the bottom and 70 percent for the middle of total height. Damage parameter ξ was studied separately in the three regions. Figure 8.5 shows the parameter changes of the three regions at each damage step in HMA. The middle region was selected based on the graph plots in the figures below:

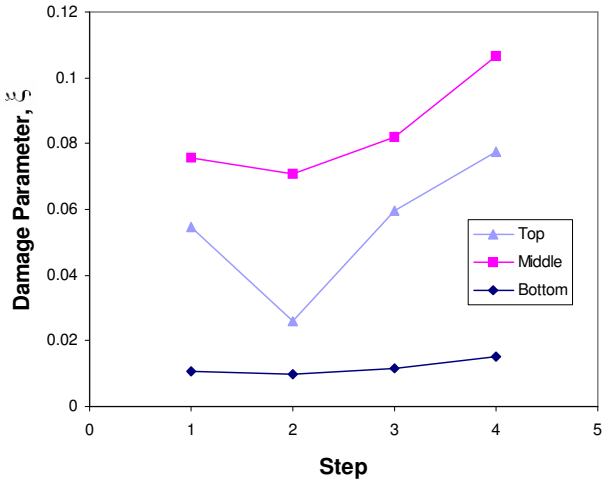

(a)

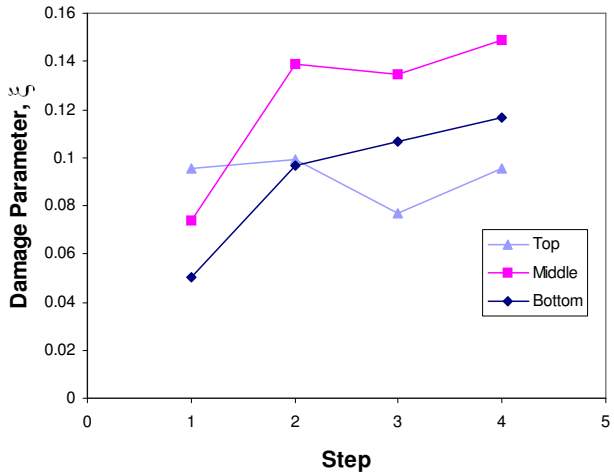

(b)

Figure 8.5. Damage Parameter ξ Changes of Three Distinct Regions at Each Damage Step in (a) Dry Condition and (b) Wet Condition in HMA.

Figure 8.6 shows the average values of damage parameter ξ changes by dynamic creep test from both dry and wet conditioned specimens at the defined four steps. As expected, the wet conditioned specimens experienced higher damage throughout the steps.

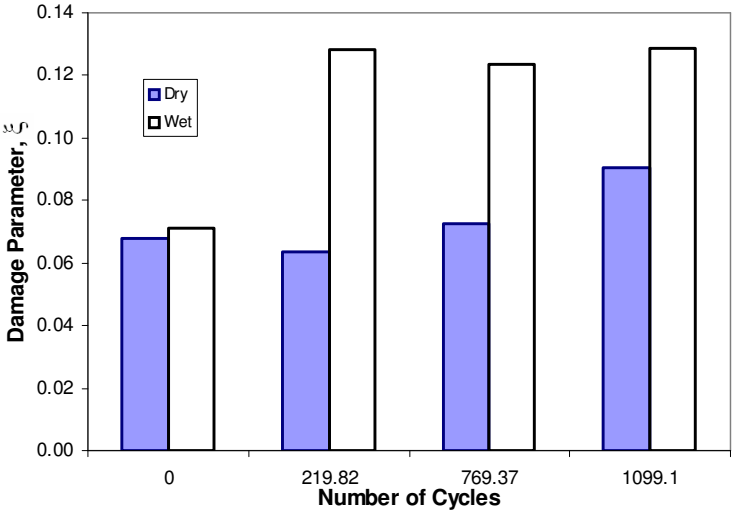

Figure 8.6. Comparison of Damage Parameter ξ at Dry and Wet Condition in HMA.

The calculated standard deviation was also adopted for supplementary way to show the HMA damage status at each damage step. Table 8.3 summarized the standard deviation and ξ values from HMA. Because the sand asphalts used for DMA have relatively homogeneous properties and does not show significant degree of dispersions in the results, only HMA results from dynamic creep test were included to estimate standard deviation. The standard deviation based on the data from the dynamic creep test was estimated and plotted in Table 8.3 and Figure 8.7.

The standard deviation is a measure of how widely values are dispersed from the average value (the mean). Following Equation 8.1 was used for standard deviation.

$$S.D. = \sqrt{\frac{n\sum x^2 - \left(\sum x\right)^2}{n(n-1)}} \quad (8.\ 1)$$

Where $S.D.$ = standard deviation,

n = number of samples, and

x = measured damage parameter value.

Table 8.3 and Figure 8.7 show that standard deviation in wet condition has more degree of scattering than in dry condition and there is a relatively big shift at Step2 as shown in Figure 8.4. On the contrary, no significant increase was detected at Step2 in dry condition.

Table 8.3. Data Summary of Standard Deviation and Average Parameter Value ξ from HMA.

	Standard Deviation	Average ξ
Dry		
Step 1	0.376	0.076
Step 2	0.348	0.071
Step 3	0.407	0.082
Step 4	0.531	0.107
Wet		
Step 1	0.027	0.074
Step 2	0.037	0.139
Step 3	0.053	0.135
Step 4	0.055	0.149

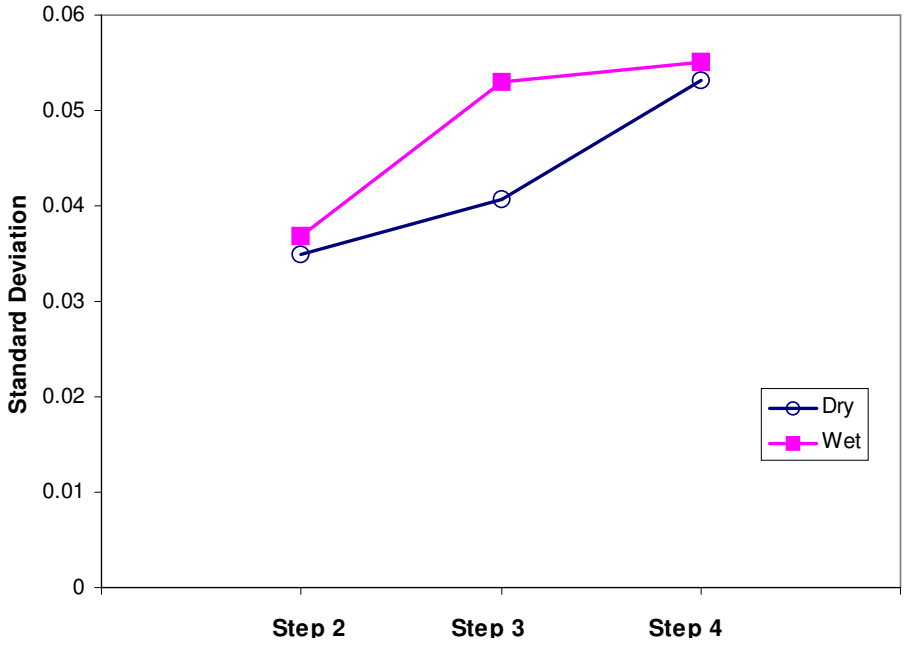

Figure 8.7. Standard Deviation at Each Damage Step in HMA.

Sand Asphalt

Figures 8.8 and 8.9 show the increasing damage parameter ξ values after DMA tests with sand asphalt specimens. Each curve represents the amount of damage measured at each damage step. Four curves are plotted for the same condition. Each curve is composed of 700 points and indicates the amount of damage with two replicates measured at pre-determined steps. The points in the two figures are calculated values from image analysis technique based on the thickness of 0.03148 mm images without offset. Assuming that the damage status in the same tested samples is symmetric, half of

the total length of a specimen was scanned by X-ray and the images were analyzed. Therefore, the height ratio in the figures was defined as the ratio of vertical distance from the bottom to a half of height of sample.

The applying torsional stress and accumulation of fatigue loose the structure of the specimen with increasing the amount of air voids and cracks. The degree of scattering data, however, did not change significantly throughout the steps. The damage distribution in a same step is quite different from that of HMA. It is believed that the different type of materials caused the different results. In other words, as described earlier, small loose sand asphalt samples using only binder and Ottawa standard sand have more homogeneous characteristics than dense graded HMA samples with Georgia granite. Also, the different mixing and compaction method and loadings types - compression (dynamic creep test) and torsional (DMA test) stress - can be considered for the reasons.

Figure 8.8 shows that a significant change of damage parameter values occurred between Step3 and Step4 in dry condition while the parameters in the first three steps show smooth increasing.

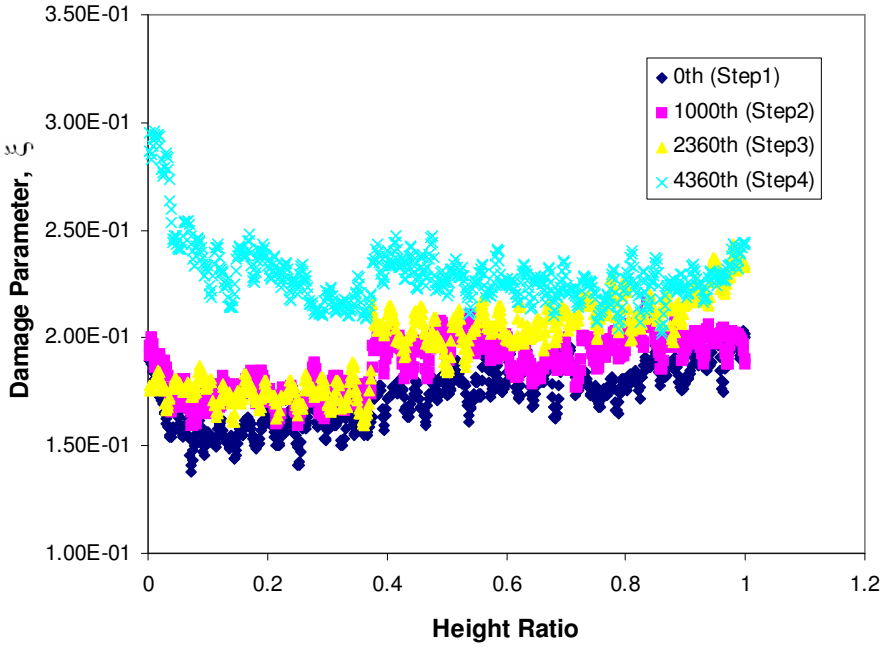

Figure 8.8. Damage Parameter ξ Distribution in Sand Asphalt (Dry Condition).

Samples in wet condition experienced a significant change of damage parameter between Step1 and Step2 as shown in Figure 8.9. The rate of damage changes is decreasing after the relatively big shift from Step1 to Step2. The same patterns of parameter changes were investigated in the wet conditioned HMA specimens.

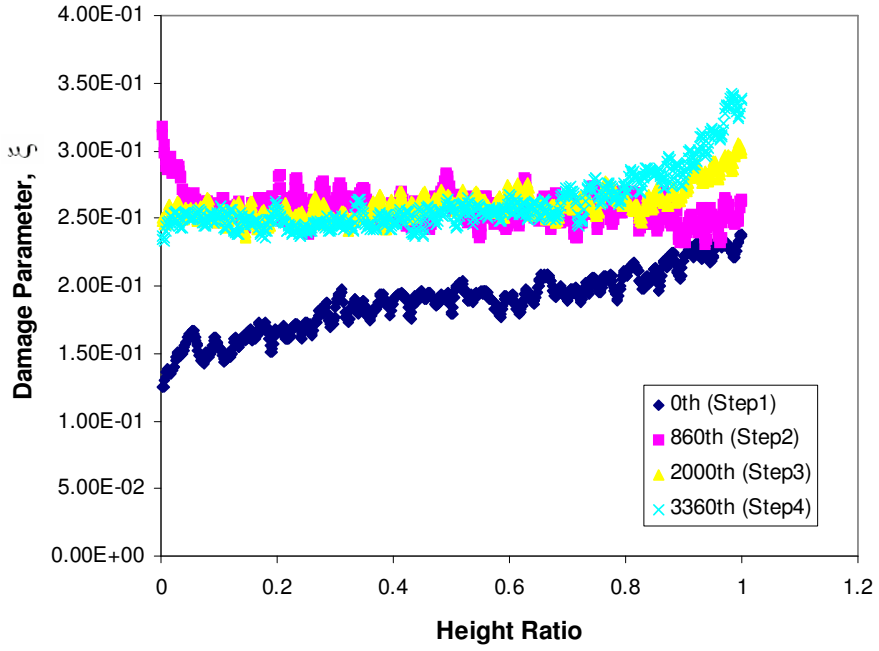

Figure 8.9. Damage Parameter ξ Distribution in Sand Asphalt (Wet Condition).

The average values from the each curve in Figures 8.8 and 8.9 are plotted in the following Figures 8.10 and 8.11 for both dry and wet condition. Figure 8.10 (a) shows the change of damage levels in dry condition while Figure 8.10 (b) is in wet condition. The patterns of average values in the following figures exhibit the similar results as the whole data values in Figures 8.8 and 8.9.

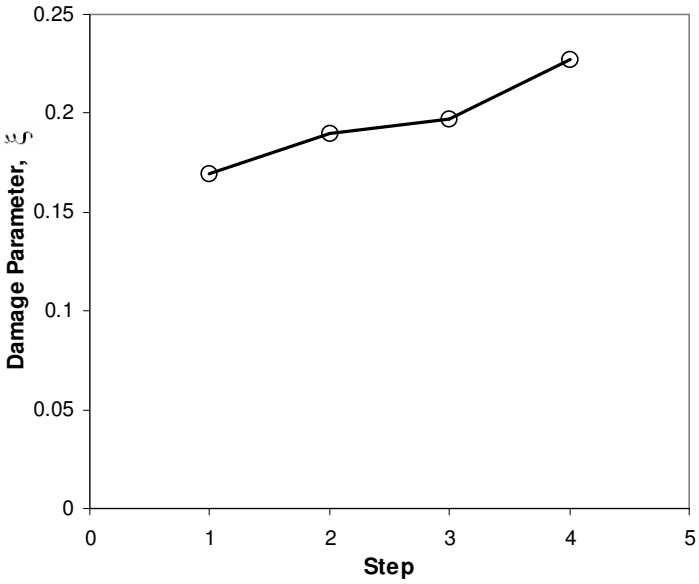

(a)

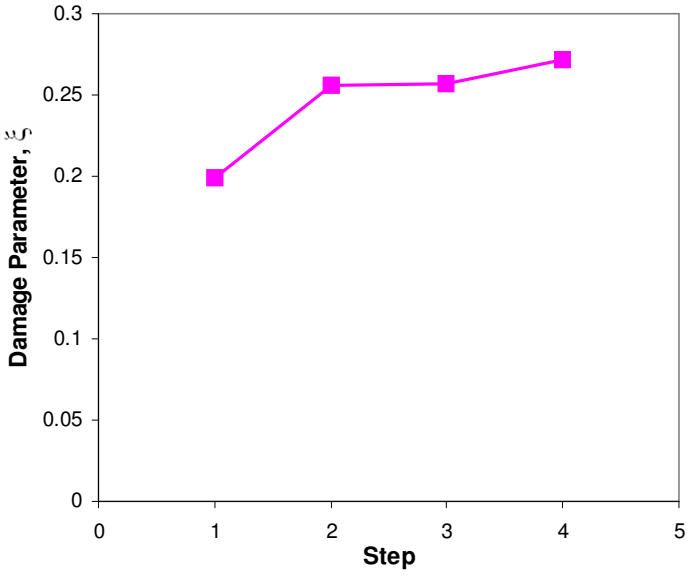

(b)

Figure 8.10. Damage Parameter ξ Changes at Each Damage Step in Sand Asphalt in (a) Dry Condition and (b) Wet Condition.

Figure 8.11 is a plot of damage parameter ξ results from both dry and wet conditioned specimens at pre-defined steps. As expected, the wet conditioned specimens experienced higher damage throughout the steps.

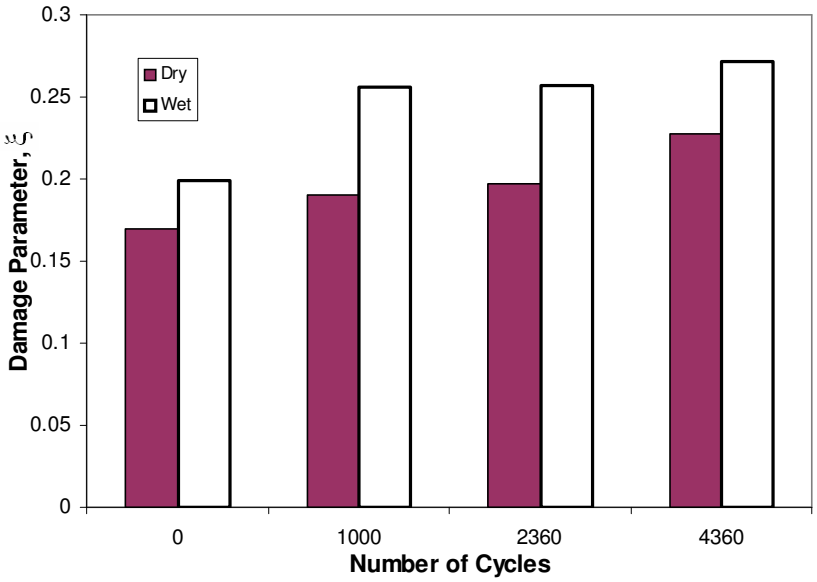

Figure 8.11. A Comparison of Damage Parameter ξ in Dry and Wet Condition in Sand Asphalt.

Although there were a couple of differences between HMA and sand asphalt test such as geometric, materials, and loading condition, both results of damage parameters ξ showed similar performance characteristics in the both dry and wet condition. Using average values of the damage parameter ξ produced similar results as whole data were

used. Therefore, the average values are adopted and used to analyze and compare with different types of parameters representing damage in the HMA and sand asphalt specimens.

DATA ANALYSIS FOR *S*

Dynamic creep test with HMA and DMA with sand asphalt samples are fabricated in dry and wet condition and then damage parameter *S* is calculated based on the results from the two laboratory experiments. Equations 2.17 and 2.18 in Chapter II are for the calculating damage parameter *S* which is calculated at each discrete cycle by obtaining the peak pseudo strain (ε_m^R or $\gamma_{m,i}^R$) and pseudo stiffness (C_i) corresponding time (t_i). Kim et al. (1995) suggested a method to predict the relaxation modulus of HMA from the calculated creep compliance $D'(t) = D_1 \times t^{n'}$ in creep test as shown in Equation 2.29 in Chapter II. Equation 2.19 also defined pseudo stiffness S^R in terms of peak pseudo strain and corresponding stress (Lee et al. 2000a). Based on the Equations 2.19 and 2.33, pseudo stiffness was calculated for dry and wet conditioned HMA. Pseudo stiffness in torsional mode stress is calculated by DMA with controlled-strain and measured stress.

The following Figure 8.12 illustrates that the stiffness calculated from HMA has similar features like it from sand asphalt with DMA. The initial stiffness, before applying stress, of the dry sample is bigger and the performance life is longer than wet conditioned sample as expected. After getting the pseudo stiffness from HMA and sand asphalt samples, it is easy to calculate damage parameter *S* by using Equations 2.17 and

2.18. There were reasonable experimental results when parameter *S* was used as a damage parameter to reflect conditions of damaged sand asphalt samples and compare with other steps and parameters. The calculated *S* from both dry and wet conditioned HMA with increasing stress shows similar results as ξ. In other words, the wet conditioned samples were damaged more than dry conditioned ones. In controlled-stress mode experiment such as dynamic creep test, the strain is increasing which results in the similar graph plots like Figure 8.6 when Equation 2.17 is used. Figure 8.13 depicts the changes of damage parameter *S* with increasing loading stress. Theoretically, the value *S* at the initial step (Step1) is set to zero. Figure 8.13, therefore, shows just the steps after starting damage procedures, that is, Step2, Step3, and Step4.

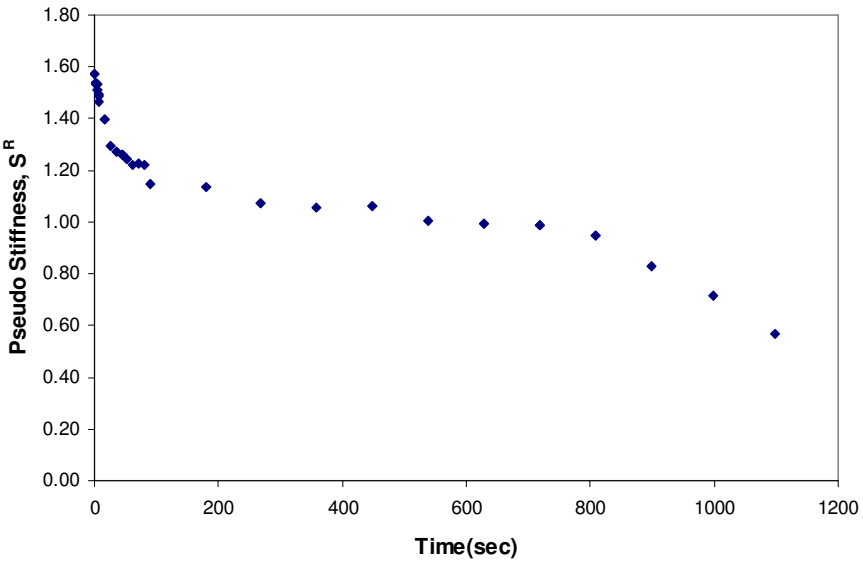

(a)

Figure 8.12. Plots of Pseudo Stiffness versus Loading Time in (a) Dry Condition and (b) Wet Condition.

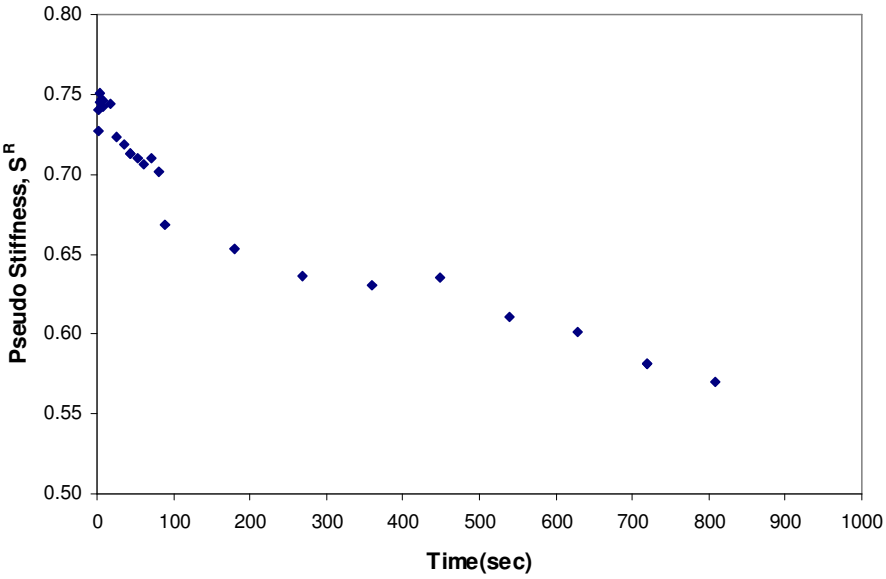

(b)

Figure 8.12. Continued.

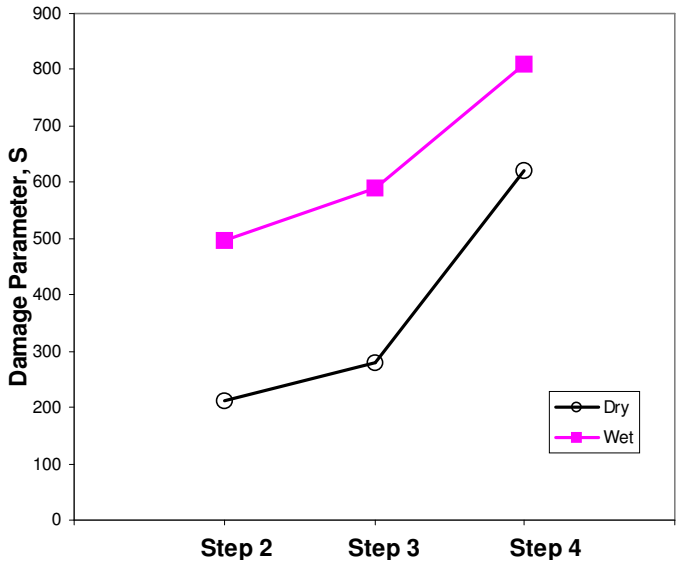

(a)

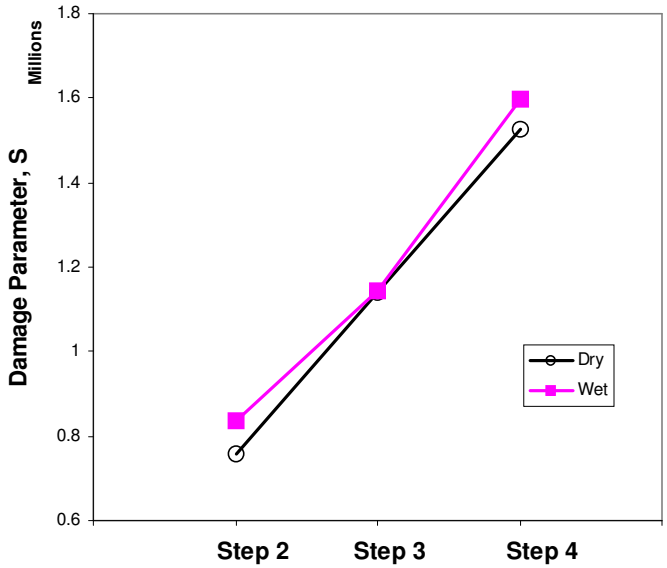

(b)

Figure 8.13. Damage Parameter *S* Changes at Each Damage Step in Dry and Wet Condition in (a) HMA and (b) Sand Asphalt.

DATA ANALYSIS FOR DPSE

Chapter VI described the DPSE by plotting the measured stress against pseudo strain. The sample undergoing fatigue testing exhibits hysteresis loop in both plotting of measure stress against physical strain and pseudo strain. The inner area of the hysteresis loop by plotting measured stress against pseudo strain is defined DPSE. As can be seen in Equation 2.26, the DPSE is composed of pseudo strain (ε^R) and changing stiffness of the material due to changes in microstructure of the material such as increasing damage and/or healing. Lee et al. (2000b) and Si et al. (2002) also explained the calculation of DPSE by obtaining pseudo strain for damaged nonlinear asphalt concrete as shown in Figure 2.5. DPSE which should be related to the fatigue fracture and healing can be used as a real damage indicator since it represents energy dissipation after eliminating material viscoelasticity.

Figure 8.14 shows the variations of DPSE in controlled-stress and controlled-strain mode each. Slope of variances in the early stage and in the final stage is stiffer than in the middle stage of growing damage. As shown in Figure 8.14 (a), HMA under controlled-stress increase DPSE with increasing pseudo strain values. On the contrary, controlled-strain loading mode decreases DPSE as displayed in Figure 8.14 (b). However, Figure 8.14 indicates that wet conditioned samples are more damaged than dry ones at every step as expected. The damage expressed by DPSE is independent of loading modes and can be used as an indicator for damage levels.

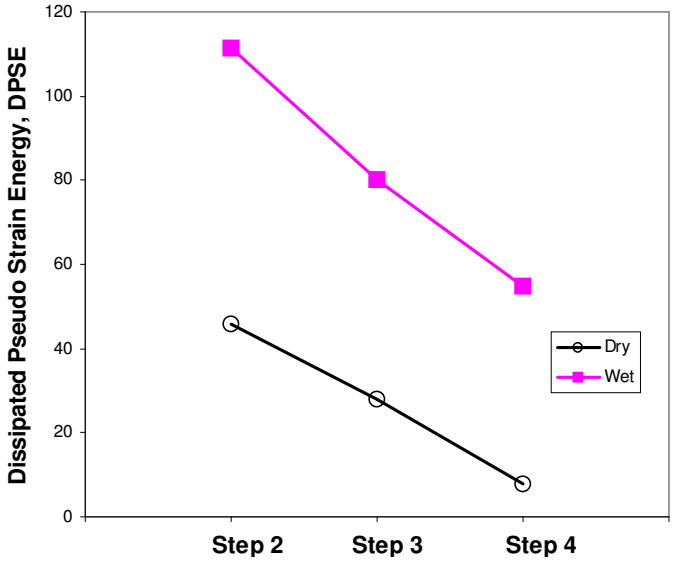

(a)

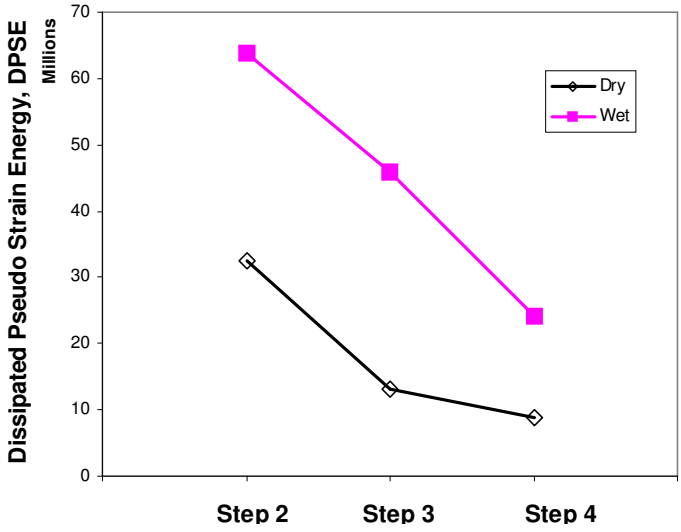

(b)

Figure 8.14. DPSE W^R Changes at Each Damage Step in Dry and Wet Condition in (a) HMA and (b) Sand Asphalt.

SURFACE AREA PARAMETER AND AVERAGE RADIUS

"Surface Area Parameter" and "Average Radius" are added to the three parameters. The "Surface Area Parameter" is defined as average of void perimeters summation as Equation 8.2. Equation 8.3 is used for "Average Radius".

$$Surface\ Area\ Parameter = \frac{1}{n}\sum_{i=1}^{n}\frac{P_i}{\pi \cdot r_i^2} \tag{8.2}$$

Where n = number of air voids and cracks, and

P = perimeter of each void and crack.

$$Average\ Radius = \sqrt{\frac{\sum_{i=1}^{n} A_i}{n \cdot \pi}} \tag{8.3}$$

Where A = area of each void and crack.

Figures 8.15 (a) and 8.16 (a) show HMA surface area parameter and average radius at each damage step in dry and wet conditioned specimens. The calculated values of the two parameters in sand asphalt are plotted in Figures 8.15 (b) and 8.16 (b) as well. As expected, the values are increasing with increasing accumulated damage in both dry and wet conditioned samples. All the wet specimens have experienced high damage. All the following four figures showed rapid changes between at the first step and at the second step in wet conditioned samples as shown in previous results of Figures 8.4 and 8.9.

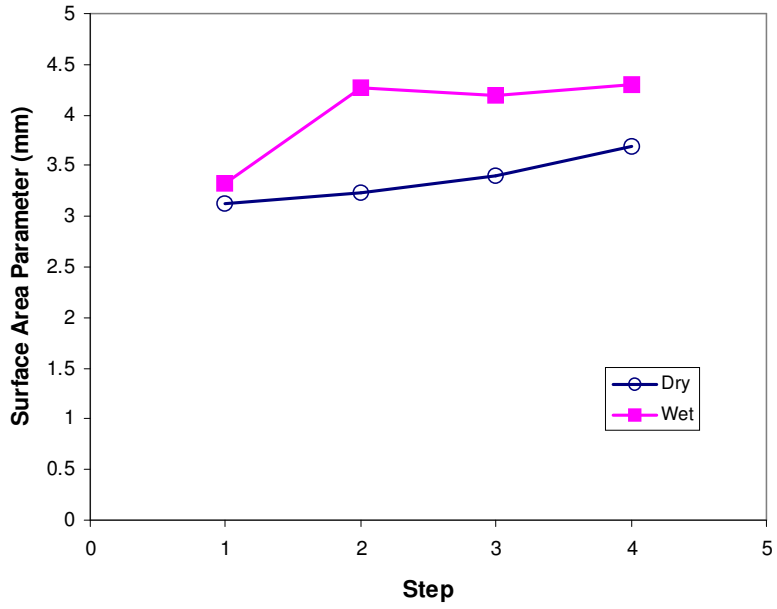

(a)

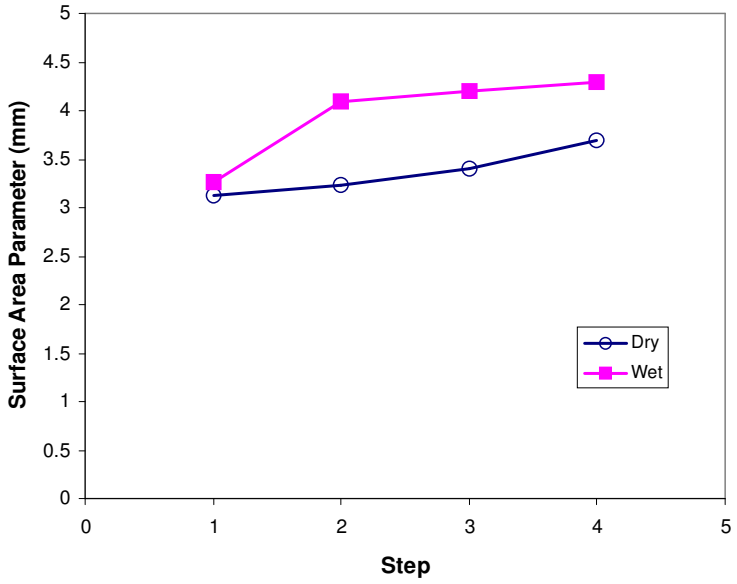

(b)

Figure 8.15. Calculated Surface Area Parameter from (a) HMA and (b) Sand Asphalt at Each Damage Step.

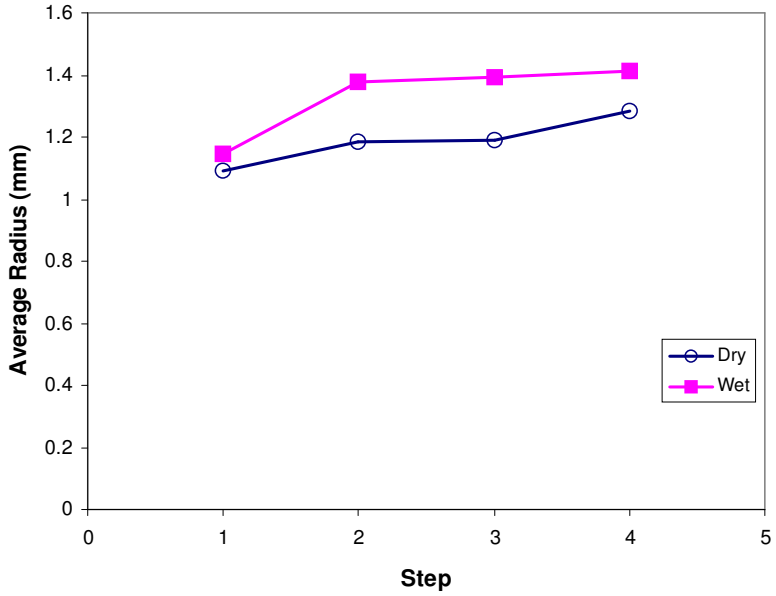

(a)

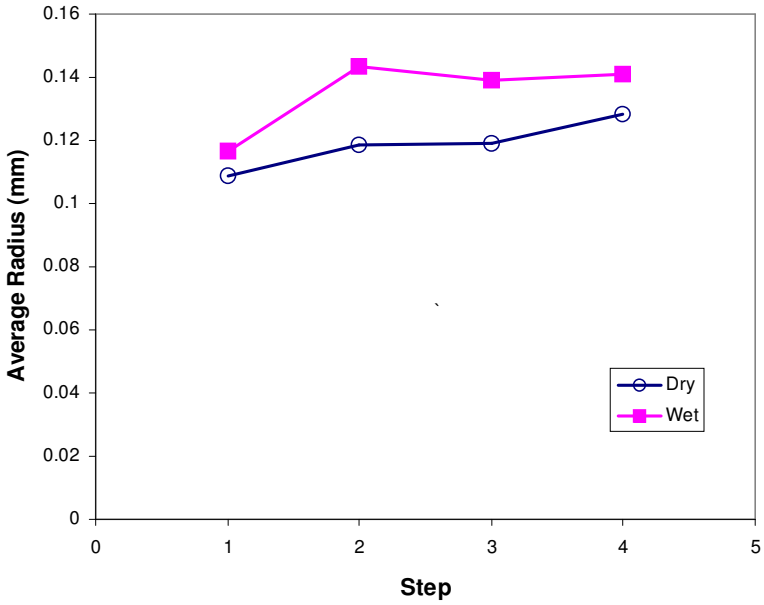

(b)

.

Figure 8.16. Calculated Average Radius from (a) HMA and (b) Sand Asphalt at Each Damage Step.

THE RATIO OF DAMAGE INDICATOR

The pseudo stiffness values from each dynamic test were used for calculating the percentage of aggregate surface area that is replaced by moisture (P_i) with previously determined adhesive surface energies both under dry and wet condition as shown in Equation 8.5. Figures 8.17 and 8.18 show the results of ratio of damage indicator at each damage step and the percentage of the aggregate surface area that has been exposed to water.

Cheng (2002) defined the ratio of stiffness under wet conditions to stiffness under dry conditions by the work of adhesion ratio between asphalt and aggregate in wet and dry conditions. The stiffness ratio in dynamic creep and DMA test is defined by normalized pseudo stiffness as shown in Equation 8.4.

$$\frac{NS_{i,w}^{R}}{NS_{i,d}^{R}} = \frac{\Delta G_d^a (1 - P_i) + \Delta G_w^a P_i}{\Delta G_d^a} \tag{8.4}$$

Where $NS_{i,d}^{R}$ = normalized pseudo stiffness under dry condition at i th cycle,

$NS_{i,w}^{R}$ = normalized pseudo stiffness under wet condition at i th cycle,

ΔG_d^a = bond energy of adhesion between asphalt and aggregate under dry condition,

ΔG_w^a = bond energy of adhesion between asphalt and aggregate under wet condition, and

P_i = percentage of surface area of the aggregate that is replaced by water in the

mixture.

The Equation 8.4 can be expressed for P_i as shown:

$$P_i = \frac{\Delta G_d^a \left(\frac{NS_{i,w}^R}{NS_{i,d}^R} - 1\right)}{\Delta G_w^a - \Delta G_d^a} \tag{8.5}$$

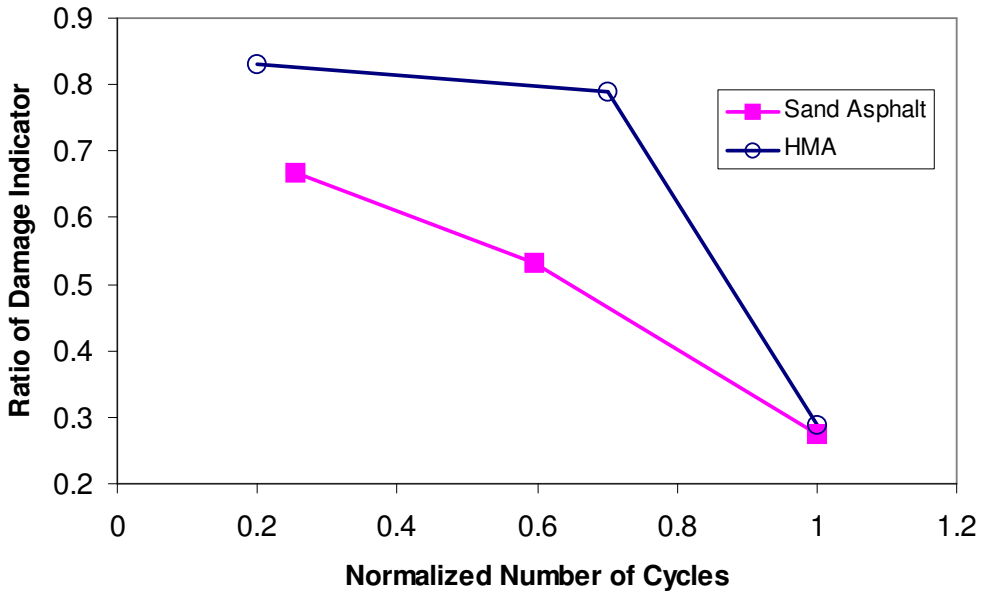

Figure 8.17. Ratio of Damage Indicator at Each Damage Step.

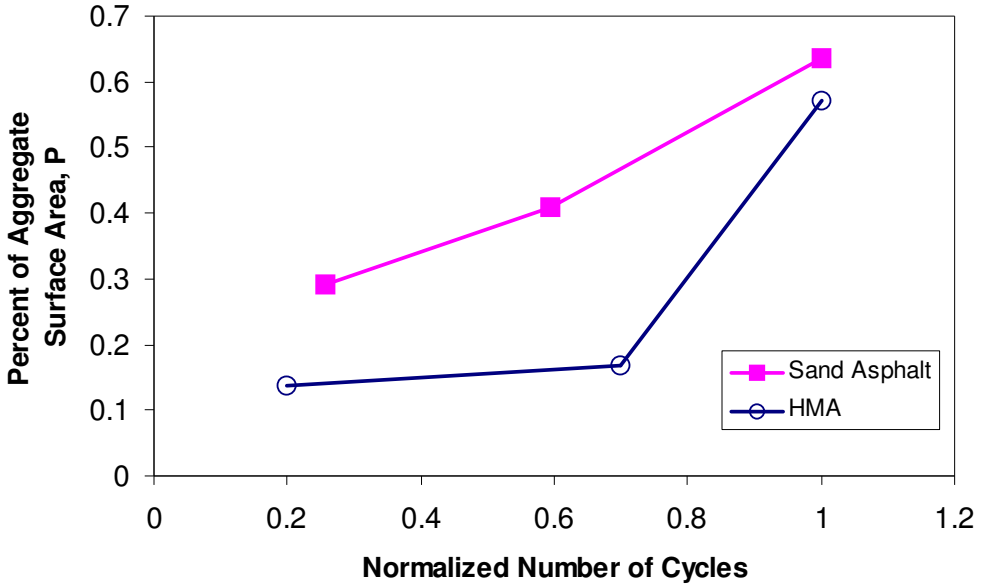

Figure 8.18. Percentage of the Aggregate Surface Area Exposed to Water at Each Damage Step.

CHARACTERIZING DAMAGE IN ASPHALT MIXTURES BY DAMAGE PARAMETER RELATIONSHIP (METHOD I)

Detailed comparison methods among damage indicators were presented in Chapter VI. As shown in Figure 6.9, the first method for characterizing damage in asphalt mixtures is direct comparisons between the same parameters from HMA and sand asphalt.

Both HMA and sand asphalt specimens under dynamic stress were used to get the three damage indicators ξ, *S,* and DPSE. The concept of the parameters was introduced and their values were plotted in the previous figures. The results from HMA are correlated to those from sand asphalt samples by means of the three damage indicators as shown in Tables 8.4, 8.5, Figures 8.19, 8.20, and 8.21.

Figure 8.19 shows damage parameter ξ from X-ray CT at different four states in dry and wet condition. The results from HMA and sand asphalt specimens show that they increase in number as shown previously. There is a good agreement between HMA and sand asphalt results for ξ. As explained early, damage in both HMA and sand asphalt increase rapid in the early and end stages while middle stages are almost same states or shows slow increases. Figure 8.20 displays damage parameter *S* from the two dynamic mechanical tests. The results from HMA agree well with calculated values in sand asphalt. Each state of damage shows similar slopes variances in dry and wet conditioned samples as shown in Figure 8.20. Figure 8.21 shows the variation of DPSE during the change of damage states in dry and wet condition. To compare results from different stress mode in a graph, values from HMA are expressed in reverse order in the

figures. There are also good agreements between HMA and sand asphalt results in the two conditions.

Table 8.4. Correlation of HMA and Sand Asphalt in Dry Condition.

Sand \ HMA	ξ	S	DPSE
ξ	0.8823	-	-
S	-	0.9894	-
W^R	-	-	0.9924

Table 8.5. Correlation of HMA and Sand Asphalt in Wet Condition.

Sand \ HMA	ξ	S	DPSE
ξ	0.9962	-	-
S	-	0.9487	-
W^R	-	-	0.7561

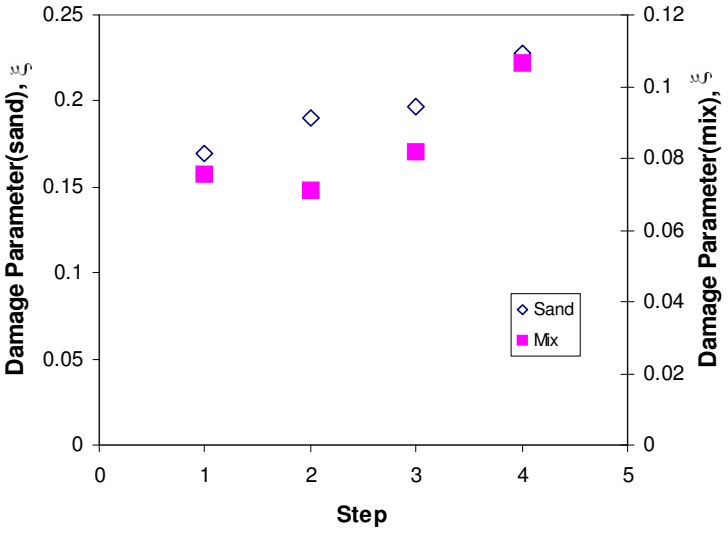

(a)

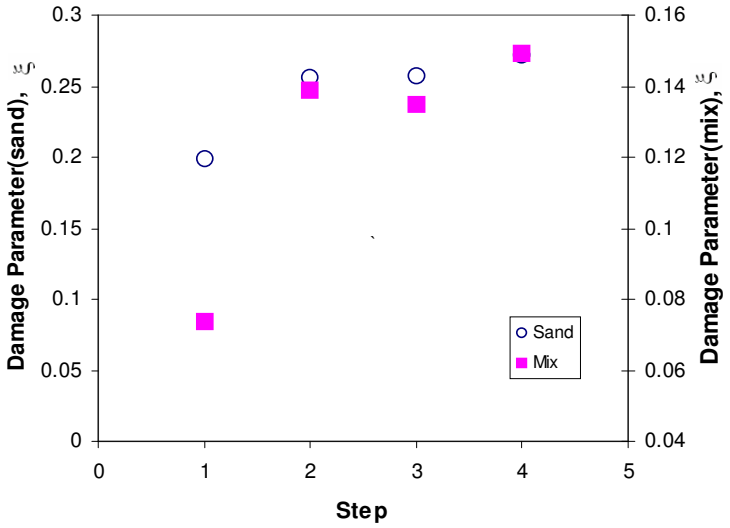

(b)

Figure 8.19. Comparison of Damage Parameter ξ from HMA and Sand Asphalt in (a) Dry Condition and (b) Wet Condition.

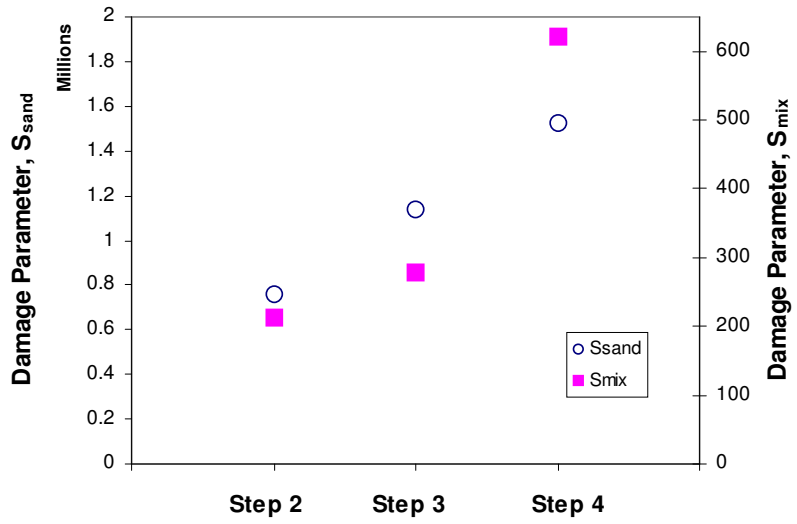

(a)

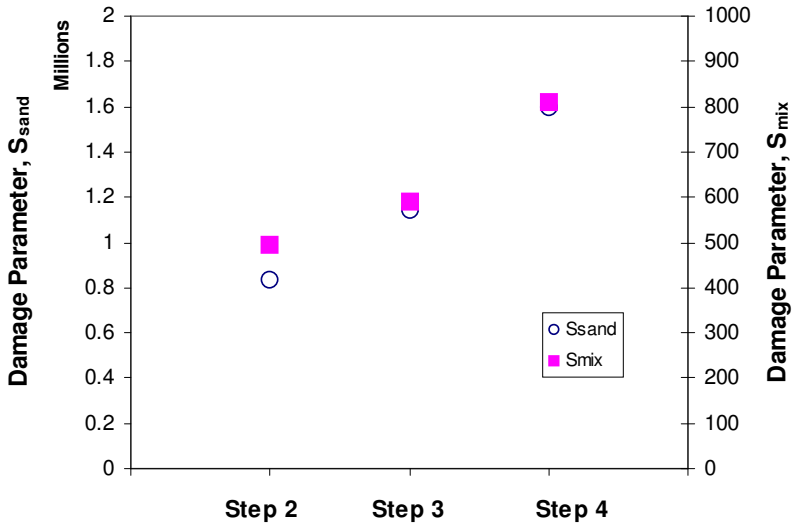

(b)

Figure 8.20. Comparison of Damage Parameter *S* from HMA and Sand Asphalt in (a) Dry Condition and (b) Wet Condition.

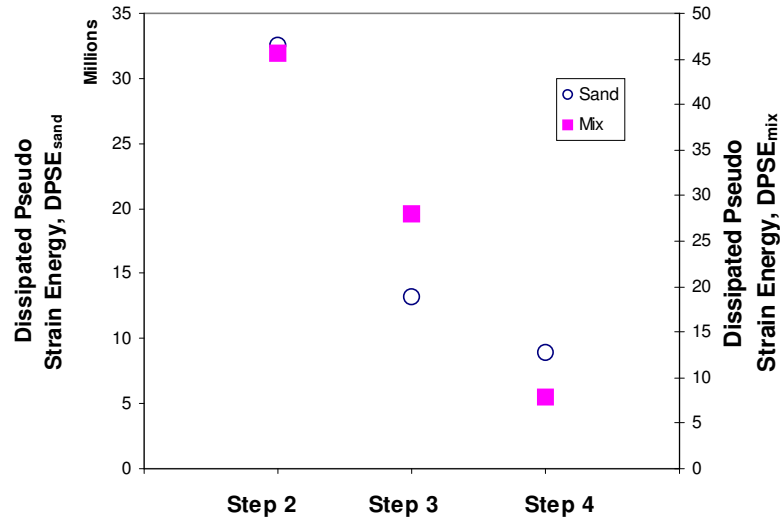

(a)

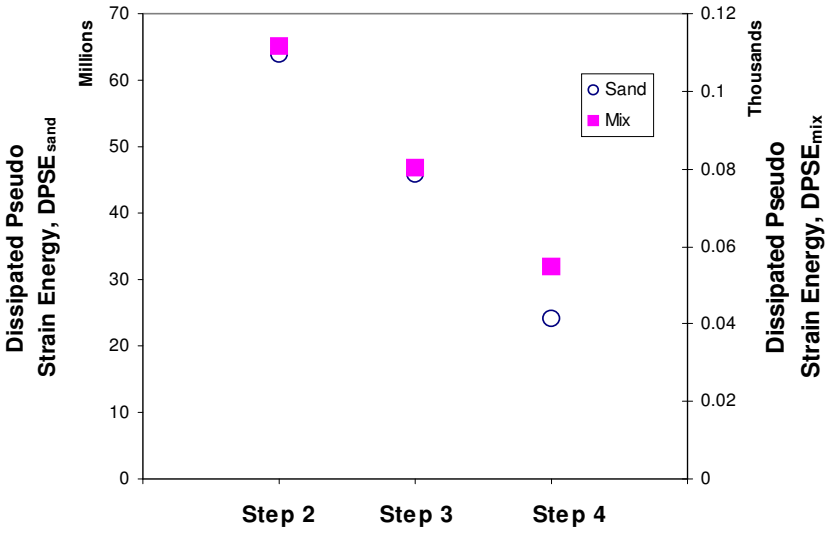

(b)

Figure 8.21. Comparison of DPSE from HMA and Sand Asphalt in (a) Dry Condition and (b) Wet Condition.

CORRELATE PARAMETERS AT SAME DAMAGE STATES (METHOD II)

Chapter VI introduced the second characterizing the method with Figure 6.10. As shown in the figure, the method relates one parameter from HMA to the other different damage indicators results from sand asphalt and vice versa. This method does not compare the same parameters, but between the different ones. Parameter ξ from X-ray CT is compared with the parameters, *S* and DPSE, from DMA to see whether or not the parameters can explain the damage progressions acquired by X-ray CT.

Correlation of ξ with *S* and DPSE in Sand Asphalt

DMA has been used to characterize material properties and fatigue life, which is a simple mechanical testing can be used to characterize damage states in asphalt mixtures. In this research, the mechanical testing results are shown and correlated with each other. Finally, DMA testing can substitute for X-ray CT method if the relation between DMA and X-ray CT result is defined.

Figure 8.22 presents that average parameter value of ξ at each state in dry and wet condition agree well with *S* from sand asphalt.

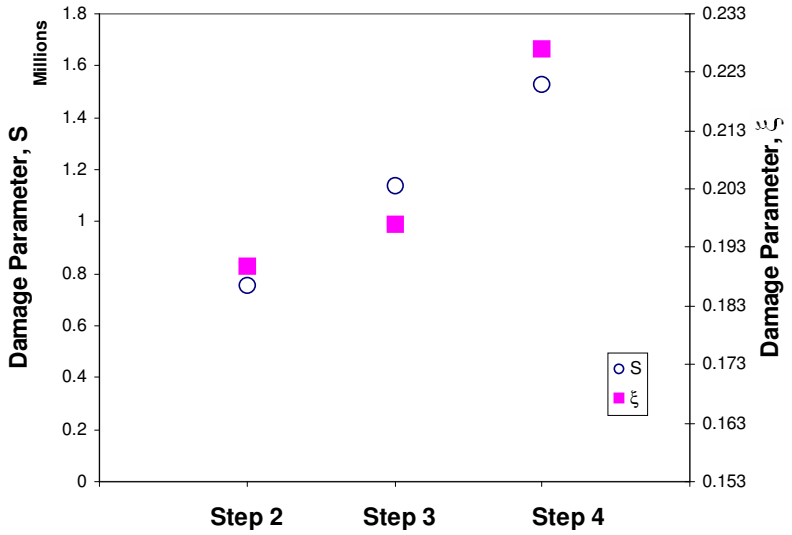

(a)

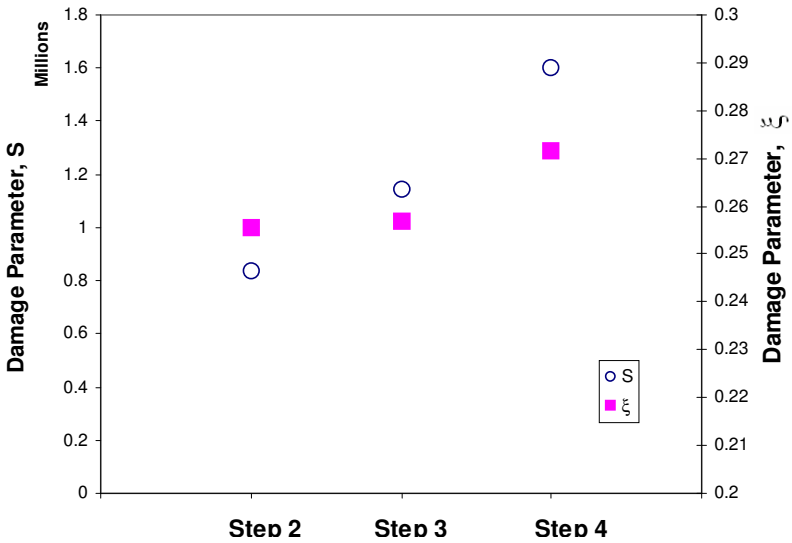

(b)

Figure 8.22. Damage Parameter *S* versus ξ in Sand Asphalt in (a) Dry Condition and (b) Wet Condition.

DPSE is plotted with ξ at each state in dry and wet condition as illustrated in Figure 8.23. The relationship in dry condition is better than wet condition. Better results are acquired at Step2 and Step3.

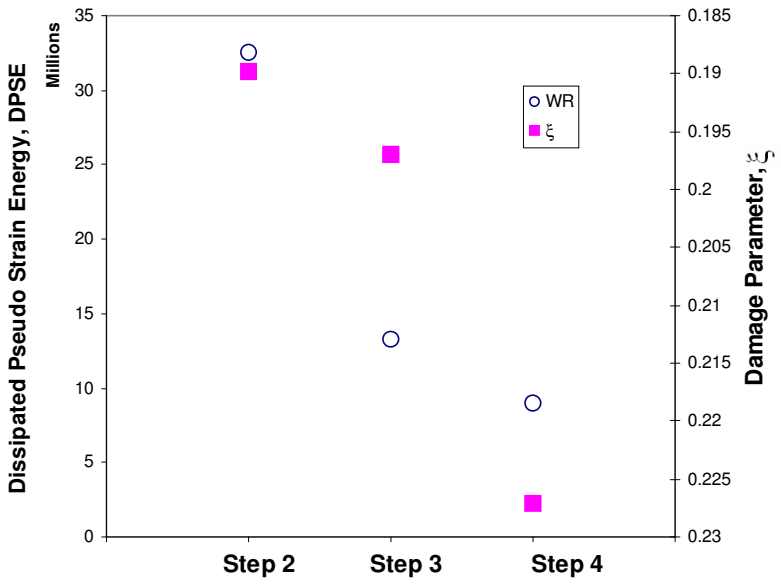

(a)

Figure 8.23. DPSE versus ξ in Sand Asphalt in (a) Dry Condition and (b) Wet Condition.

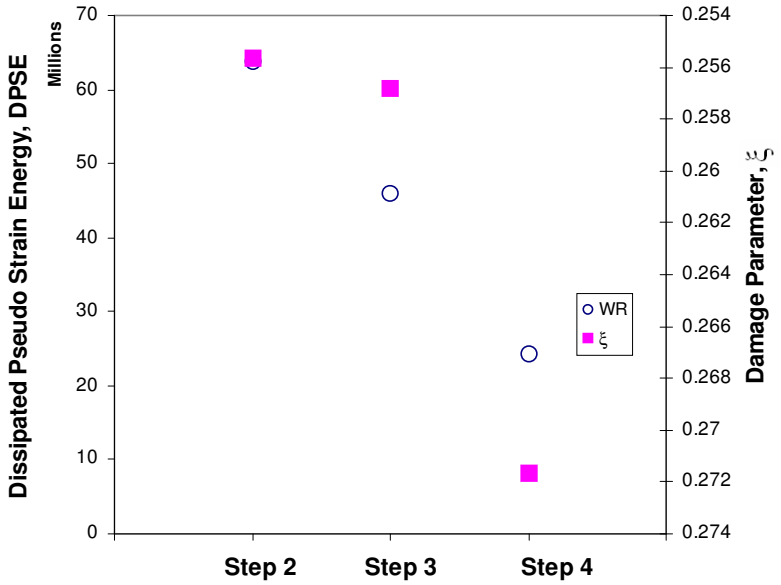

(b)

Figure 8.23. Continued.

Correlation of ξ in HMA with *S* and DPSE in Sand Asphalt

The average values of damage parameter ξ at each damage step from HMA are presented below in Figures 8.24 and 8.25 with *S* and DPSE from sand asphalt. All the three parameters are plotted for the relationship between results from X-ray CT and DMA. Expecting damage parameter ξ in HMA by *S* and DPSE in sand asphalt makes possible to verify and/or compare the results in Figures 8.22 and 8.23.

Figure 8.24 displays the damage parameter *S* in sand asphalt plots on parameter ξ in HMA with both dry and wet conditioned specimens. Calculated parameter DPSE from DMA is compared to ξ in HMA in Figure 8.25.

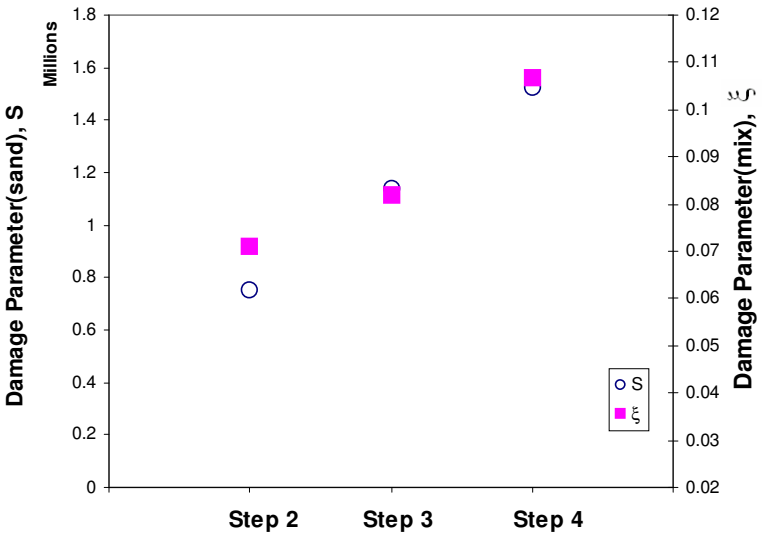

(a)

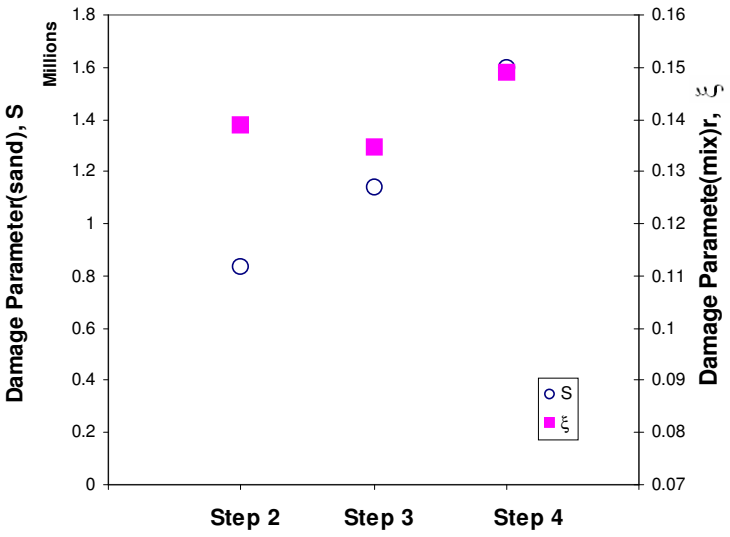

(b)

Figure 8.24. Damage Parameter *S* in Sand Asphalt versus ξ in HMA in (a) Dry Condition and (b) Wet Condition.

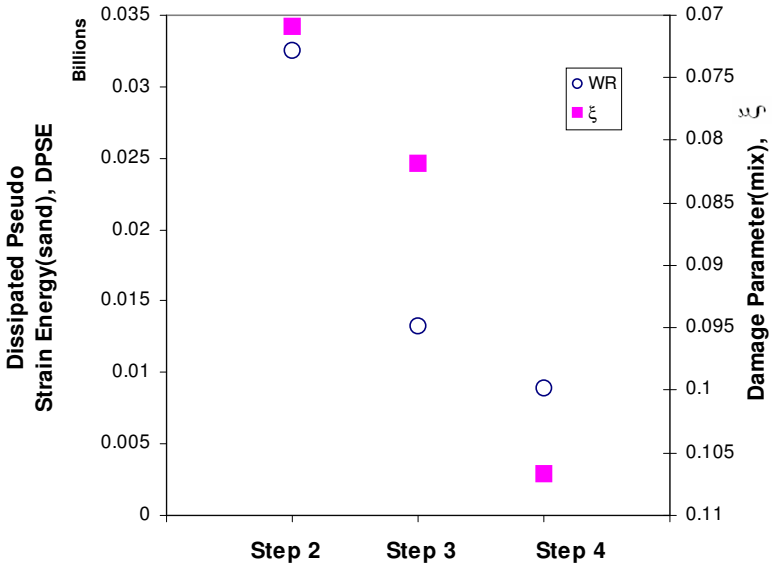

(a)

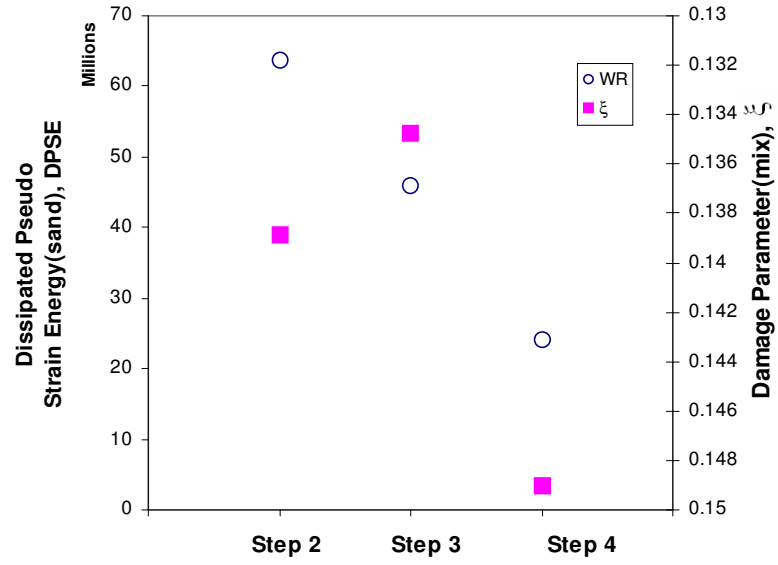

(b)

Figure 8.25. DPSE in Sand Asphalt versus ξ in HMA in (a) Dry Condition and (b) Wet Condition.

EXPECTING ASPHALT CONCRETE PAVEMENT PERFORMANCE IN TERMS OF DAMAGE PARAMETER ξ, *S*, and DPSE

Generally, to relate mechanical properties to predict pavement performance or distress, modulus of materials or stiffness have been used for permanent deformation and fatigue cracking. Modulus of a material is an important property to predict material distress by stress. Kim (2003) showed and defined fatigue life by means of material stiffness loss due to fatigue damage accumulation. Witczak et al. (2002), however, used creep compliance, D(t), to relate stress to strain and noted that using compliance is more advantageous than the modulus for viscoelastic materials since it separates time-dependent components.

Tables 8.6 and 8.7 show the correlations of each parameter from sand asphalt in dry and wet condition. Tables 8.8 and 8.9 show the variances of normalized parameter values.

Table 8.6. Correlation of Each Parameter from Sand Asphalt in Dry Condition.

	ξ	G^*	*S*	DPSE
ξ	1.0000	0.9950	0.9535	0.9996
G^*	-	1.0000	0.9642	0.9977

Table 8.7. Correlation of Each Parameter from Sand Asphalt in Wet Condition.

	ξ	G^*	S	DPSE
ξ	1.0000	0.9784	0.9616	0.6217
G^*	-	1.0000	0.9642	0.9977

Table 8.8. Variance of Normalized Parameter Value from Sand Asphalt in Dry Condition.

	ξ	G^*	S	DPSE
ξ	1.0000	0.1000	0.2289	0.1139
G^*	-	1.0000	0.0966	0.0012

Table 8.9. Variance of Normalized Parameter Value from Sand Asphalt in Wet Condition.

	ξ	G^*	S	DPSE
ξ	1.0000	0.1565	0.2544	0.0489
G^*	-	1.0000	0.0142	0.1199

From Figure 8.26 to Figure 8.31, results from damage parameter ξ, *S*, and DPSE are plotted on the original graph plots from the mechanical testings such as dynamic creep and DMA. Once the plots show well agreements with D(t) and G*, the parameters representing damage can substitute for them so that DMA mechanical test method can be used for X-ray CT or even HMA test in terms of calculated DMA results such as *S*, and DPSE.

Figures 8.26, 8.27, and 8.28 plotted the parameter ξ, *S,* and DPSE at each state on the stiffness G* calculated from DMA in both dry and wet conditioned sand asphalt. The results show that all the three parameters follow the same trend as the calculated stiffness by DMA. As can be seen in the figures, the G* explains relatively well the parameter ξ and dry conditioned samples show better agreements as well.

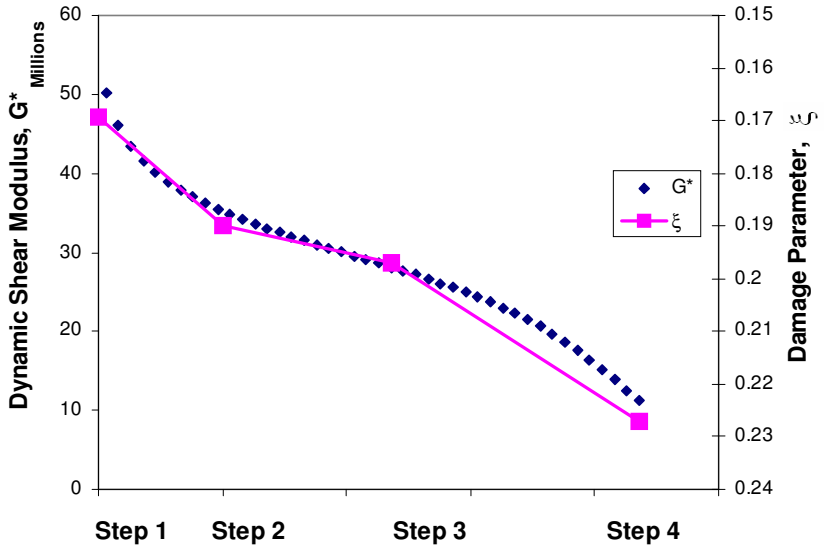

(a)

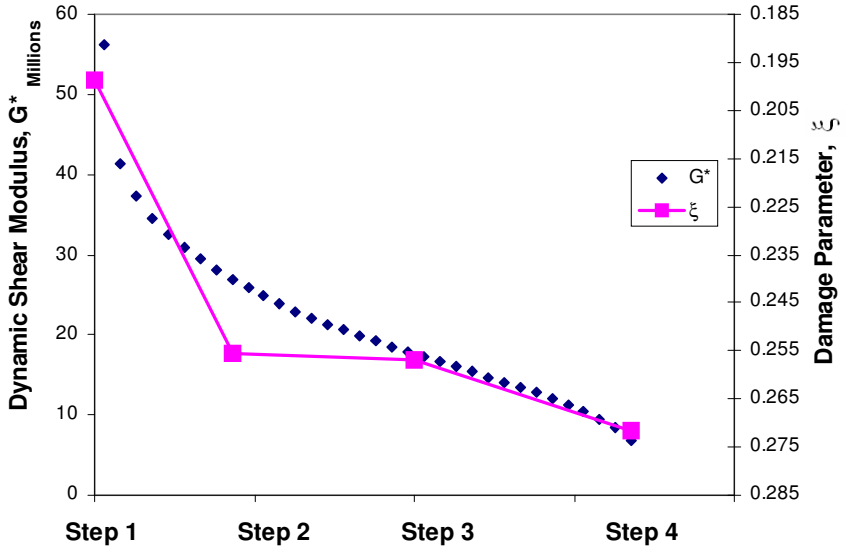

(b)

Figure 8.26. Comparison of Damage Parameter ξ and Stiffness G* from DMA in (a) Dry Condition and (b) Wet Condition.

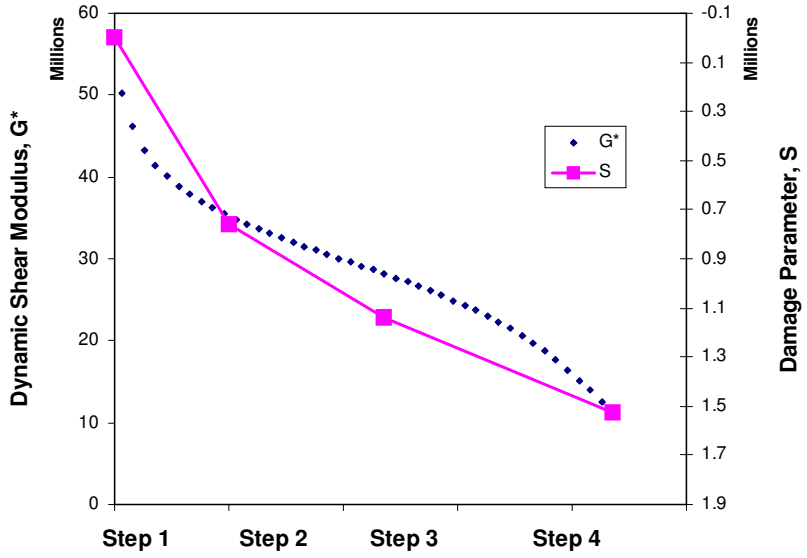

(a)

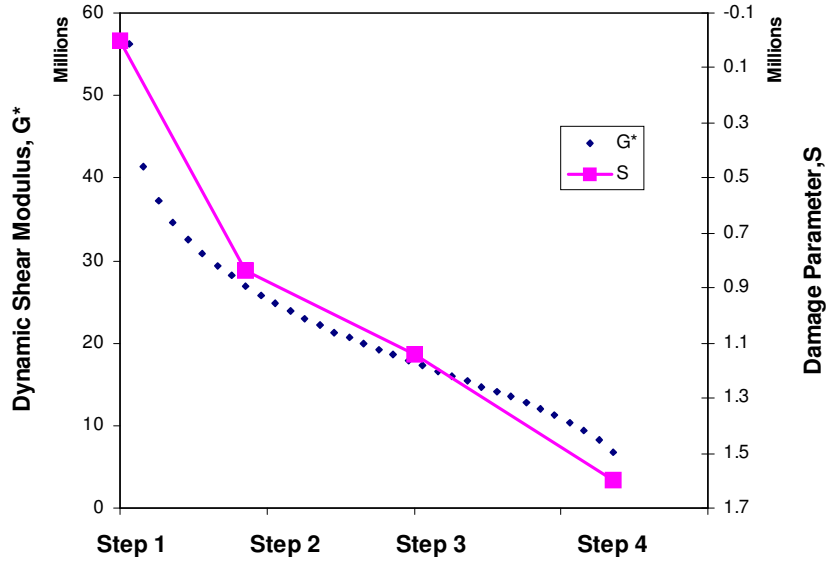

(b)

Figure 8.27. Comparison of Damage Parameter *S* and Stiffness G* from DMA in (a) Dry Condition and (b) Wet Condition.

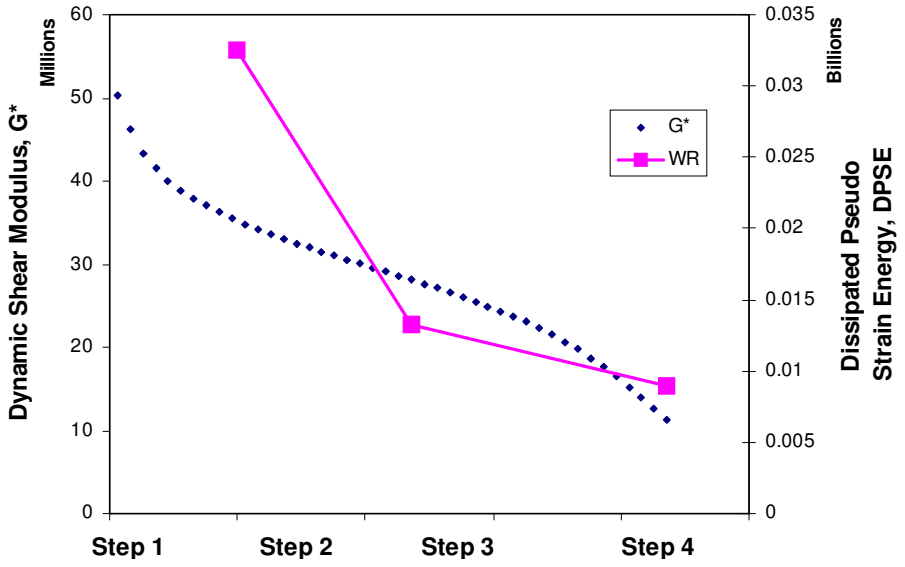

(a)

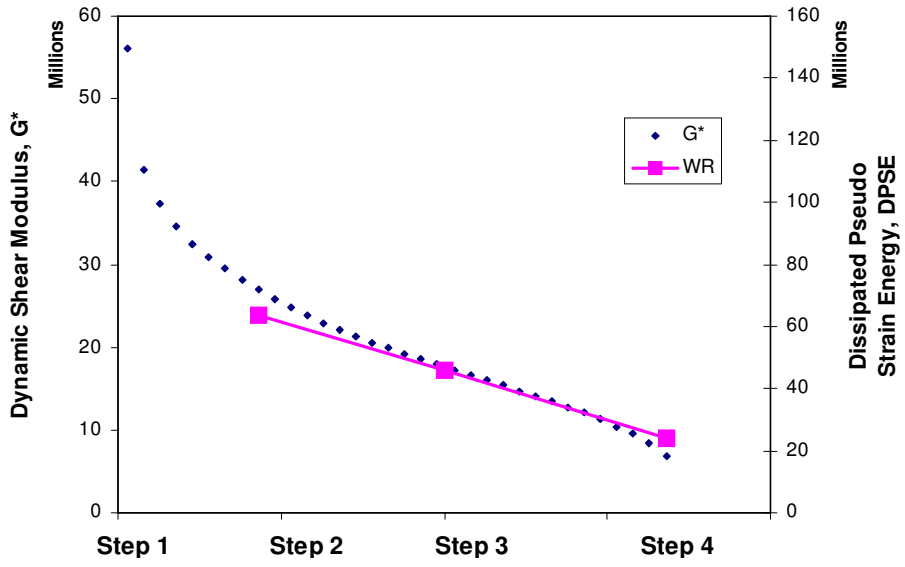

(b)

Figure 8.28. Comparison of Damage Parameter DPSE and Stiffness G* from DMA in (a) Dry Condition and (b) Wet Condition.

Tables 8.10 and 8.11 show the correlations of each parameter from HMA in dry and wet condition. Tables 8.12 and 8.13 show the variances of normalized parameter values.

Table 8.10. Correlation of Each Parameter from HMA in Dry Condition.

	ξ	*D(t)*	*S*	DPSE
ξ	1.0000	0.9155	0.6791	0.8165
D(t)	-	1.0000	0.9083	0.9797

Table 8.11. Correlation of Each Parameter from HMA in Wet Condition.

	ξ	*D(t)*	*S*	DPSE
ξ	1.0000	0.8282	0.8180	0.8722
D(t)	-	1.0000	0.9981	0.9962

Table 8.12. Variance of Normalized Parameter Value from HMA in Dry Condition.

	ξ	*D(t)*	*S*	DPSE
ξ	1.0000	0.0835	0.1682	0.3002
D(t)	-	1.0000	0.0377	0.0405

Table 8.13. Variance of Normalized Parameter Value from HMA in Wet Condition.

	ξ	*D(t)*	*S*	DPSE
ξ	1.0000	0.0347	0.2671	0.3206
D(t)	-	1.0000	0.1373	0.1619

Figures 8.29, 8.30, and 8.31 plotted the parameter ξ, *S,* and DPSE at each state on the creep compliance D(t) calculated from dynamic creep test in both dry and wet conditioned HMA.

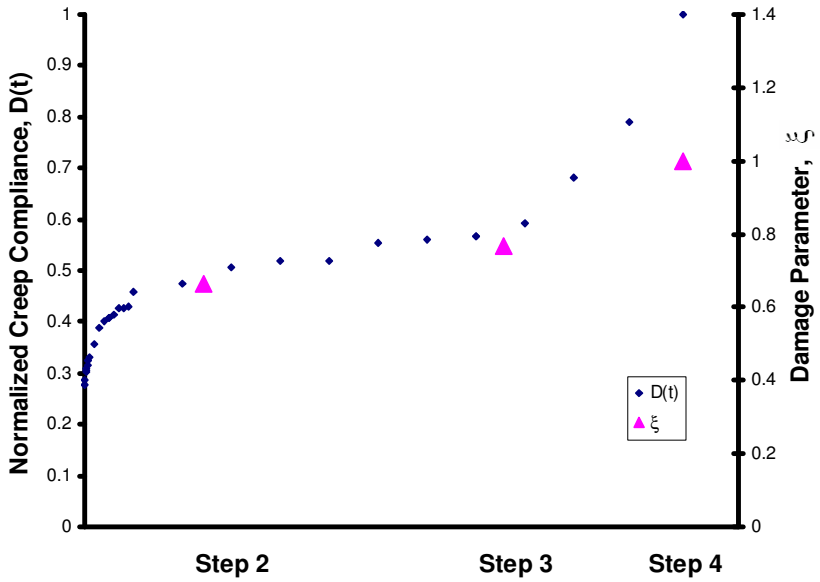

(a)

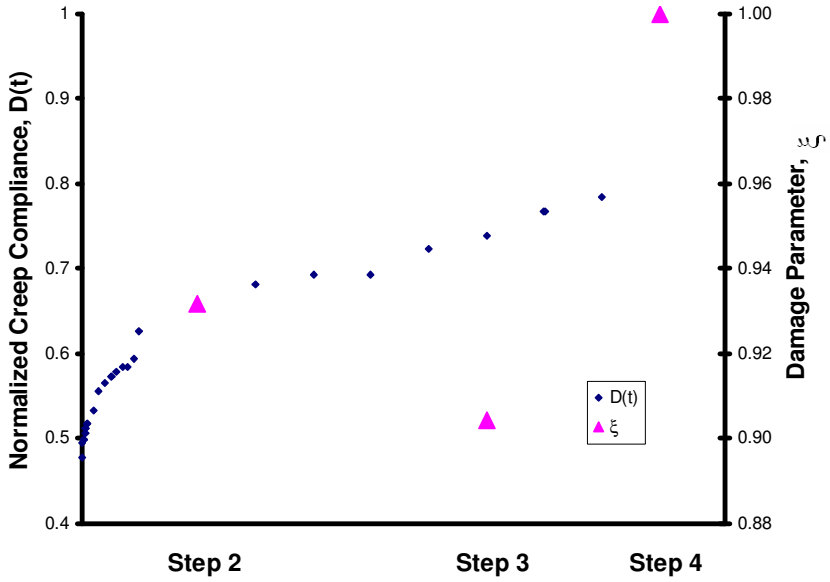

(b)

Figure 8.29. Comparison of Damage Parameter ξ and Creep Compliance D(t) from Dynamic Creep Test in (a) Dry Condition and (b) Wet Condition.

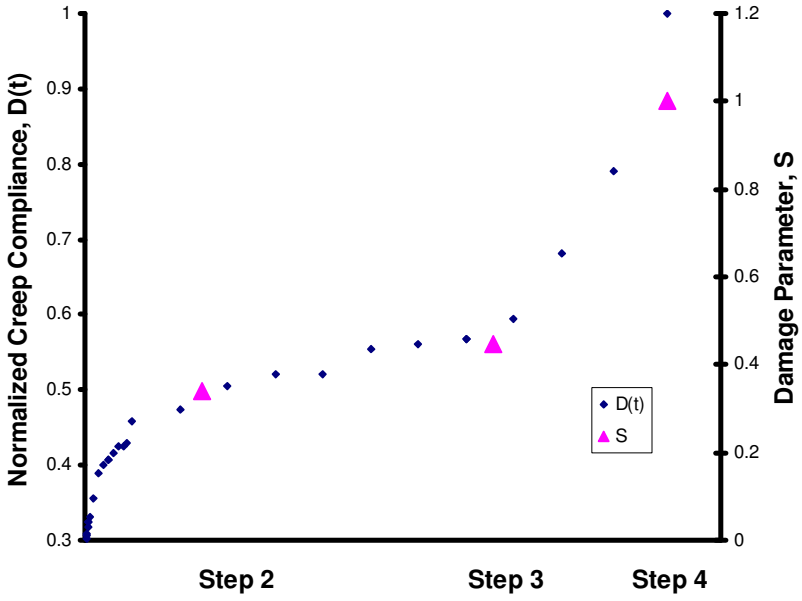

(a)

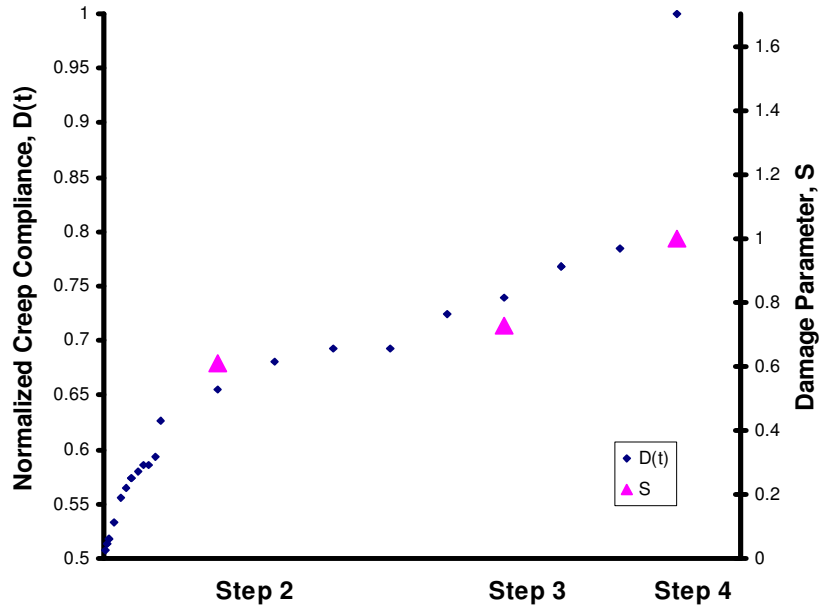

(b)

Figure 8.30. Comparison of Damage Parameter *S* and Creep Compliance D(t) from Dynamic Creep in (a) Dry Condition and (b) Wet Condition.

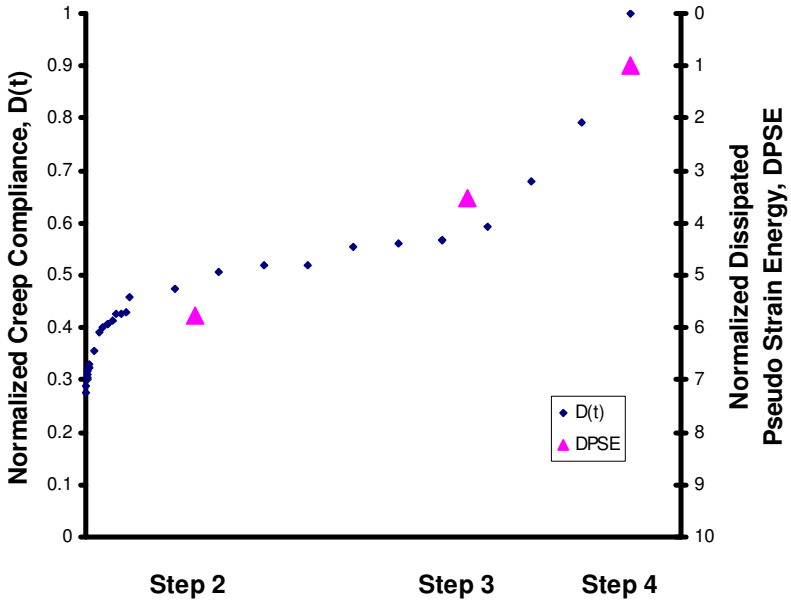

(a)

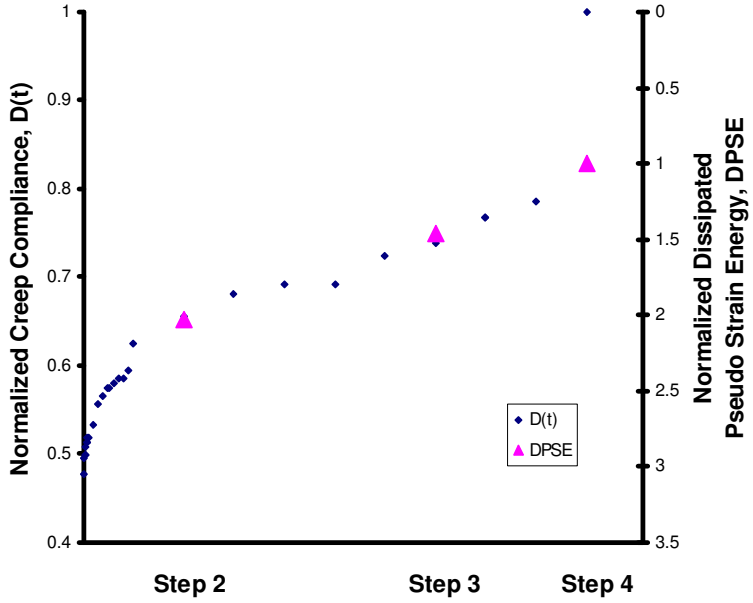

(b)

Figure 8.31. Comparison of DPSE and Creep Compliance D(t) from Dynamic Creep in (a) Dry Condition and (b) Wet Condition.

MICROMECHANICS COHESIVE AND ADHESIVE MODEL (METHOD III)

The properties of the fine and coarse aggregate define the aggregate matrix. If the aggregate shape, form, and texture properties of the matrix as well as the adhesive bond strength between the mastic and aggregate are known, then the impact of the aggregate matrix can be integrated with the impact of the mastic to assess damage. The adhesive bond between the mastic and the aggregate can be calculated based on bond energy measurements of these components to assess the potential for adhesive fracture or debonding in the dry state or in the presence of moisture.

Lytton (2004) developed equations, based on micromechanical analysis of cohesive and adhesive damage in asphalt-aggregates mixture, for the ratio of the damaged modulus to the undamaged modulus of the binder. Mechanical and chemical asphalt properties, i.e., stiffness, stress, and bond energy, were used to see the relation between damaged and undamaged modulus of asphalt. Lytton (2004) showed dependence of mixture stiffness and strength on film thickness with the equations of cohesive and adhesive fracture for the relationship. A thin film of asphalt of thickness, t, between two platens with a cross-sectional area, A, and subjected to a constant strain loading will have the relation between damaged E' and undamaged modulus E for cohesive fracture as shown in Equation 8.6. All the cracks on the cross-sectional area are assumed circular plan view.

$$\frac{E'}{E} = \left[1 - 2\pi^2 \left(\frac{m}{A}\right) \frac{\bar{c}^3}{t} \left(1 - \frac{E\Delta G_f^c}{\pi\sigma^2 \bar{c}}\right)\right] \tag{8.6}$$

Where t = the film thickness, and

ΔG_f^c = the total cohesive fracture bond energy of the asphalt.

The average number of cracks m can be calculated on cross-sectional areas by obtaining damage parameter ξ and mean crack radius $\bar{c}$ from X-ray CT. Once the parameter ξ is calculated in Equations 2.6 and 2.7, the number of cracks is simply obtained by following Equation 8.7.

$$m = \xi \frac{A}{\pi \bar{c}^2} \tag{8.7}$$

The asphalt cement film thickness t is calculated using the following equation (Roberts et al. 1996):

$$t = \frac{V_{asp}}{SA \cdot W_{agg}} \times 1000 \tag{8.8}$$

Where t = average film thickness (microns),

V_{asp} = effective volume of asphalt cement (liters),

SA = surface area of the aggregate (m^2/kg of aggregate), and

W_{agg} = weight of aggregate (kg).

Following Equation 8.9 defines the stress σ with constant strain ε_0 for the Equation 8.6.

$$\sigma = E\varepsilon_0 \tag{8.9}$$

Equation 8.10 shows the modulus relation between the damaged and the undamaged modulus for adhesive fracture under constant strain loading.

$$\frac{E_f^{'}}{E_f} = \left\{1 - \pi^2 \left(\frac{m}{A}\right) \frac{\bar{c}^3}{t} \left[\left(1 + \frac{E_f}{E_s}\right) - \frac{4E_f\left(\Delta G_f^a\right)}{\pi\sigma^2 \bar{c}}\right]\right\}$$

(8.10)

Where E_f, E_s = the modulus of the fluid (asphalt) and the solid (aggregate),

Respectively, and

ΔG_f^a = the total adhesive fracture bond energy of the material.

Equation 8.11 shows the modulus relation between the damaged and the undamaged modulus for cohesive fracture under constant stress loading.

$$\frac{E}{E'} = \left[1 + 2\pi^2 \left(\frac{m}{A}\right) \frac{\bar{c}^3}{t} \left(1 - \frac{E\Delta G_f^c}{\pi\sigma^2 \bar{c}}\right)\right] \tag{8.11}$$

Equation 8.12 shows the modulus relation between the damaged and the undamaged modulus for adhesive fracture under constant stress loading.

$$\frac{E_f}{E_f^{'}}=\left\{1+\pi^2\left(\frac{m}{A}\right)\frac{\bar{c}^3}{t}\left[\left(1+\frac{E_f}{E_s}\right)-\frac{4E_f\left(\Delta G_f^a\right)}{\pi\sigma^2\bar{c}}\right]\right\} \tag{8.12}$$

Applying the definitions above for the shear stress mode, the four equations can be rewritten as Table 8.14.

Table 8.14. Cohesive and Adhesive Fracture Equations in Shear Stress Mode Loading.

Loading	Fracture Mode	Equation
Strain Controlled	Cohesive	$\frac{G'}{G}=\left[1-2\pi^2\left(\frac{m}{A}\right)\frac{\bar{c}^3}{t}\left(1-\frac{G\Delta G_f^c}{\pi\tau^2\bar{c}}\right)\right]$
	Adhesive	$\frac{G_f^{'}}{G_f}=\left\{1-\pi^2\left(\frac{m}{A}\right)\frac{\bar{c}^3}{t}\left[\left(1+\frac{G_f}{G_s}\right)-\frac{4G_f\left(\Delta G_f^a\right)}{\pi\tau^2\bar{c}}\right]\right\}$
Stress Controlled	Cohesive	$\frac{G}{G'}=\left[1+2\pi^2\left(\frac{m}{A}\right)\frac{\bar{c}^3}{t}\left(1-\frac{G\Delta G_f^c}{\pi\tau^2\bar{c}}\right)\right]$
	Adhesive	$\frac{G_f}{G_f^{'}}=\left\{1+\pi^2\left(\frac{m}{A}\right)\frac{\bar{c}^3}{t}\left[\left(1+\frac{G_f}{G_s}\right)-\frac{4G_f\left(\Delta G_f^a\right)}{\pi\tau^2\bar{c}}\right]\right\}$

Cheng (2002) presented the bond energy of cohesion (ΔE_f^c and ΔG_f^c) and adhesion (ΔE_f^a) under dry and wet condition. The cohesive and adhesive bond energy

values from Cheng (2002) for binder and mixtures were adopted and the adhesive values for sand asphalt (ΔG_f^a) were calculated based on the following Equations 8.13, 8.14 and Table 8.15.

$$\Delta G_d^a = 2\left(\sqrt{\Gamma_b^{LW}\Gamma_a^{LW}} + \sqrt{\Gamma_b^+\Gamma_a^-} + \sqrt{\Gamma_b^-\Gamma_a^+}\right) \tag{8.13}$$

$$\Delta G_w^a = 2\Gamma_w^{LW} + 2\sqrt{\Gamma_b^{LW}\Gamma_a^{LW}} - 2\sqrt{\Gamma_b^{LW}\Gamma_w^{LW}} - 2\sqrt{\Gamma_a^{LW}\Gamma_w^{LW}} + 4\sqrt{\Gamma_w^+\Gamma_w^-} - 2\sqrt{\Gamma_w^+}\left(\sqrt{\Gamma_b^-} + \sqrt{\Gamma_a^-}\right) - 2\sqrt{\Gamma_w^-}\left(\sqrt{\Gamma_b^+} + \sqrt{\Gamma_a^+}\right) + 2\sqrt{\Gamma_b^+\Gamma_a^-} + 2\sqrt{\Gamma_b^-\Gamma_a^+} \tag{8.14}$$

Where ΔG_d^a , ΔG_w^a = adhesive surface energies for dry and wet condition, respectively,

Γ^{LW} = Lifshitz-van der Waals component of the bond energy,

Γ^+ = Lewis acid component of the bond energy,

Γ^+ = Lewis base component of the bond energy, and

subscript a , b , w = each means aggregate, binder, and water, respectively.

Table 8.15. Component Values for Adhesive Bond energy Calculation in Dry and Wet Condition of Sand Asphalt.

Γ_a^{LW}	Γ_b^{LW}	Γ_a^+	Γ_b^+	Γ_a^-	Γ_b^-	Γ_w^{LW}	Γ_w^+	Γ_w^-
64.8	7.34	11.0	18.38	250.8	28.76	21.8	25.5	25.5

Table 8.16 shows the determined surface energies for cohesive and adhesive fractures in dry and wet condition.

Table 8.16. Calculated Cohesive and Adhesive Surface Energies in Dry and Wet Condition.

Specimen	Fracture Mode	Surface Energies (J/m^2)			
		Step 1	Step 2	Step 3	Step 4
HMA	Cohesive	0.1062	0.1062	0.1062	0.1062
	Adhesive	0.1992	0.1992	0.1992	0.1992
Sand Asphalt	Cohesive	0.1062	0.1062	0.1062	0.1062
	Adhesive	0.2150	0.2150	0.2150	0.2150

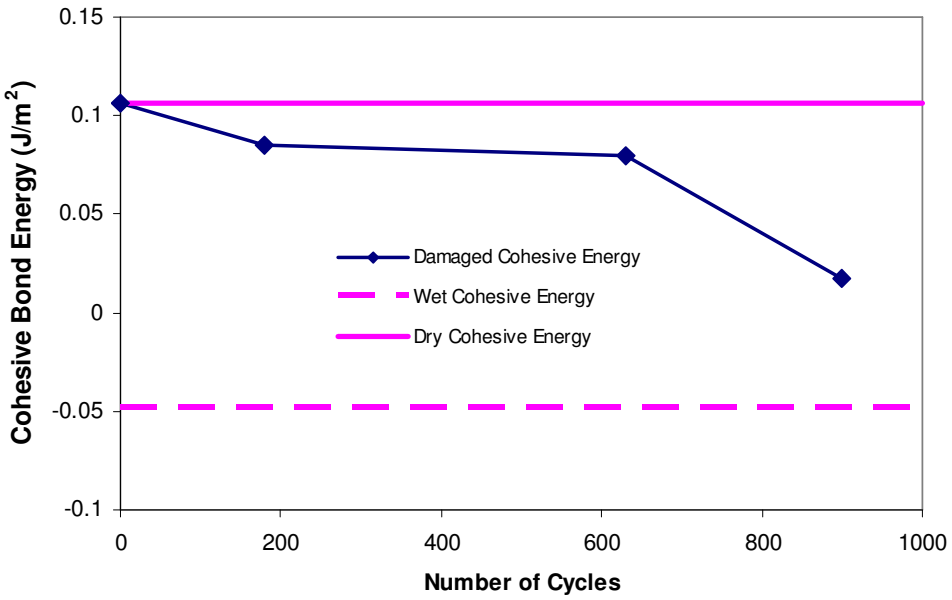

Figure 8.32. The Cohesive Bond Energy Measured for Dry and Wet Conditions in HMA, and Cohesive Bond Energy Back Calculated from the Micromechanics Model for Partially Damaged Material.

The bond energy values that gave the best fitting to the experimental measurements of ($E_f / E_f^{'}$ or $G_f^{'} / G_f$) were back calculated from the micromechanics models for the damaged materials under wet condition. The back calculated values are between those measured for the dry and wet condition as shown in Figure 8.32. Table 8.17 shows the back calculated bond energy values under wet condtion.

Table 8.17. Back Calculated Surface Energies under Wet Condition.

Specimen	Fracture Mode	Surface Energies under Wet Condition (J/m^2)			
		Step 1	Step 2	Step 3	Step 4
HMA	Cohesive	0.1062	0.0850	0.0801	0.0178
	Adhesive	0.1992	0.1652	0.1574	0.0575
Sand Asphalt	Cohesive	0.1062	0.0662	0.0502	0.0192
	Adhesive	0.2150	0.1432	0.1145	0.0590

The fittings of the model results to the experimental measurements are shown in Figure 8.33 through Figure 8.36. Figures 8.33 and 8.34 show the calculated and measured modulus ratios from cohesive and adhesive models each based on micromechanics which were applied using the data from sand asphalt. Results from HMA were used for the controlled-stress model as shown in Figures 8.35 and 8.36. To exclude the variability from different tests and conditions and compare the results, normalized value was used.

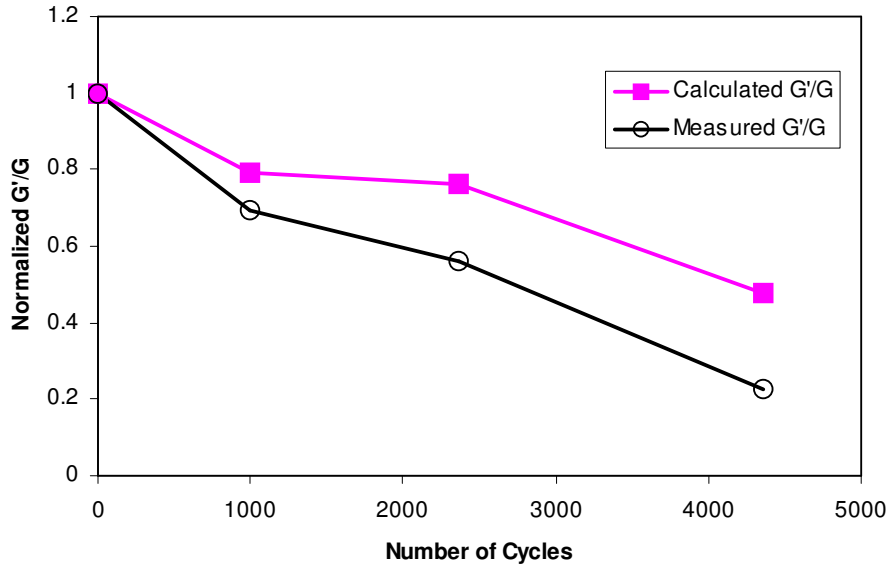

(a)

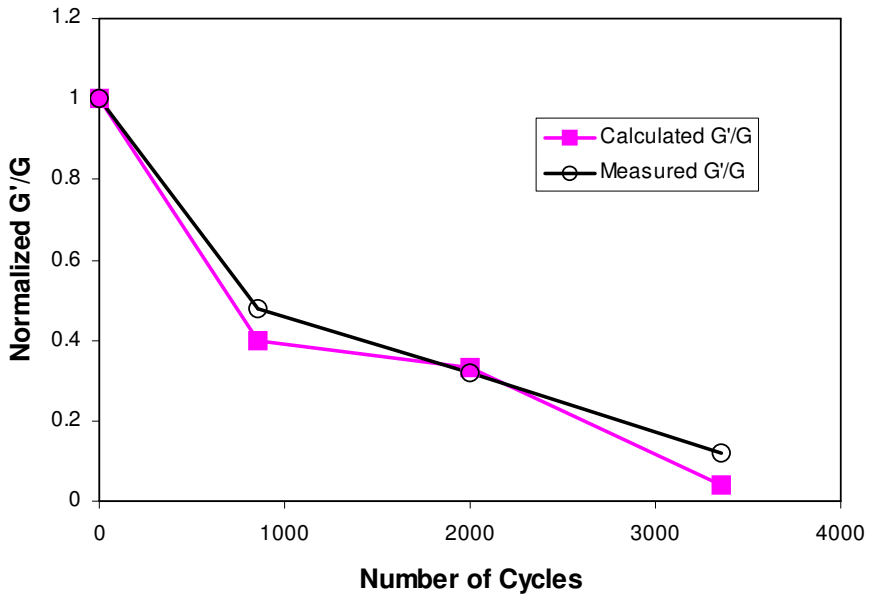

(b)

Figure 8.33. Cohesive Fractures in (a) Dry Condition and (b) Wet Condition under Controlled-Strain.

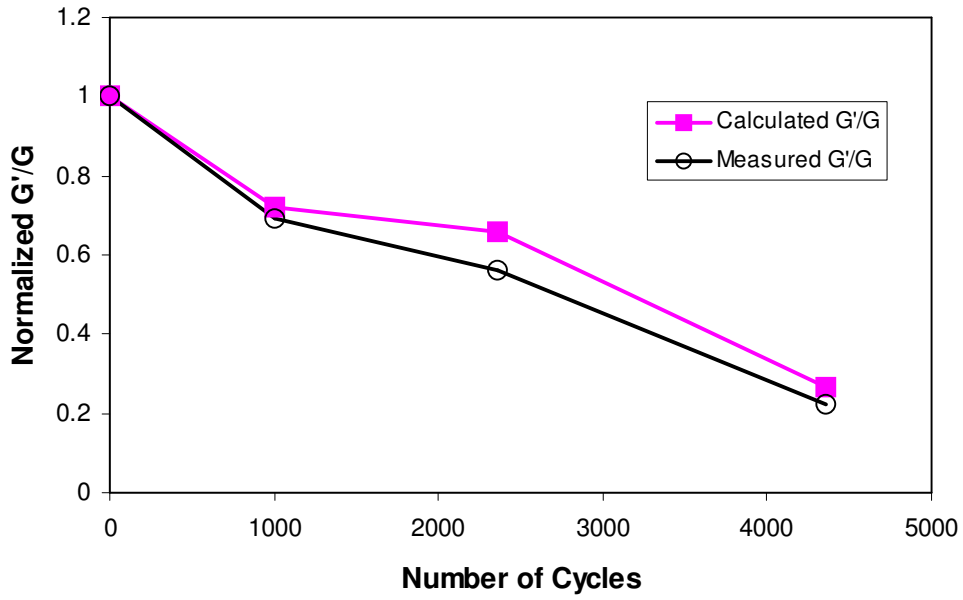

(a)

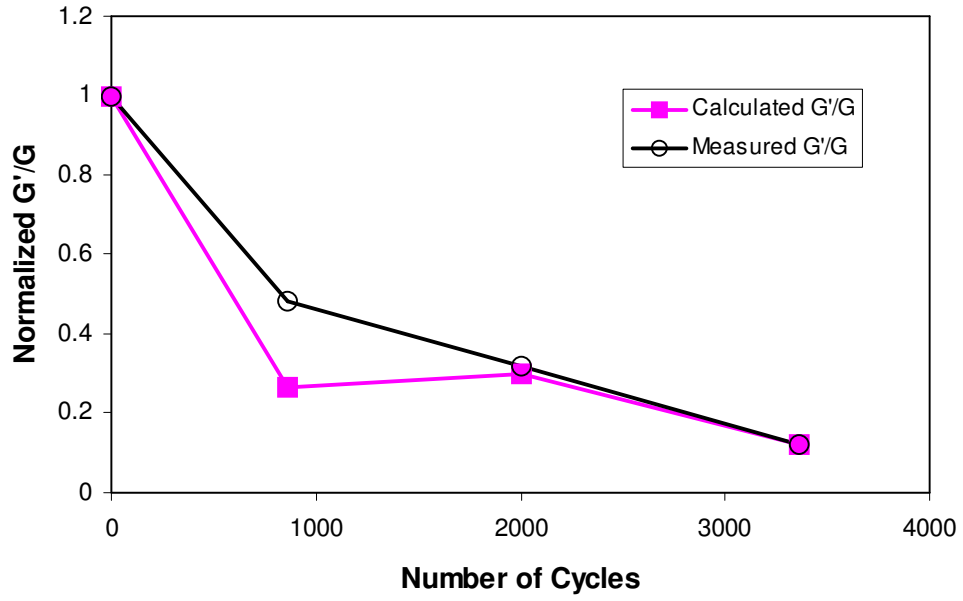

(b)

Figure 8.34. Adhesive Fractures in (a) Dry Condition and (b) Wet Condition under Controlled-Strain.

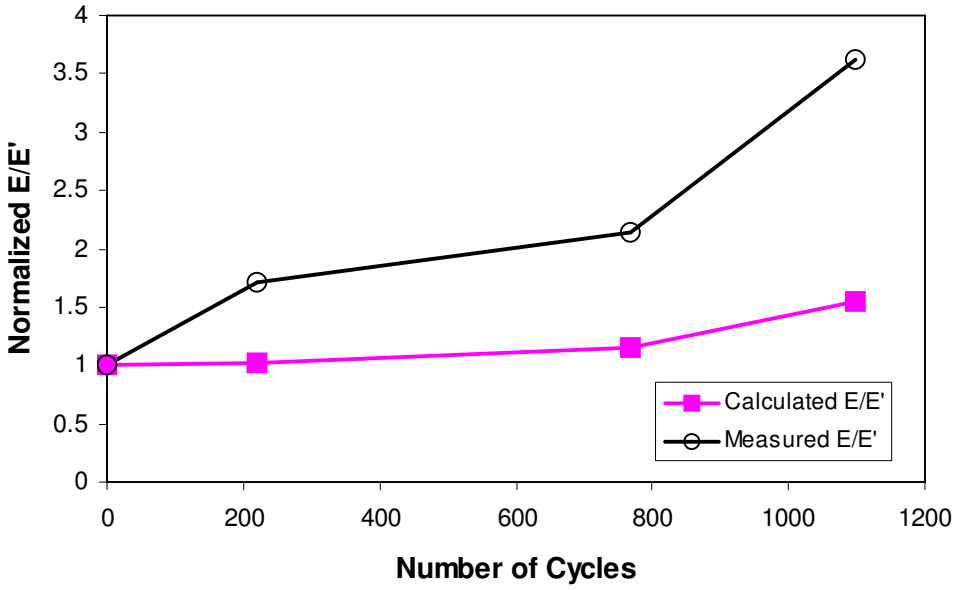

(a)

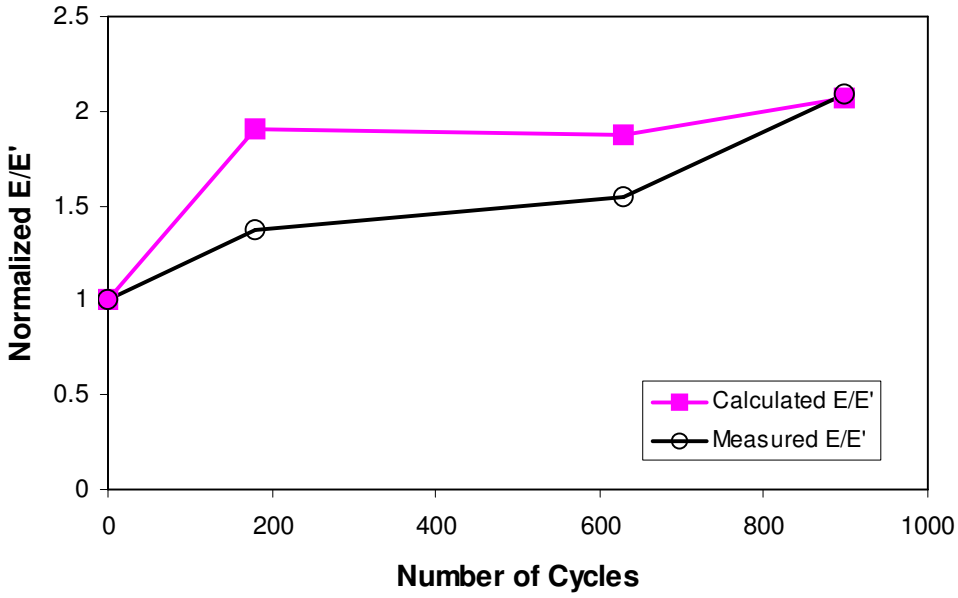

(b)

Figure 8.35. Cohesive Fractures in (a) Dry Condition and (b) Wet Condition under Controlled-Stress.

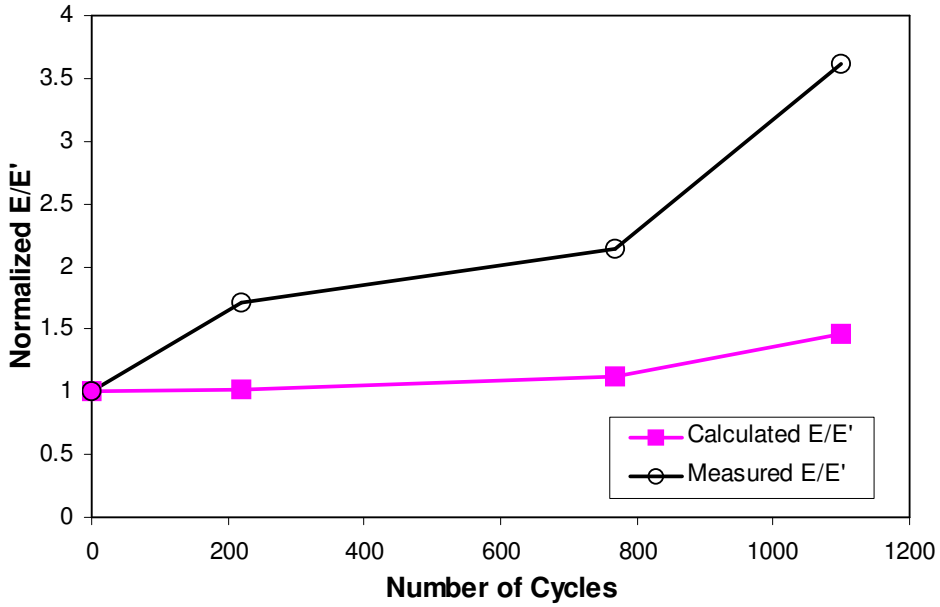

(a)

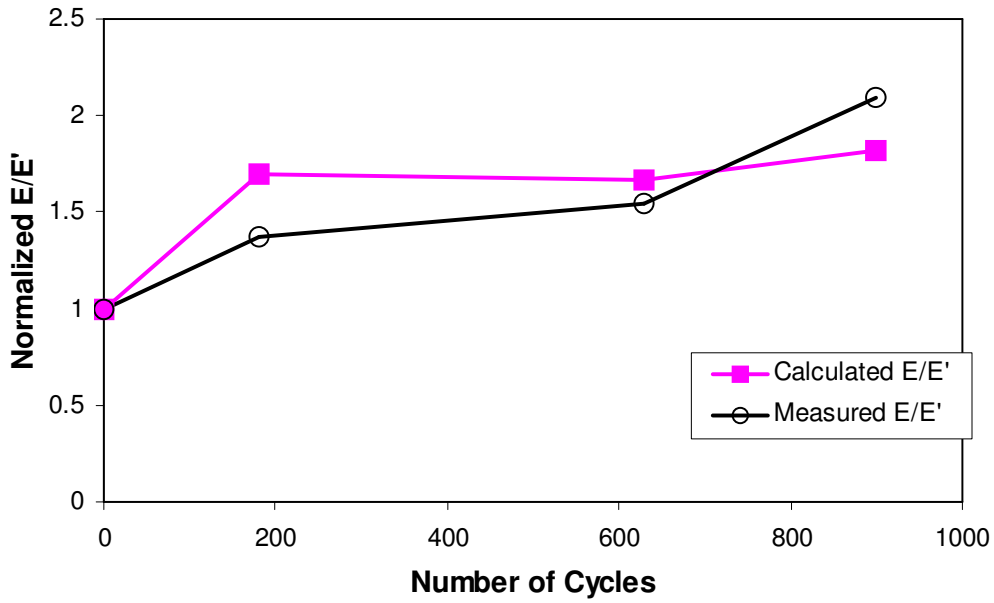

(b)

Figure 8.36. Adhesive Fractures in (a) Dry Condition and (b) Wet Condition under Controlled-Stress.

Table 8.18 listed parameter values used for calculating the modulus ratios both under controlled-strain and controlled-stress mode of loading. The dynamic shear rheometer (DSR) measured the rheological properties complex shear modulus at room temperature of 25°C with 10Hz of frequency for the modulus of the asphalt (E_f or G_f). Barksdale (1996) presented modulus of granite which was used for fabricating HMA and Carmichael (1989) measured stiffness of sand. The suggested each modulus is adopted for the adhesive micro mechanics models. Film thickness values used for the micro mechanics models for both HMA and sand asphalt were calculated by using image analysis technique.

Table 8.18. Parameters Used for Micro Mechanics Models.

Specimen	Condition	E_f or G_f (MPa)	E_s or G_s (MPa)	Film Thickness, t (μm)
HMA	Dry	0.28	45000	115
	Wet	0.28	45000	220
Sand Asphalt	Dry	0.28	38000	93
	Wet	0.28	38000	125

Following two figures, Figures 8.37 and 8.38, show the comparisons between measured and calculated modulus changes by means of the cohesive and adhesive model. The both measured and calculated shear modulus at any number of cycles are normalized with respect to the initial modulus, and the damage parameter is normalized

with respect to the maximum damage at the end of loading. It can be seen that the normalized modulus ratio and damage parameter follow the same trend as the normalized shear modulus confirming the relationship between microcracking and the degradation in the shear modulus measured and calculated from the micromechanics model and the DMA.

It is evident that the micromechanics model is capable of describing the experimental measurements under dry and wet conditions.

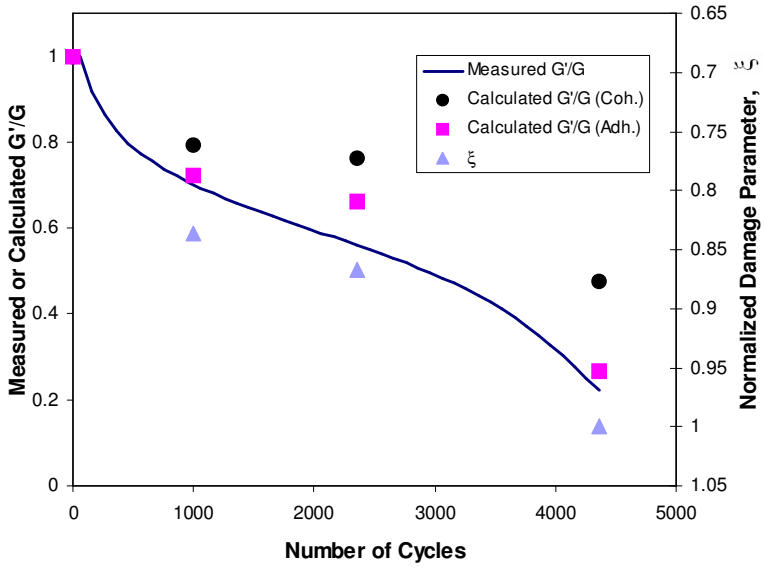

(a)

Figure 8.37. Comparison of Measured and Calculated Shear Modulus by Cohesive and Adhesive Fracture Model in (a) Dry Condition and (b) Wet Condition.

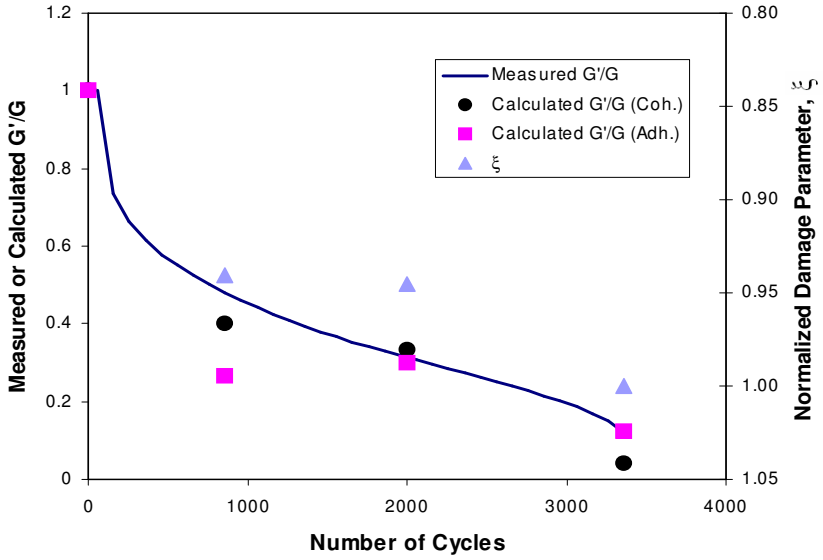

(b)

Figure 8.37. Continued.

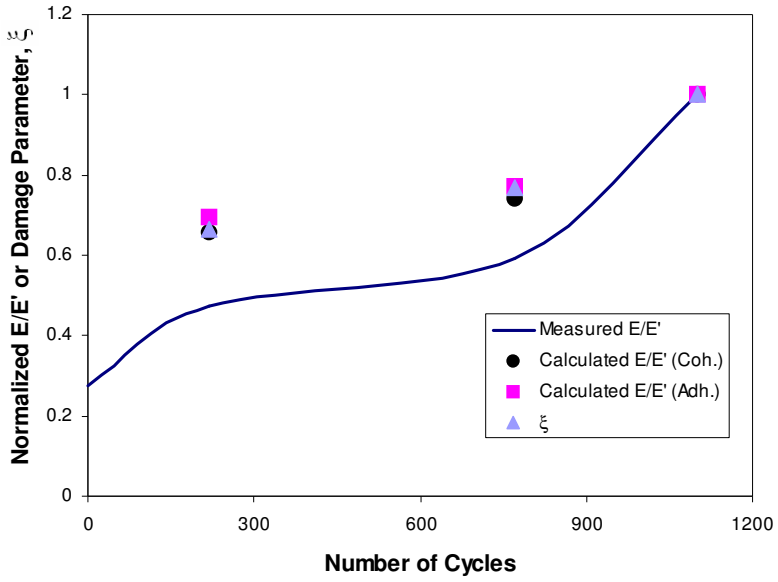

(a)

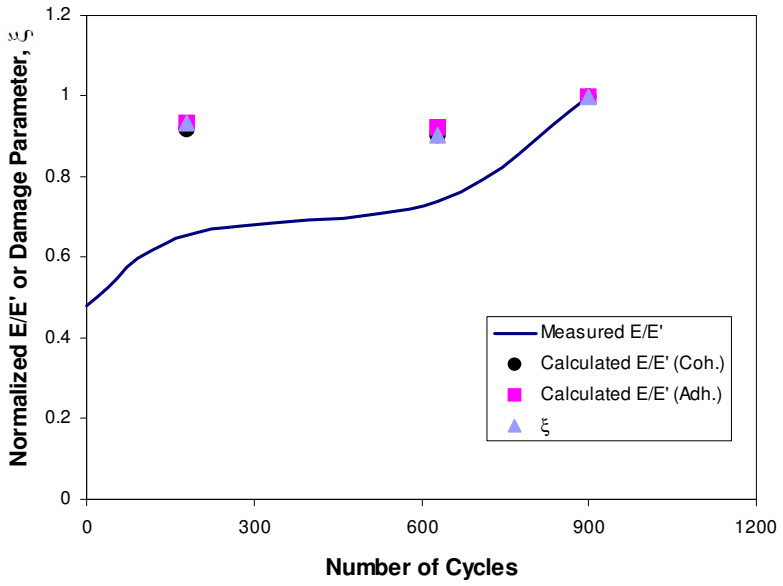

(b)

Figure 8.38. Comparison of Measured HMA Stiffness Ratio with Cohesive and Adhesive Fracture Model in (a) Dry Condition and (b) Wet Condition.

INFLUENCE OF HEALING IN THE MASTICS

As described in the previous chapters, DMA was used for fatigue test at 25 °C under controlled – strain cyclic loading mode. Kim (2003) showed that microdamage due to the fatigue loading can be healed when rest periods applied during fatigue testing. The fatigue life increase in terms of healing process with rest periods was evident.

Damage parameters ξ, *S* and DPSE were used for observing healing in the sand asphalt by recovery of the damage indicators. The parameters before and after rest periods were monitored to calculate healing potential of the sand asphalts. The rest periods of ten two-minute were conducted with applying 0.28 percent of torsional shear cyclic loading at 25 °C for the sand asphalt specimens under dry condition. The number of load repetitions applied before each rest period is equal to one tenth of failure point which was defined earlier as the fourth step in the fatigue life without rest periods. The controlled – strain cyclic loading was continued after the last rest period.

Figure 8.39 shows the microdamage healing effect due to rest periods by illustrating dynamic modulus data set for with and without rest periods. The modulus increases after each rest period, and then decreases as the loading continues after the rest. It is evident that the ten two-minute rest period increases the fatigue life.

Four damage steps were defined earlier based on the fatigue test data from DMA. Damage parameters ξ at the steps with rest periods were calculated by using image analysis technique and Figure 8.40 plotted the results with dynamic shear modulus.

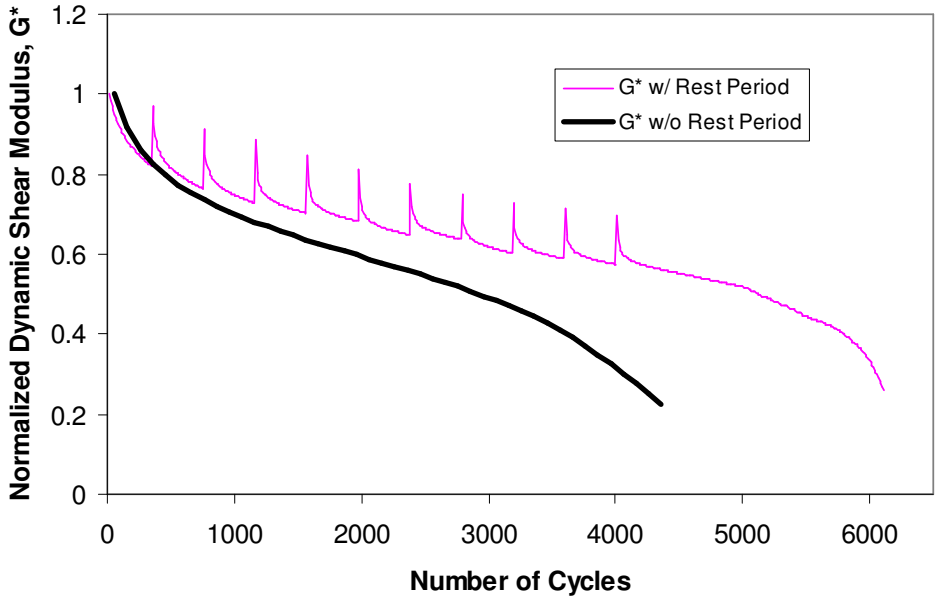

Figure 8.39. Dynamic Modulus Recovery after Applying Rest Period.

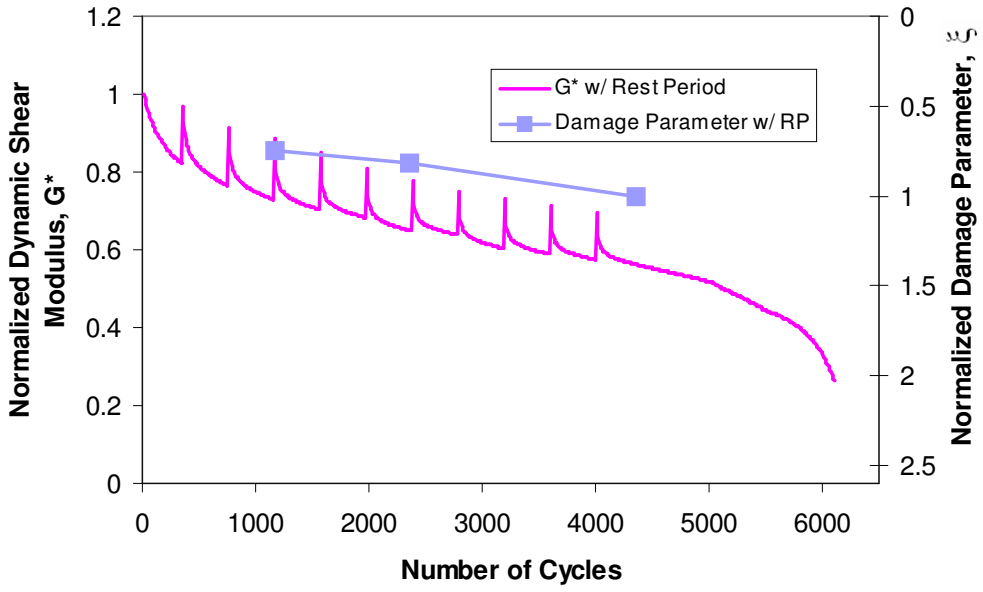

Figure 8.40. Damage Parameter ξ Changes with Rest Periods.

The three damage indicators, that is damage parameters ξ, S and DPSE, were calculated for both with and without rest periods and compared. Figure 8.41 to Figure 8.43 demonstrate the comparison of each parameter at the defined steps.

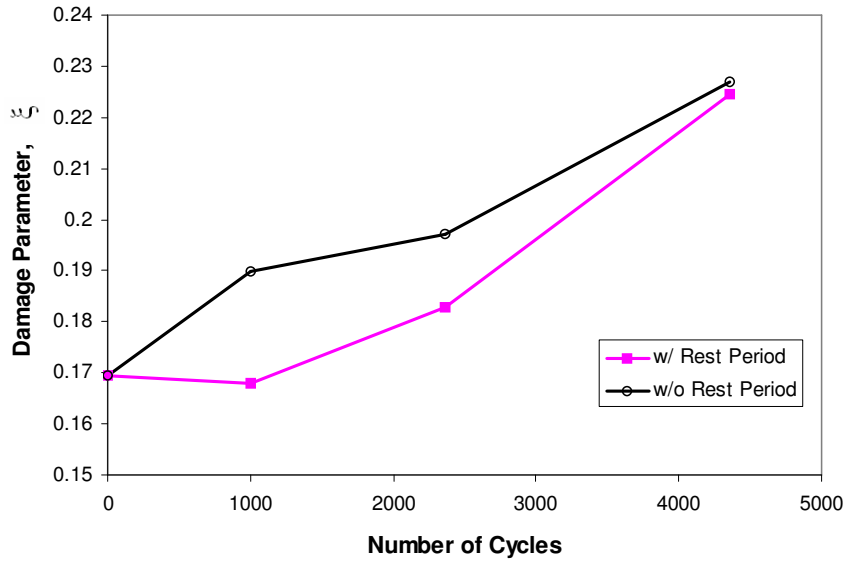

Figure 8.41. Damage Parameter ξ with and without Rest Periods.

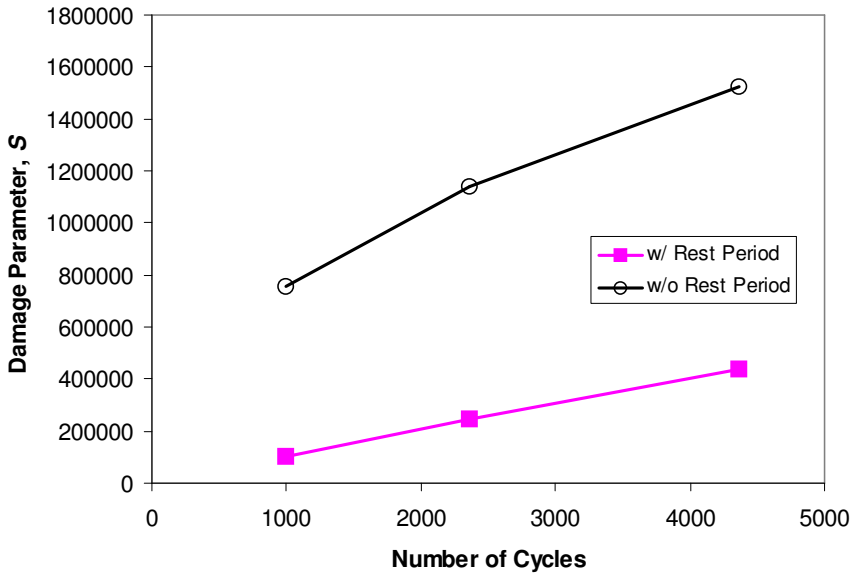

Figure 8.42. Damage Parameter *S* with and without Rest Periods.

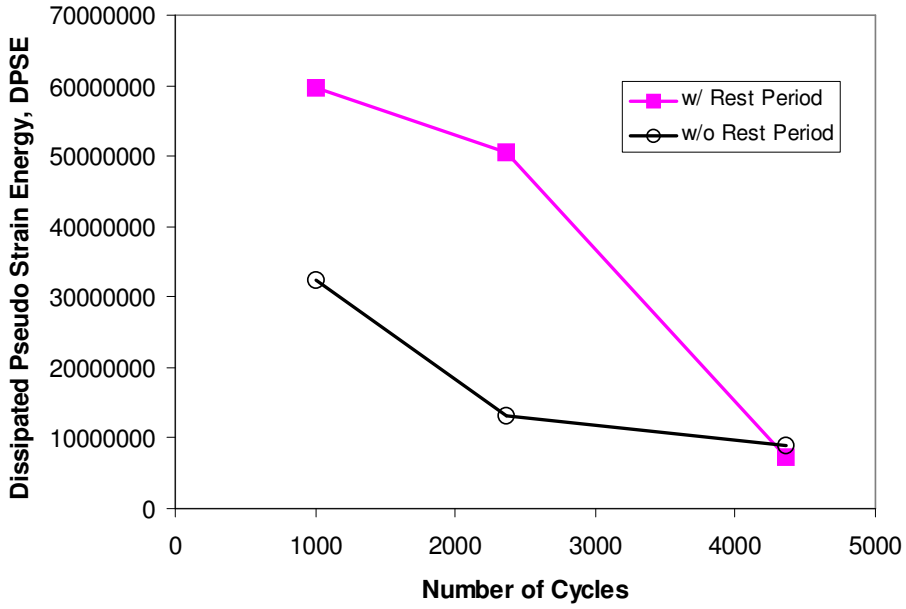

Figure 8.43. DPSE with and without Rest Periods.

CONCLUSIONS

- Permanent deformation is composed of two different mechanisms: densification and repetitive shear deformation. Fatigue cracking in asphalt mixtures is generally considered by three states, those are crack initiation, crack propagation, and disintegration. Permanent deformation and fatigue cracking test are performed and two critical points on both tests are defined based on the results.
- The best fitting third order polynomial regression model has been developed and used to determine FIP and SIP by second derivatives of the equations in DMA test results. The two inflection points were adopted as critical points not only for fatigue test analysis but also permanent deformation test.
- Sand asphalt cylindrical specimens were fabricated using the specially designed mold for 50 mm long and 12 mm diameter. DMA as a simple and accurate method was successfully used to evaluate the damage mechanics of the asphalt mixtures. DMA was also validated to monitor the progression of microcrack damage through CT and micromechanics models. The normalized shear modulus at any number of cycles and the normalized damage parameters were plotted. The normalized damage follows the same trend as the normalized shear modulus confirming the relationship between microcracking and the degradation in the shear modulus measured in the DMA.
- Computer imaging technology is a nondestructive technique and make it possible to characterize engineering materials based on the distribution of its internal structure. It is well established that air voids play an important role in

determining resistance of asphalt mixtures to major pavement distress including fatigue cracking, permanent deformation, and low-temperature cracking. Therefore, X-ray CT experiment was used to quantify the damage in asphalt mixtures for image analysis. Data analysis showed that X-ray CT was a valuable method to characterize and monitor the damage under different loading levels in asphalt mixtures.

- Damage levels were investigated in terms of different damage indicators of ξ, *S,* and DPSE at different loading status. Parameter ξ was calculated values from X-ray CT and image analysis software. Parameter *S*, and DPSE were calculated at each discrete cycle by obtaining the peak pseudo strain (ε_m^R or $\gamma_{m,i}^R$) and pseudo stiffness (C_i) corresponding time (t_i).
- Three methods were developed to compare the results from mechanical and image analysis experiments such as DMA, dynamic creep and X-ray CT. The first method was direct comparisons of the three damage indicators between HMA and sand asphalts. The second is between parameter ξ from X-ray CT and *S* and DPSE. The third is comparisons of the three indicators in terms of cohesive and adhesive micromechanics model.
- There are well agreements among the parameters and the relationships such as correlation and variances were presented.

- Damage captured from X-ray in asphalt mixtures in dry condition are less than the specimens in the presence of water which is consistent with the other parameters.
- In general, it can be seen that the damage increased with an increase in loading cycles. Also, there was slight change in damage in the first three stages of loading the dry specimen. However, damage increased significantly between the first and second steps of loading the wet specimens. The results indicate the low resistance of wet specimens to damage compared with the dry specimens.
- Lytton (2004) developed an equation, based on micromechanicsanalysis of cohesive damage in asphalt-aggregates mixture, for the ratio of the damaged modulus to the undamaged modulus of the binder. The model validated results from X-ray CT and DMA. It is evident that the micromechanics model is capable of describing the experimental measurements under dry and wet conditions.

REFERENCES

Asphalt Institute (1982). "Research and Development of the Asphalt Institute's Thickness Design Manual (MS-1), 9th ed." Research Report 82-2, Asphalt Institute, Lexington, Kentucky.

Barksdale, R. D. (1996). *The Aggregate Handbook.* National Stone Association, Washington, D.C.

Bhairampally, R. K. (1998). "Study of Permanent Deformation Characteristics of Aspahlt Mixes in Relation to Microcrack Growth." M.S. thesis. Texas A&M University, College Station, Texas.

Brown, E. R. and Cross, S. (1992). "A National Study of Rutting in Asphalt Pavement." *Journal of the Association of Asphalt Paving Technologists*, 61, 535-582.

Brown, S. F., and Bell, C. A. (1977). "The Validity of Design Procedures for the Permanent Deformation of Asphalt Pavements." *Proceedings, 4th International Conference on the Structural Design of Asphalt Pavements*, Vol. I, Ann Arbor, Michigan, 467-482.

Brown, S. F., and Bell, C. A. (1979). "The Prediction of Permanent Deformation in Asphalt Pavements." *Proceedings, Journal of Association of Asphalt Paving Technologists*, 48, 438-476.

Carmichael, R. S. (1989). *Practical Handbook of Physical Properties of Rocks and Minerals.* CRC Press, Boca Raton, Florida.

Cheng, D. (2002). "Surface Free Energy of Asphalt-Aggregate System and Performance Analysis of Asphalt Concrete Based on Surface Free Energy." Ph.D. dissertation, Texas A&M University, College Station, Texas.

Denison, C., Carlson, W. D., and Ketcham, R. A. (1997). " Three-Dimensional Quantitative Textural Analysis of Metamorphic Rocks Using High-Resolution Computed X-ray Tomography: Part I. Methods and Techniques." *Journal of Metamorphic Geology,* 15:29-44.

Domke, C. H., Liu, M., Davison, R. R., Bullin, J. A., and Glover, C. J. (1997). "Study of Strategic Highway Research Program Pressure Aging Vessel Procedure Using Long-Term, Low-Temperature Aging Experiments and Asphalt Kinetics." *Transportation Research Record*, *1586,* Transportation Research Board, Washington, D. C., 10-15.

Eriksen, K., and Wegen, V. (1993). "Optical Methods for the Evaluation of Asphalt Concrete and Polymer-Modified Bituminous Binders." *Note 244*, Danish Road Institute, Roskilde, Denmark.

Finn, F. N., Monismith, C. L., and Markevich, N. J. (1983). "Pavement Performance and Asphalt Concrete Mix Design." *Proceedings*, *Journal of Association of Asphalt Paving Technologists*, 52, 121-150.

Ghuzlan, K. A. (2001). "Fatigue Damage Analysis in Asphalt Concrete Mixtures Based Upon Dissipated Energy Concepts." Ph.D. dissertation. University of Illinois at Urbana-Champaign.

Hills, J. F., Brien, D., and Van de loo, P. J. (1974). "The Correlation of Rutting and Creep Tests on Asphalt Mixes." *Institute of Petroleum*, Paper IP 74-001, January.

Hiltunen, D. R. and Roque, R. (1994). "A Mechanistic-Based Prediction Model for Thermal Cracking of Asphaltic Concrete Pavements." *Journal of the Association of Asphalt Paving Technologists*, 63, 81-113.

Huang, Y. H. (1993). *Pavement Analysis and Design.* Prentice Hall, Englewood Cliffs, New Jersey.

Image-Pro Plus Version 4. (1998). Media Cybernetics, Georgia, Maryland.

Izzo, R. P. (1997). "Evaluation of the Filler Effects on Fatigue Cracking and Permanent Deformation of Asphalt Concrete Mixtures." M.S. thesis, Texas A&M University, College Station, Texas.

Jacobs, M. M. J. (1995). "Crack Growth in Asphaltic Mixes." Ph.D. dissertation, Delft University of Technology, Delft, The Netherlands.

Kachnov, L. M. (1958). "Time to Rupture Process Under Creep Conditions." In. Izv. Akad. Nauk, USSR, Otd. Tekh. Nauk., 26-31.

Kaloush, K.E. and Witczak, M.W. (2002). "Tertiary Flow Characteristics of Asphalt Mixtures", *Journal of the Association of Asphalt Paving Technologists*, 71, 248-280.

Kandhal, P. S., and Mallick, R. B. (1999) "Evaluation of Asphalt Pavement Analyzer for HMA Mix Design." NCAT Rep. No. 99-4, National Center for Asphalt Technology, Auburn, Alabama.

Kim, Y. S. (1988). "Evaluation of Healing and Constitutive Modeling of Asphalt Concrete by Means of the Theory of Nonlinear Viscoelasticity and Damage Mechanics." Ph.D. dissertation, Texas A&M University, College Station, Texas.

Kim, Y., and Little, D. N. (1990). "One Dimensional Constitutive Modeling of Asphalt Concrete." *Journal of Engineering Mechanics*, 116(4), 751-772.

Kim, Y. R., Whitmoyer, S. L., and Little, D. N. (1994). "Healing in Asphalt Concrete Pavements: Is It Real?" *Transportation Research Record*, *1454,* Transportation Research Board, Washington, D. C., 89-96.

Kim, Y. R., Lee, Y. C., and Lee, H. J. (1995). "Correspondence Principle for Characterization of Asphalt Concrete." *Journal of Materials in Civil Engineering*, ASCE, 7(1), 59-68.

Kim, Y. R., Lee, H. J., and Little, D. N. (1997). "Fatigue Characterization of Asphalt Concrete Using Viscoelasticity and Continuum Damage Theory." *Journal of the Association of Asphalt Paving Technologists*, 66, 520-569.

Kim, Y., Little, D. N., and Lytton, R. L. (2001). "Evaluation of Microdamage, Healing, and Heat Dissipation of Asphalt Mixtures Using a Dynamic Mechanical Analyzer (DMA)." *Transportation Research Record*, *1767,* Transportation Research Board, Washington, D. C., 62-66.

Kim, Y. R., Little, D. N., and Lytton, R. L. (2002). "Use of Dynamic Mechanical Analysis (DMA) to Evaluate the Fatigue and Healing Potential of Asphalt Binders in Sand Asphalt Mixtures." *Journal of the Association of Asphalt Paving Technologists*, 71, 176-206.

Kim, Y. R. (2003). "Mechanistic Fatigue Characterization and Damage Modeling of Asphalt Mixtures." Ph.D. dissertation, Texas A&M University, College Station, Texas.

Kirwan, R. W., Snaith, M. S. and Glynn, T. E. (1977). "A Computer Based Subsystem for the Prediction of Permanent Deformation." *Proceedings, 4th International Conference on the Structural Design of Asphalt Pavements*, Vol. II, Ann Arbor, Michigan, 509-518.

Lee, H. J. (1996). "Uniaxial Constitutive Modeling of Asphalt Concrete Using Viscoelasticity and Continuum Damage Theory." Ph. D. dissertation, North Carolina State University, Raleigh, North Carolina.

Lee, H.-J., and Kim, Y. R. (1998). "Viscoelastic Continuum Damage Model of Asphalt Concrete with Healing." *Journal of Engineering Mechanics,* ASCE, 124(11), 1224-1232.

Lee, H.-J., Daniel, J. S., and Kim, Y. R. (2000a). "Continuum Damage Mechanics-Based Fatigue Model of Asphalt Concrete." *Journal of Materials in Civil Engineering,* ASCE, 12(2), 105-112.

Lee, H.-J., Daniel, J. S., Kim, Y. R. (2000b). "Laboratory Performance Evaluation of Modified Asphalt Mixtures for Inchon Airport Pavements." *International Journal of Pavement Engineering*, 1(2), 151-169.

Little, D. N., Button, J. W., and Youssef, H. (1993). "Development of Criteria to Evaluate Uniaxial Creep Data and Asphalt Concrete Permanent Deformation Potential." *Transportation Research Record*, *1417,* Transportation Research Board, Washington,

D. C., 49-57.

Little, D.N. (1995). *Handbook for Stabilization of Pavement Subgrades and Base Courses with Lime.* The National Lime Association, Dubuque, Iowa.

Little, D. N., Lytton, R. L., Williams, D., and Chen, J. W. (1998). "Fundamental Properties of Asphalts and Modified Asphalts." *Final Research Report. Texas Transportation Institute*, Texas A&M University, College Station, Texas, Vol. I.

Little, D. N., and Kim, Y. R. (2002). "Using Dynamic Mechanical Analysis As a Tool to Access the Suitability of Fillers in Asphalt Mixtures Based on the Mastic Properties." *Proceedings, 10th Annual Symposium Proceedings, International Center for Aggregate Research*. Austin, Texas.

Lytton, R. L. (2000). "Characterizing Asphalt Pavements for Performance." *Transportation Research Record*, *1767,* Transportation Research Board, Washington, D. C., 5-16.

Lytton, R. L. (2004). "Adhesive Fracture in Asphalt Concrete Mixtures," Chapter in Book Edited by Youtcheff, J., In Press.

Masad, E., Muhunthan, B., Shashidhar, N., and Harman T. (1999a). "Internal Structure Characterization of Asphalt Concrete Using Image Analysis." *Journal of Computing in Civil Engineering (Special Issue on Image Processing)*, ASCE, 13(2), 88-95.

Masad, E. A., Muhunthan, B., Shashidhar, N., and Harman, T. (1999b). "Quantifying Laboratory Compaction Effects on the Internal Structure of Asphalt

Concrete." *Transportation Research Record*, *1681,* Transportation Research Board, Washington, D. C., 179-185.

Masad, E., Jandhyala, V. K., Dasgupta, N., Somadevan, N., and Shashidhar, N. (2002). "Characterization of Air Void Distribution in Asphalt Mixes using X-Ray Computed Tomography.*" Journal of Materials in Civil Engineering*, ASCE, 14(2), 122-129.

Miner, M. A. (1945). "Cumulative Damage in Fatigue." *Journal of Applied Mechanics*, 67, A159-A164.

Mohammad, L. N., Abadie, C., Gokmen, R., and Puppala, A. J. (2000). "Mechanistic Evaluation of Hydrated Lime in Hot-Mix Asphalt Mixtures." *Transportation Research Record*, *1767,* Transportation Research Board, Washington, D. C., 26-36.

Monismith, C. L., Inkabi, K. Freeme, C. R., and McLean, D. B. (1977). "A Subsystem to Predict Rutting in Asphalt Concrete Pavement Structures." *Proceedings, 4th International Conference on the Structural Design of Asphalt Pavements*, Vol. I, Ann Arbor, Michigan, 529-539.

Monismith, C. L., and Tayebali, A. A. (1988). "Permanent Deformation (Rutting) Considerations in Asphalt Concrete Pavement Sections." *Journal of the Association of Asphalt Paving Technologists*, 71, 76-206.

Monismith, C. L. (1992). "Analytically Based Asphalt Pavement Design and Rehabilitation." *Transportation Research Record*, *1354,* Transportation Research Board, Washington, D. C., 5-26.

Paris, P., and Erdogan, F. (1963). "A Critical Analysis of Crack Propagation Laws." Transaction of The ASME, *Journal of Basic Engineering*, 85(D), No. 4.

Perzyna, P. (1984). "Constitutive Modeling of Dissipative Solids for Postcritical Behavior and Fracture." *Journal of Engineering Materials and Technology*, ASME, 106, 410 - 419.

Reese, R. (1997). "Properties of Aged Asphalt Binder Related to Asphalt Concrete Fatigue Life." *Journal of the Association of Asphalt Paving Technologists*, 66, 604-632.

Roberts, F. L., Kandhal, P. S., Brown, E. R., Lee, D. and Kennedy, T. (1996). *Hot Mix Asphalt Materials, Mixture Design and Construction.* NAPA Educational Foundation, Lanham, Maryland.

Rowe, G. M. (1993). "Performance of Asphalt Mixtures in the Trapezoidal Fatigue Test." *Journal of the Association of Asphalt Paving Technologists*, 62, 344-384.

Rowe, G. M. and Bouldin, M. G. (2000). "Improved Techniques to Evaluate the Fatigue Resistance of Asphaltic Mixes." *Proceedings, Second Enraphalt and Eurobitume Congress,* Barcelona, Spain, 754-763.

Schapery, R. A. (1984). "Correspondence Principles and a Generalized J-integral for Large Deformation and Fracture Analysis of Viscoelastic Media." *International Journal of Fracture Mechanics*, 25, 195-223.

Schmidt, J. (1997). "Two additives are sometimes better than one, Lime makes believers out of cold in-place recycling contractors." *The Asphalt Contractor Paving America*, 3(5), 18-25.

Shami, H. I., Lai, J. S., D'Angelo, J. A., and Harman, T. P. (1997). "Development of Temperature-Effect Model for Predicting Rutting of Asphalt Mixtures Using Georgia Loaded Wheel Tester." *Transportation Research Record*, *1590,* Transportation Research Board, Washington, D. C., 17-22.

Si, Z. (2001). "Characterization of Microdamage and Healing of Asphalt Concrete Mixtures." Ph.D. dissertation, Texas A&M University, College Station, Texas.

Si, Z., Little, D. N., and Lytton, R. L. (2002). "Characterization of Microdamage and Healing of Asphalt Concrete Mixtures." *Journal of Materials in Civil Engineering*, ASCE, 14(6), 461-470.

Sousa, J. B., Craus, J. and Monismith, C. L. (1991). "Summary Report on Permanent Deformation in Asphalt Concrete." Report SHRP-A-318, Strategy Highway Research Program, National Research Council, Washington, D.C.

Sousa, J. B. (1995). "Asphalt-Aggregate Mix Design Using the Repetitive Simple Shear Test (Constant Height)." *Journal of the Association of Asphalt Paving Technologists*, 64, 298-345.

Tangella, S. C. S. R, Craus, J., Deacon, J. A., and Monismith, C. L. (1990). "Summary Report on Fatigue Response of Asphalt Mixtures." Report No. SHRP-A/IR-90-011, Strategic Highway Research Program, National Research Council, Washington, D.C.

Tashman, L., Masad, E., Peterson, B., and Saleh, H. (2001). "Internal Structure Analysis of Asphalt Mixes to Improve the Simulation of Superpave Gyratory

Compaction to Field Conditions." *Journal of the Association of Asphalt Paving Technologists*, 70, 605-645.

Tashman, L., Masad, E., Zbib, H., Little, D., and Kaloush, K. (2004). "Anisotropic Viscoplastic Continuum Damage Model for Asphalt Mixes." *Conference Proceeding,* ASCE, 111-125.

Tayebali, A., Deacon, J. A., Coplantz, J., Harvey, J. and Monismith, C. (1994). "Mixture and Mode-of-Loading Effects on Fatigue Response of Asphalt-Aggregate Mixtures." *Journal of the Association of Asphalt Paving Technologist*, 63, 118-143.

Transportation Research Circular E-C016. (2000). "Load Wheel Testers in the United States." Transportation Research Board, National Research Council, Washington, D. C.

Tseng, K.-H. and Lytton, R. L. (1989). "Prediction of Permanent Deformation in Flexible Pavement Materials." Implications of Aggregates in the Design, Construction, and Performance of Flexible Pavements, ASTM STP 1016, Philadelphia, Pennsylvania, 154-172.

Ueshita, K. and Meyerhof, G. G. (1968). "Surface Displacement of an Elastic Layer Under Uniformly Distributed Loads." *Highway Research Record 288*, Highway Research Board, 1-10.

Wang, J.-N., Yang, C.-K., and Luo, T.-Y. (2002). "Mechanistic Analysis of Asphalt Pavements, Using Superpave Shear Tester and Hamburg Wheel-Tracking Device." *Transportation Research Record*, *1767,* Transportation Research Board, Washington, D. C., 102-110.

Witczak, M. W., Kaloush, K., Pellinen T., El-Basyouny M. and Von Quintus H. (2002). "Simple Performance Test for Superpave Mix Design." National Cooperative Highway Research Program Rep. No. 465, Transportation Research Board, Washington, D. C.

Yoder, E. J., and Witczak, M. W. (1975). *Principles of Pavement Design.* John Wiley & Sons Inc, New York.

Yue, Z. Q., Bekking, W., and Morin, I. (1995). "Application of Digital Image Processing to Quantitative Study of Asphalt Concrete Microstructure." *Transportation Research Record, 1492,* Transportation Research Board, Washington, D. C., 53-60.

APPENDIX A

COMPARISON OF DAMAGE PARAMETERS IN DIFFERENT CONDITIONS

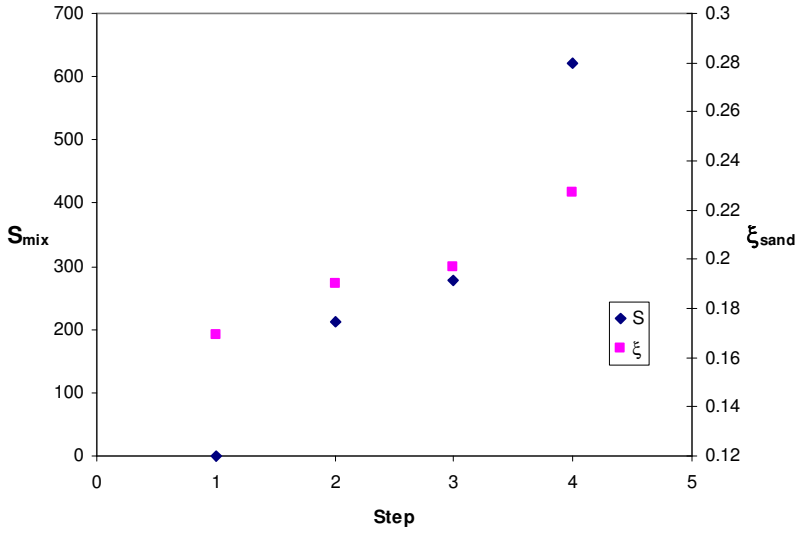

(a)

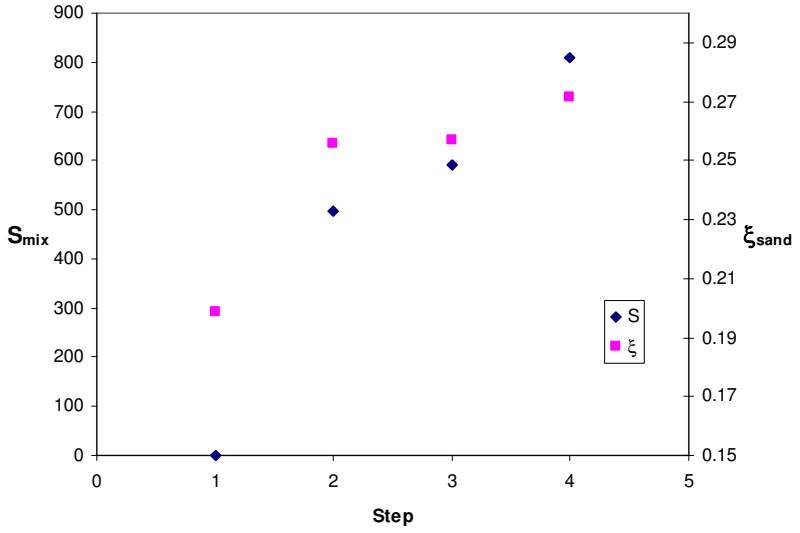

(b)

Figure A.1 Comparison of Damage Parameter *S* from Creep Test and ξ from DMA in (a) Dry Condition and (b) Wet Condition.

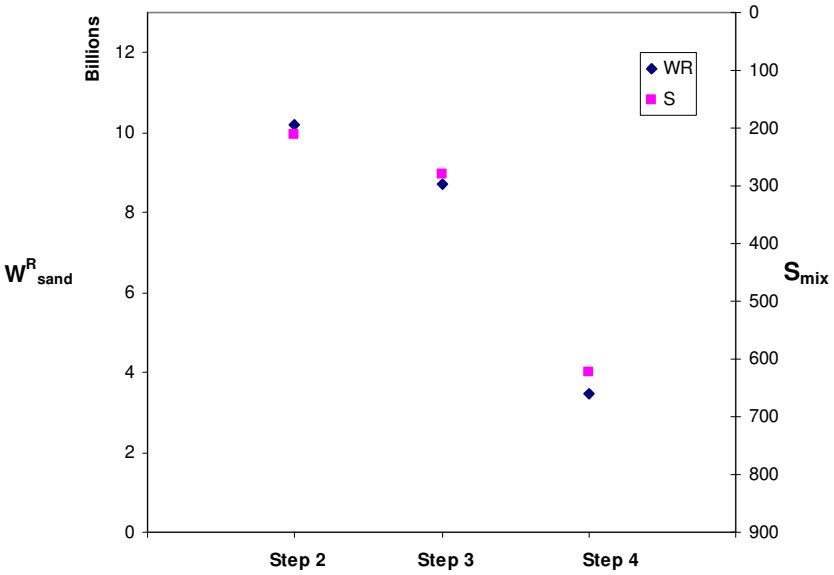

(a)

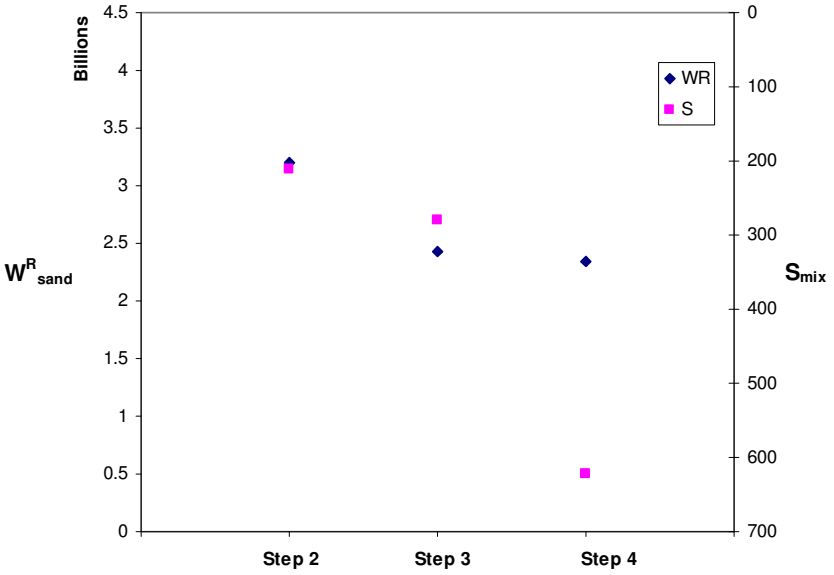

(b)

Figure A.2. Comparison of Dissipated Pseudo Strain Energy W^R from DMA and S from Creep Test in (a) Dry Condition and (b) Wet Condition.

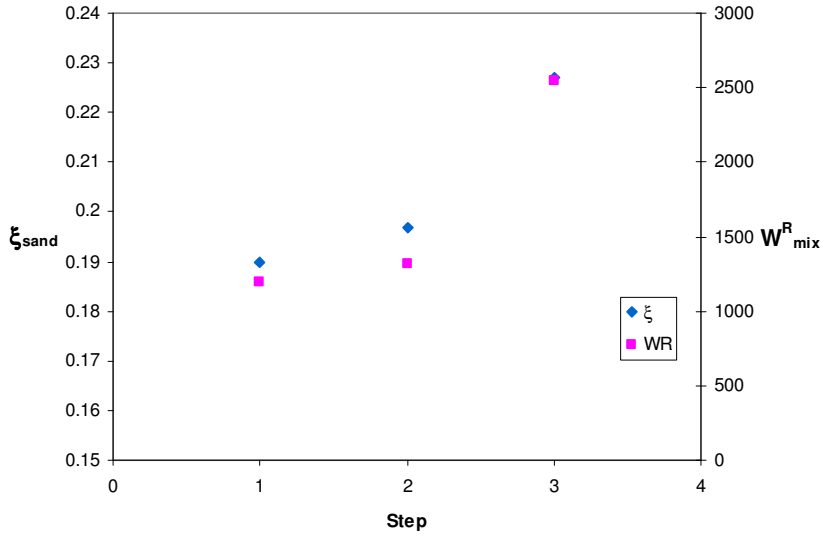

(a)

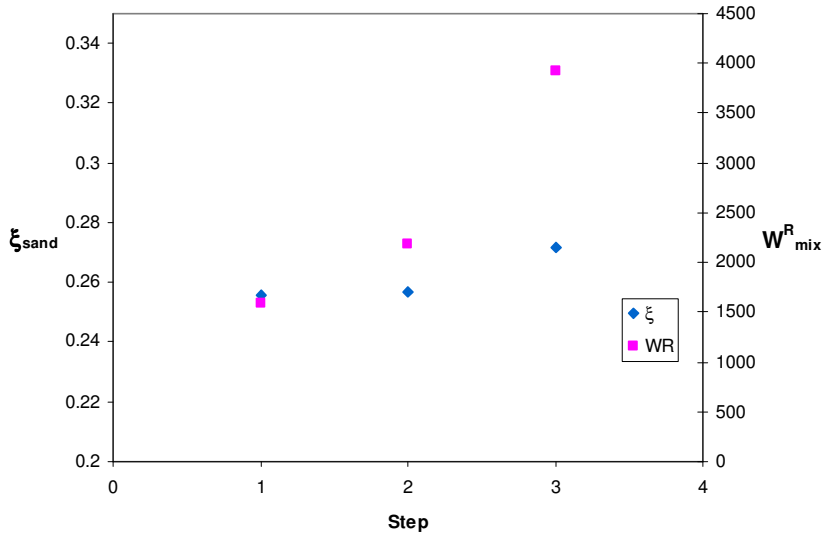

(b)

Figure A.3. Comparison of Damage Parameter ξ from DMA and Dissipated Pseudo Strain Energy W^R from Creep Test in (a) Dry Condition and (b) Wet Condition.

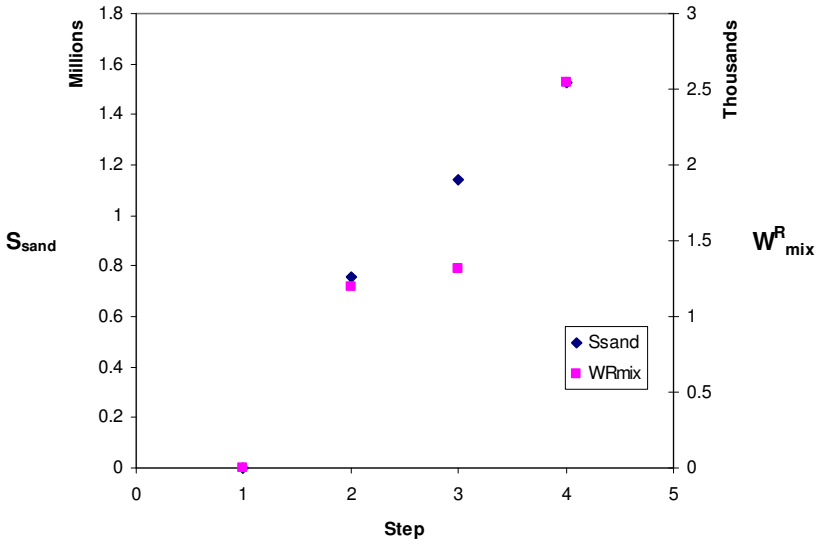

(a)

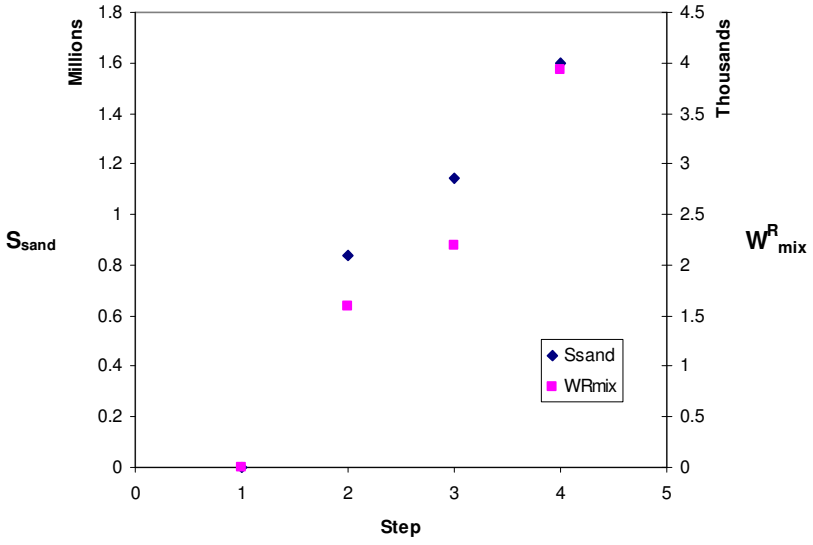

(b)

Figure A.4. Comparison of Damage Parameter *S* from DMA and Dissipated Pseudo Strain Energy W^R from Creep Test in (a) Dry Condition and (b) Wet Condition.

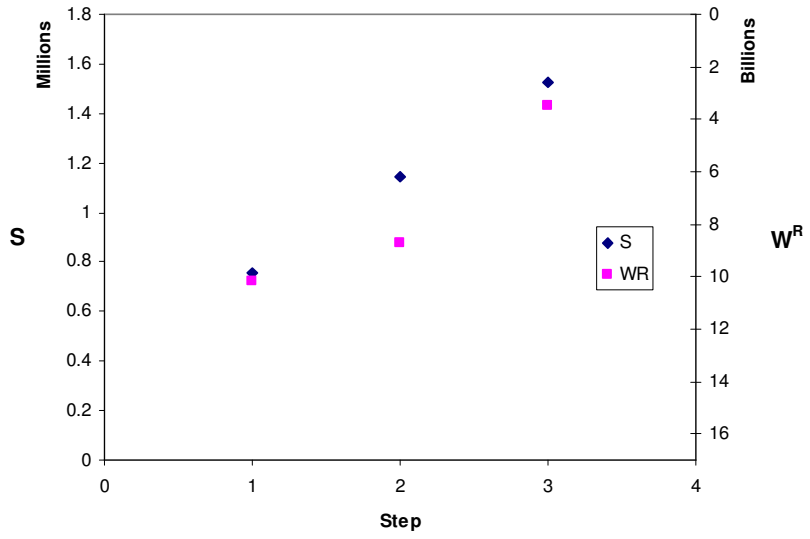

(a)

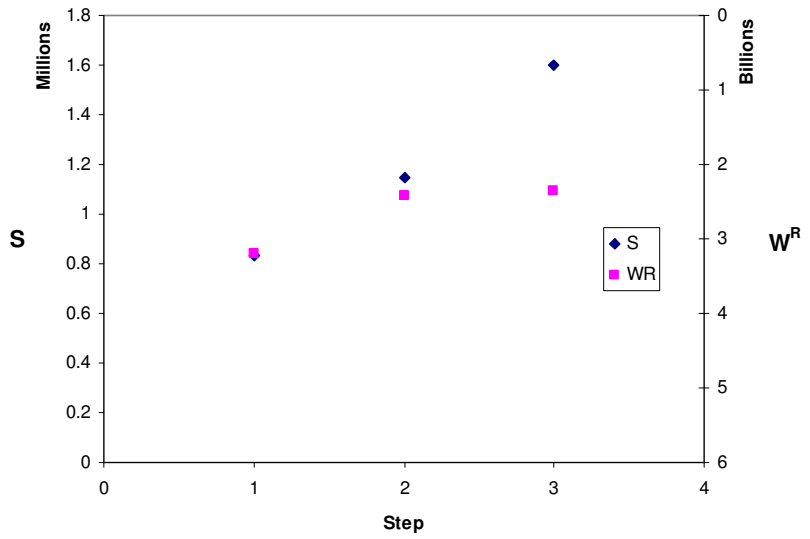

(b)

Figure A.5. Comparison of Damage Parameter *S* and Dissipated Pseudo Strain Energy W^R from DMA in (a) Dry Condition and (b) Wet Condition.

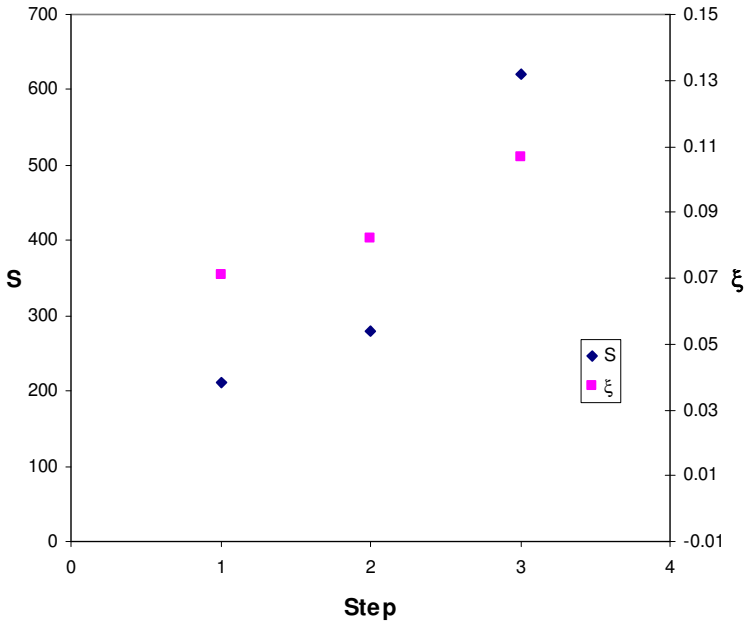

(a)

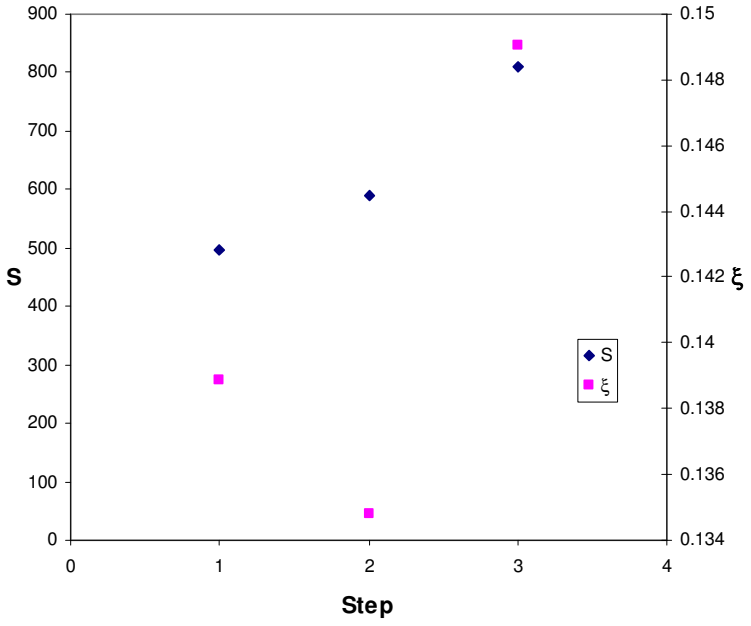

(b)

Figure A.6. Comparison of Damage Parameter *S* and ξ from Creep Test in (a) Dry Condition and (b) Wet Condition.

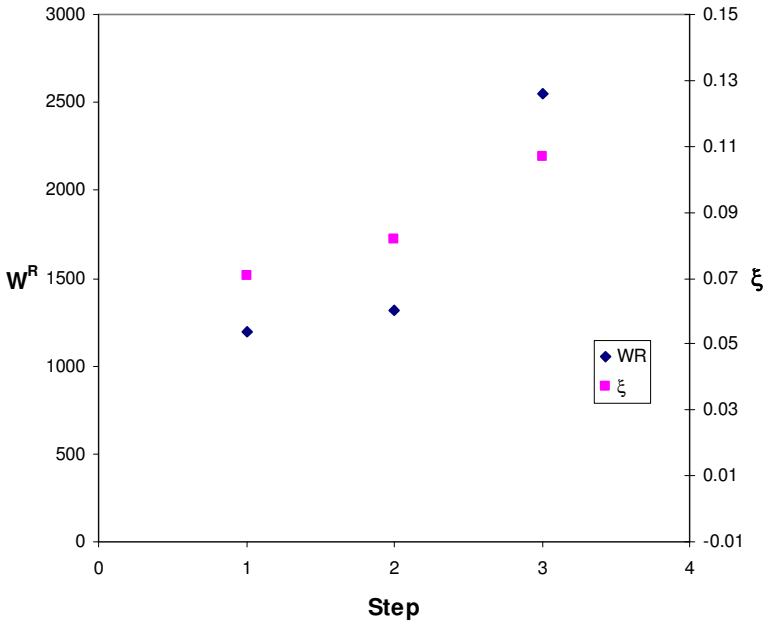

(a)

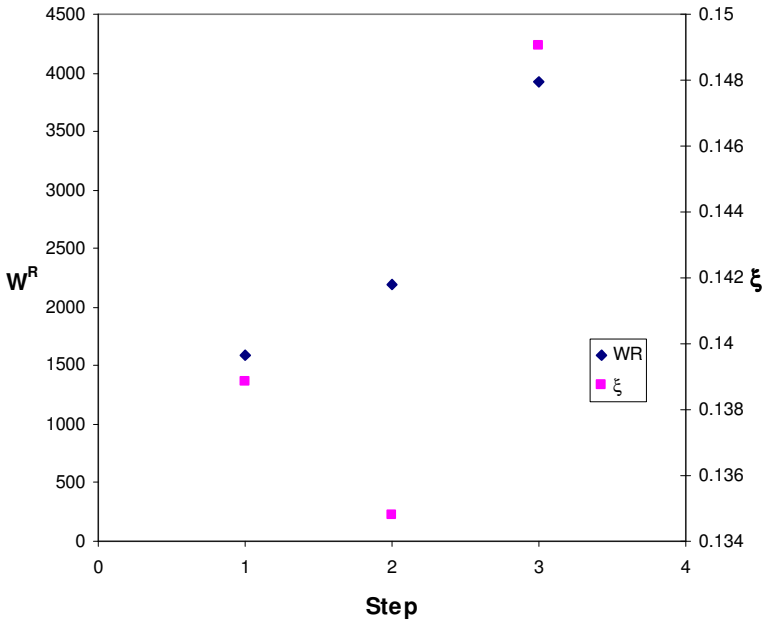

(b)

Figure A.7. Comparison of Dissipated Pseudo Strain Energy W^R and ξ from Creep Test in (a) Dry Condition and (b) Wet Condition.

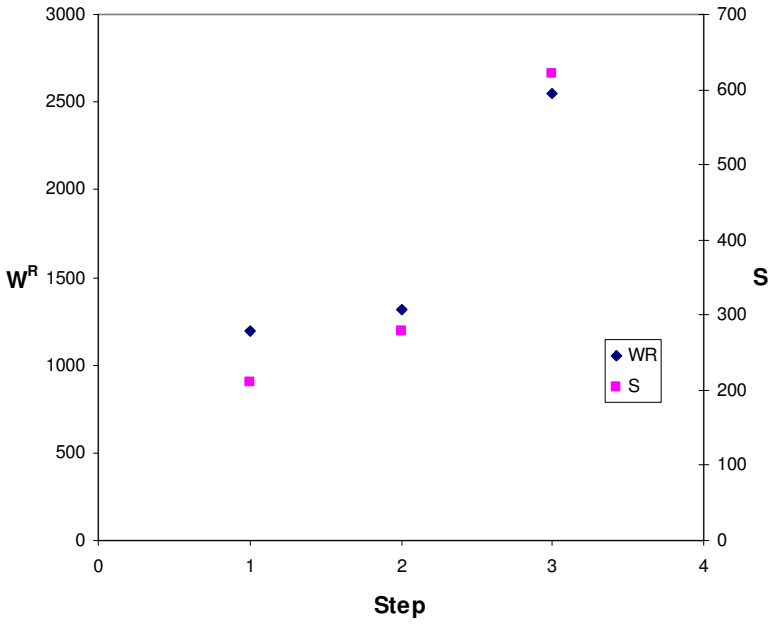

(a)

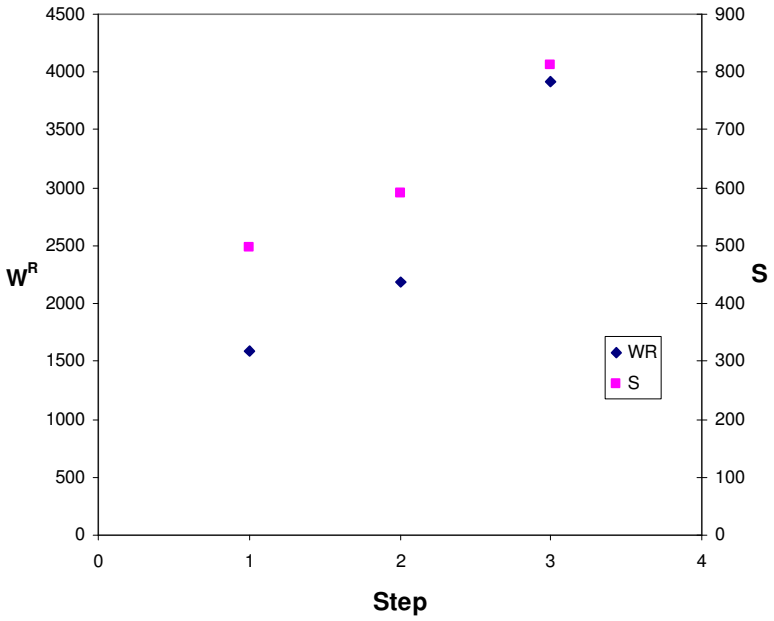

(b)

Figure A.8. Comparison of Dissipated Pseudo Strain Energy W^R and S from Creep Test in (a) Dry Condition and (b) Wet Condition.

Table A.1. Correlation of Dry and Wet Condition in HMA.

Wet \ Dry	ξ	S	W^R
ξ	0.4761	-	-
S	-	0.9283	-
W^R	-	-	0.9947

Table A.2. Correlation of Dry and Wet Condition in Sand Asphalt.

Wet \ Dry	ξ	S	W^R
ξ	0.8718	-	-
S	-	0.9984	-
W^R	-	-	0.7281

APPENDIX B

VOID CONTENTS FOR THE TESTING SPECIMENS AND BASIC PROPERTIES FOR HOT MIX ASPHALT CONCRETE

Table B.1. Void Contents of Specimens Used for Tests

Specimen	Condition	Step	Void Content Undamaged Specimens (%)	Void Content Damaged Specimens (%)
HMA	Dry	1	7.4766	8.3239
		2	7.5617	8.2753
		3	7.5167	8.1488
		4	7.3242	9.7396
	Wet	1	6.7758	7.0515
		2	7.2089	9.519
		3	6.617	8.7064
		4	7.5237	8.9798
Sand Asphalt	Dry	1	15.187	14.8816
		2	13.479	14.729
		3	14.394	16.5115
		4	14.682	16.1529
	Wet	1	13.839	14.1630
		2	13.769	15.1171
		3	14.217	14.9514
		4	13.979	16.5891

Table B.2. Basic HMA Properties for Mix Design

Properties	Value
Optimum Asphalt Content (%)	4.5000
Rice specific Gravity (G_{mm})	2.471
Bulk specific Gravity (G_{mb})	2.376

Table B.3. Measured Specific Gravity for Georgia Granite.

Size (mm)	Bulk Specific Gravity (Oven Dry)	Bulk Specific Gravity (S.S.D)	Apparent Specific Gravity
19	2.71	2.72	2.74
12.5	2.70	2.72	2.74
9.5	2.70	2.72	2.74
4.75 (#4 sieve)	2.71	2.72	2.74
Passing #4 sieve	2.67	2.70	2.75

VITA

Injun Song

Daelim APT 109-1701, Daebang-Dong, Dongjak-Gu

Seoul, Korea, 156-761

E-mail address: injunsong@yahoo.com

Injun Song was born in Daejeon, Korea on July 4, 1971. He grew up in Seoul, Korea. He received his Bachelor of Science in transportation engineering from Hanyang University in February, 1997. He entered the graduate school of Hanyang University in March 1997 and received a Master of Science in transportation engineering in February 1999. After graduation, he worked for Korea Institute of Construction Technology until June 2000. He started his Ph.D. study in August, 2000 and received a Ph.D. in civil engineering in August, 2004. He is married to Sun Young and has a daughter Yoonah.